

# NASA TECHNICAL MEMORANDUM

NASA TM X-73326

## STARSAT - A SPACE ASTRONOMY FACILITY



By Program Development

July 1976

(NASA-TM-X-73326) STARSAT: A SPACE  
ASTRONOMY FACILITY (NASA) 83 p HC \$5.00  
CSCL 14B

N76-29340-

Unclas

63/14

48418

**NASA**



*George C. Marshall Space Flight Center  
Marshall Space Flight Center, Alabama*

1. REPORT NO. NASA TM X-73326		2. GOVERNMENT ACCESSION NO.		3. RECIPIENT'S CATALOG NO.	
4. TITLE AND SUBTITLE Starsat — A Space Astronomy Facility				5. REPORT DATE July 1976	
				6. PERFORMING ORGANIZATION CODE	
7. AUTHOR(S).				8. PERFORMING ORGANIZATION REPORT #	
9. PERFORMING ORGANIZATION NAME AND ADDRESS George C. Marshall Space Flight Center Marshall Space Flight Center, Alabama 35812				10. WORK UNIT, NO.	
				11. CONTRACT OR GRANT NO.	
12. SPONSORING AGENCY NAME AND ADDRESS National Aeronautics and Space Administration Washington, D. C. 20546				13. TYPE OF REPORT & PERIOD COVERED Technical Memorandum	
				14. SPONSORING AGENCY CODE	
15. SUPPLEMENTARY NOTES Prepared by Program Development					
16. ABSTRACT <p>Preliminary design and analyses of a new versatile telescope for Spacelab missions are presented in this report. The system is an all-reflective Korsch three-mirror telescope with excellent performance characteristics over a wide field and a broad spectral range, making it particularly suited for ultraviolet observations. The system concept is evolved around the utilization of existing hardware and designs which were developed for other astronomy space projects.</p> <p style="text-align: center;"><b>ORIGINAL PAGE IS OF POOR QUALITY</b></p>					
17. KEY WORDS			18. DISTRIBUTION STATEMENT Unclassified — Unlimited		
19. SECURITY CLASSIF. (of this report) Unclassified		20. SECURITY CLASSIF. (of this page) Unclassified		21. NO. OF PAGES 83	22. PRICE NTIS

## CONTRIBUTORS

Study Manager	M. E. Nein
Project Engineers	E. C. Hamilton C. E. Mundie
Optical Design and Analysis	D. Korsch*
Mechanical Design	R. A. Love
Structural Analysis	F. S. Fuller
Pointing and Stabilization	J. R. Parker
Thermal Control	C. G. Fritz
Data Management and Communication	R. E. White
Electrical Power	R. J. Giudici

\*Sperry Rand in support of Electronics and Control Laboratory,  
MSFC

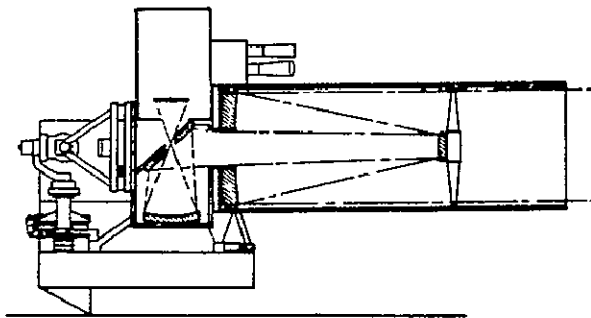


# TABLE OF CONTENTS

		Page
1.	INTRODUCTION .....	1
2.	OPTICAL CONCEPT .....	2
	2.1 BACKGROUND .....	2
	2.2 THE KORSCH THREE-MIRROR TELESCOPE.....	4
	2.3 OPTICAL ANALYSIS .....	8
	2.4 BAFFLING .....	10
	2.5 FOCAL PLANE ACCESS .....	12
	2.6 INSTRUMENT INTEGRATION CONCEPT.....	13
	2.7 ROWLAND SPECTROGRAPH CONFIGURATION .....	13
3.	STRUCTURAL DESIGN AND MECHANICS .....	15
	3.1 TELESCOPE DESCRIPTION .....	15
	3.1.1 The Three-Mirror Telescope Configurations ...	15
	3.1.2 The Modified Version for Rowland Spectrograph.....	16
	3.2 STRUCTURAL CONCEPT .....	21
	3.2.1 Requirements .....	21
	3.2.2 Primary Bulkhead .....	21
	3.2.3 Metering Shell .....	21
	3.2.4 Mirror Supports .....	23
4.	POINTING AND STABILIZATION .....	25
	4.1 COARSE POINTING .....	25
	4.2 FINE POINTING .....	27
	4.3 FINE GUIDANCE SENSOR .....	29
	4.3.1 HEAO-B Star Tracker System .....	31
	4.3.2 Charge Coupled Device .....	39
	4.3.3 Multiaperture Image Dissector.....	40
	4.3.4 Perkin-Elmer ST FGS .....	41
	4.4 SECONDARY MIRROR ALIGNMENT AND ARTICULATION MECHANISM .....	42

## TABLE OF CONTENTS (Concluded)

	Page
5. THERMAL CONTROL . . . . .	43
5.1 REQUIREMENTS . . . . .	44
5.2 CONTROL CONCEPT . . . . .	45
5.3 MATHEMATICAL MODEL . . . . .	46
5.4 ASSUMPTIONS AND INPUT PARAMETERS . . . . .	47
5.5 RESULTS . . . . .	49
5.6 THERMAL CONTROL OF INSTRUMENT MODULE . . . . .	55
5.7 RECOMMENDATIONS . . . . .	56
6. DATA MANAGEMENT AND COMMUNICATIONS . . . . .	57
6.1 DATA MANAGEMENT . . . . .	57
6.2 COMMUNICATIONS . . . . .	58
7. ELECTRICAL SYSTEM . . . . .	59
7.1 POWER REQUIREMENT . . . . .	60
7.2 WIRE HARNESS . . . . .	62
8. INTERFACES . . . . .	62
8.1 PAYLOAD BAY . . . . .	62
8.2 POINTING AND STABILIZATION . . . . .	65
8.3 DATA MANAGEMENT . . . . .	66
8.4 ELECTRICAL SYSTEM . . . . .	67
8.5 COMMUNICATIONS . . . . .	68
9. MASS PROPERTIES . . . . .	68
10. CONCLUSIONS . . . . .	70
11. REFERENCES . . . . .	71

# LIST OF ILLUSTRATIONS

Figure	Title	Page
1.	Transmission Comparison . . . . .	3
2.	Transmission loss due to one reflection . . . . .	3
3.	Examples of previous three-mirror designs . . . . .	4
4.	The Korsch three-mirror telescope (configuration I) . . . .	5
5.	The Korsch three-mirror telescope (configuration II) . . .	6
6.	Field distribution . . . . .	8
7.	Performance comparison . . . . .	9
8.	Stray light path in configuration I . . . . .	11
9.	Stray light path in configuration II . . . . .	11
10.	Telescope with instrument module . . . . .	12
11.	Three field cameras sharing focal plane . . . . .	14
12.	Korsch telescope modified as a two-mirror system with Rowland spectrograph . . . . .	14
13.	The four modules of the three-mirror telescope . . . . .	16
14.	The two configurations of the three-mirror telescope . . .	17
15.	Tertiary and instrument modules of configurations I and II . . . . .	19
16.	Rowland spectrograph module . . . . .	20
17.	Rowland spectrograph configuration . . . . .	20
18.	GEMS . . . . .	22

## LIST OF ILLUSTRATIONS (Continued)

Figure	Title	Page
19.	GEMS static test and estimated load in Starsat application . . . . .	23
20.	Primary mirror support concept . . . . .	24
21.	Error definitions . . . . .	26
22.	Pointing control block diagram . . . . .	28
23.	Image stabilization . . . . .	29
24.	Starsat — sequence flow diagram . . . . .	30
25.	Starsat fine guidance sensor . . . . .	31
26.	Martin Marietta drive mechanism . . . . .	32
27.	Guide sensor field . . . . .	32
28.	Search scan pattern . . . . .	34
29.	Acquisition mode (first guide star detection) . . . . .	34
30.	Modulation pattern and driving signal . . . . .	36
31.	Error count angle transfer curve . . . . .	37
32.	Focus sensor scan . . . . .	39
33.	Perkin-Elmer Space Telescope FGS schematic . . . . .	41
34.	Mirror control system . . . . .	43
35.	Thermal tolerances based on optical requirements . . . . .	44
36.	Thermal control concept . . . . .	45

## LIST OF ILLUSTRATIONS (Continued)

Figure	Title	Page
37.	Thermal model . . . . .	47
38.	Temperature history of each end of the optical bench for the hot case . . . . .	49
39.	Temperature history of each end of the optical bench for the cold case . . . . .	50
40.	Average temperature variation of telescope throughout an orbit for the cold case . . . . .	53
41.	Average temperature variation of telescope throughout an orbit for the hot case . . . . .	53
42.	Temperature variation of telescope throughout an orbit for the cold case . . . . .	54
43.	Temperature variation of telescope throughout an orbit for the hot case . . . . .	54
44.	Temperature history of primary mirror, graphite-epoxy tube and outside surface throughout an orbit for hot and cold cases . . . . .	55
45.	Average payload bay temperature throughout an orbit for hot and cold cases . . . . .	56
46.	Starsat in Shuttle payload bay . . . . .	62
47.	Allowable telescope motion in payload bay . . . . .	63
48.	Telescope facility in Shuttle payload bay . . . . .	64
49.	Telescope facility on pallet . . . . .	64
50.	IPS/telescope tiedown interface . . . . .	65



## LIST OF ILLUSTRATIONS (Concluded)

Figure	Title	Page
51.	IPS optical sensor package . . . . .	66
52.	Spacelab CDMS and Orbiter interface . . . . .	67
53.	Electrical power distribution and interface . . . . .	68
54.	Starsat center of mass and inertias . . . . .	69

## LIST OF TABLES

Table	Title	Page
1.	Telescope Parameters . . . . .	5
2.	Misalignment Sensitivities . . . . .	10
3.	Characteristics of the Four Modules . . . . .	18
4.	Spacelab Instrument Pointing System . . . . .	27
5.	Fine Guidance Sensor Characteristics (HEAO-B Star Tracker) . . . . .	33
6.	Thermal Properties of Surfaces and Materials . . . . .	48
7.	Heater Power in Watts to Maintain $20 \pm 1^\circ\text{C}$ . . . . .	50
8.	System Equilibrium Time . . . . .	51
9.	Starsat Thermal Control Results . . . . .	52
10.	Telescope Facility Command and Telemetry Requirements . . . . .	58
11.	Command and Telemetry Requirements . . . . .	59
12.	Electrical Power Requirements . . . . .	60
13.	System and Subsystem Weights . . . . .	69

## STARSAT — A SPACE ASTRONOMY FACILITY

### 1. INTRODUCTION

Starsat is a versatile space telescope designed to take full advantage of the space environment in performing observational astronomy. It is particularly suited for extended field and ultraviolet observations.

The specific capabilities of this telescope ideally supplement the scientific objectives of the 2.4 m Space Telescope which are oriented toward very high resolution over narrow fields.

The telescope is a Korsch three-mirror design with excellent performance characteristics. Several three-mirror telescope designs have been proposed in the past; however, significant shortcomings such as inaccessibility of the focal plane, excessive central obscuration, or generally impractical configurations have prevented their application. The main characteristics of this new design are as follows:

- All reflective
- Conventional conic surface figures for all mirrors
- Wide flat field and high performance
- Loss in efficiency only significant below 110 nm
- Fully accessible focal plane
- High degree of modularity
- Simple and effective baffling systems.

While excellent performance of a space telescope is the primary concern of scientists, it is equally important to strive for cost-effective approaches. To this end, the Starsat concept has evolved around the use of existing hardware and designs developed for the Space Telescope, High Energy Astronomy Observatory (HEAO), and other space projects. For example, the availability of a graphite-epoxy metering shell — a technological development item in the Space Telescope program — led to selection of the 1.5 m aperture. Use of this metering shell saves the high cost of a new development

item and the extensive test program associated with it. Cost savings are also realized by using scaled down designs of the Space Telescope primary bulkhead, mirror attachments, and secondary mirror actuator systems. The primary mirror can possibly be fabricated from an existing blank.

Other low cost systems proposed for Starsat are the HEAO-B star tracker and a rho-theta drive mechanism designed for the Space Telescope program.

Subsequent chapters of this report describe the concept of the three-mirror telescope and preliminary analyses of the subsystems.

## 2. OPTICAL CONCEPT

### 2.1 BACKGROUND

The performance of ground-based telescopes is principally limited by the Earth's atmosphere. The turbulent atmosphere not only limits the resolution to approximately 1 arc s but also absorbs large portions of the electromagnetic spectrum. The capability to place a telescope into space and perform extraterrestrial observations without interference from the atmosphere provides new opportunities for major advancements in the field of observational astronomy. The design of new instruments with the capability to utilize all the advantages of an extraterrestrial station is a desirable and demanding task.

The Ritchey-Chretien, an improved version of the classical Cassegrain Telescope, is today's most popular telescope. This two-mirror system, however, provides only a high resolution field of a few arc min and has a curved image surface. To widen and flatten the field, the Ritchey-Chretien telescope is normally used in combination with refractive correctors, the transmission of which is essentially limited to the visible portion of the spectrum. The transmission range of a reflective surface and of a refractive corrector, both optimized for ultraviolet transmission, are shown in comparison with the atmospheric window in the vicinity of the visible spectrum in Figure 1. Considering the fact that one major reason for putting astronomical telescopes outside the atmosphere is to expand the observable range of the electromagnetic spectrum, it becomes evident that an all-reflective space telescope is highly desirable. Improving the performance of a two-mirror telescope necessarily means increasing the number of surfaces. The addition of surfaces means a loss in transmission, particularly in the extreme ultraviolet. However, the transmission loss per reflection (Fig. 2) is insignificant compared to the total loss of large portions of the spectrum caused by refractive optics.

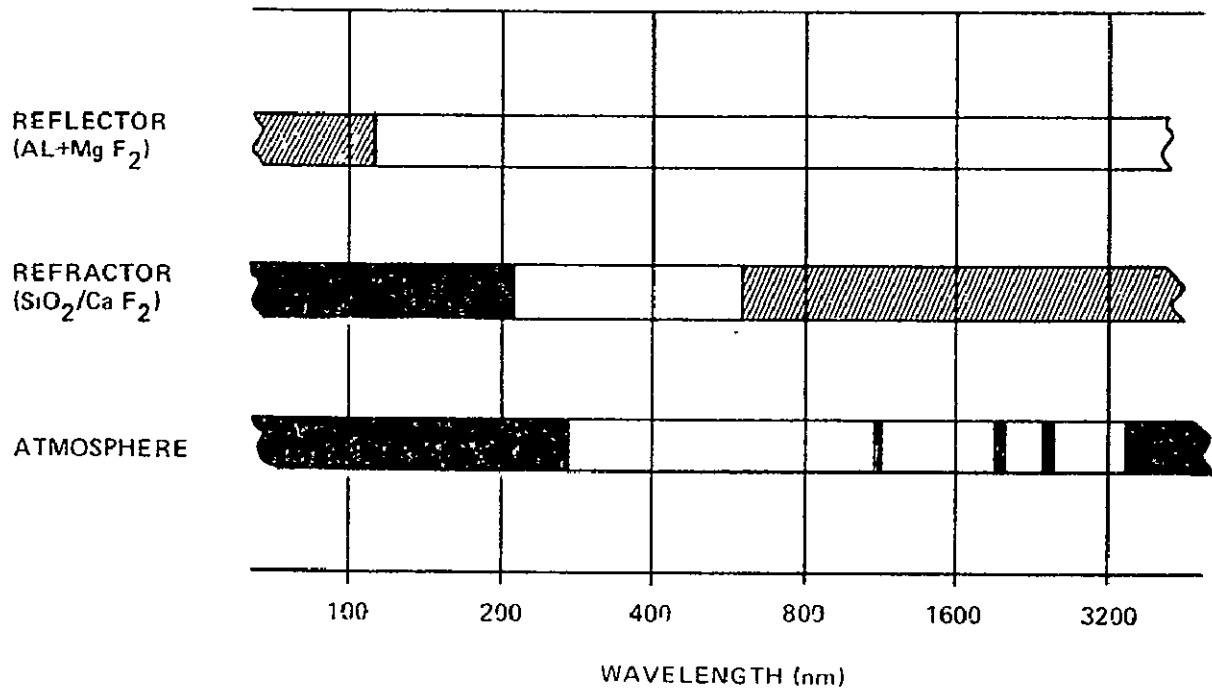


Figure 1. Transmission comparison.

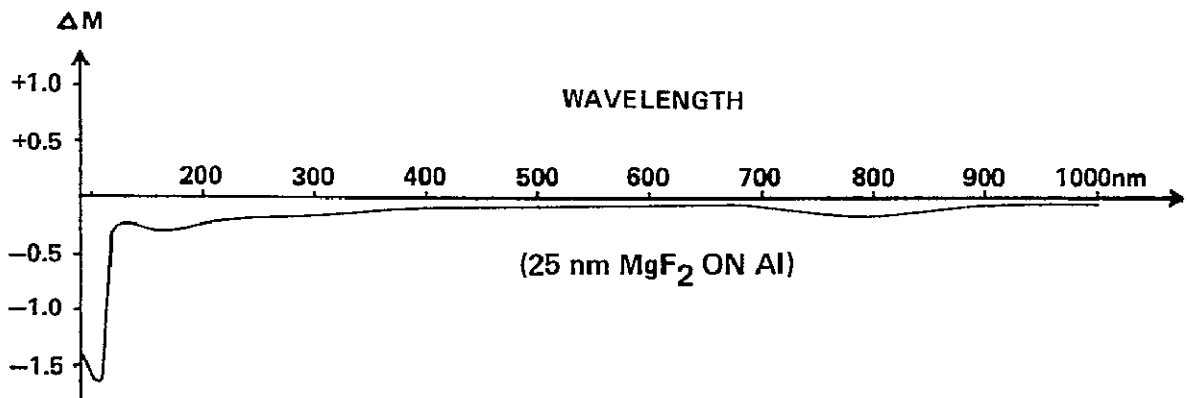


Figure 2. Transmission loss due to one reflection.

Several three-mirror telescopes have been proposed in the past [1-7], none of which provides a practical and useful solution. Examples of the most typical configurations are shown in Figure 3. The main shortcomings of the types a, b, and c are the inaccessibility of the image plane, the large central obscuration, and the practically invariable fast focal ratio forced by the

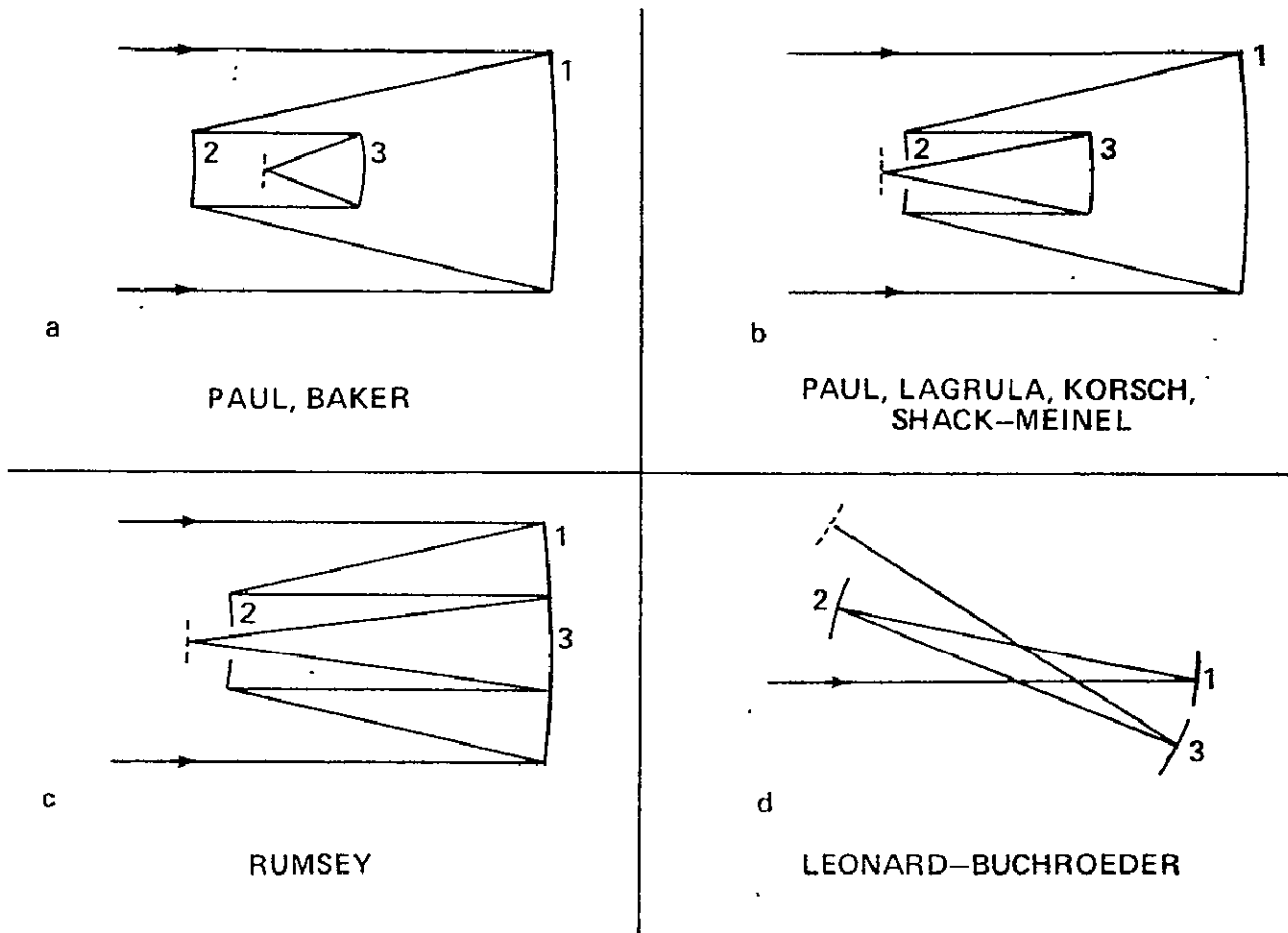


Figure 3. Examples of previous three-mirror designs.

configuration. A special class of tilted-component telescopes is summarized in a report by Buchroeder [8]; Figure 3d is one example. Apart from the fact that the largely asymmetric configurations are not very attractive, none of the designs meets the requirements of a high performance space telescope.

## 2.2 THE KORSCH THREE-MIRROR TELESCOPE

While any practical two-mirror telescope configuration can only be corrected for maximally two aberrations, usually spherical aberration and coma, the Korsch three-mirror telescope presented here is corrected for four aberrations: spherical aberration, coma, astigmatism, and field curvature. The primary/secondary configuration resembles the Cassegrain, forming a

real image closely behind the primary (Fig. 4). This secondary image is then reimaged by a tertiary mirror at approximately unit magnification. A small, flat mirror placed at the exit pupil, which is located between the primary mirror and the tertiary mirror, folds the light away from the axis of the telescope where the final image is formed. The pertinent telescope parameters are summarized in Table 1.

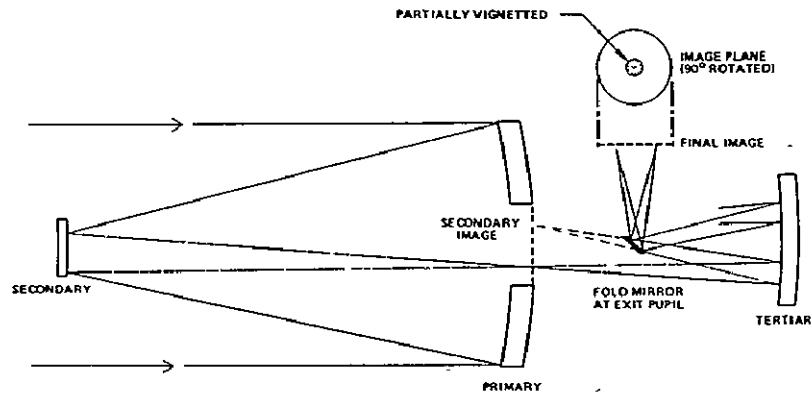


Figure 4. The Korsch three-mirror telescope (configuration I).

TABLE 1. TELESCOPE PARAMETERS

CLEAR APERTURE	150 cm
PRIMARY F-NO.	2.2
SYSTEM F-NO.	12
SYSTEM FOCAL LENGTH	1800 cm
SECONDARY DIAMETER	35 cm
TERTIARY DIAMETER	80 cm
EXIT PUPIL DIAMETER	5.2 cm
SECONDARY IMAGE DIAMETER	48.3 cm (1.5°)
FINAL IMAGE DIAMETER	47.1 cm (1.5°)
PRIMARY RADIUS	660.0000 cm
SECONDARY RADIUS	-126.9495 cm
TERTIARY RADIUS	155.1436 cm
PRIMARY DEFORMATION	-0.969825155 (ELLIPSOID)
SECONDARY DEFORMATION	-1.739742501 (HYPERBOLOID)
TERTIARY DEFORMATION	-0.558565085 (ELLIPSOID)
SECONDARY MAGNIFICATION	-5.6
TERTIARY MAGNIFICATION	0.9740
DISTANCE:	
PRIMARY-SECONDARY	277.8600 cm
SECONDARY-TERTIARY	449.1962 cm
TERTIARY-EXIT PUPIL	92.0000 cm
EXIT PUPIL-IMAGE PLANE	61.1287 cm

In an alternate configuration shown in Figure 5, a flat perforated mirror is placed diagonally between primary and tertiary. This configuration minimizes obscuration by avoiding the spider that holds the small fold mirror and significantly improves the baffling of the system.

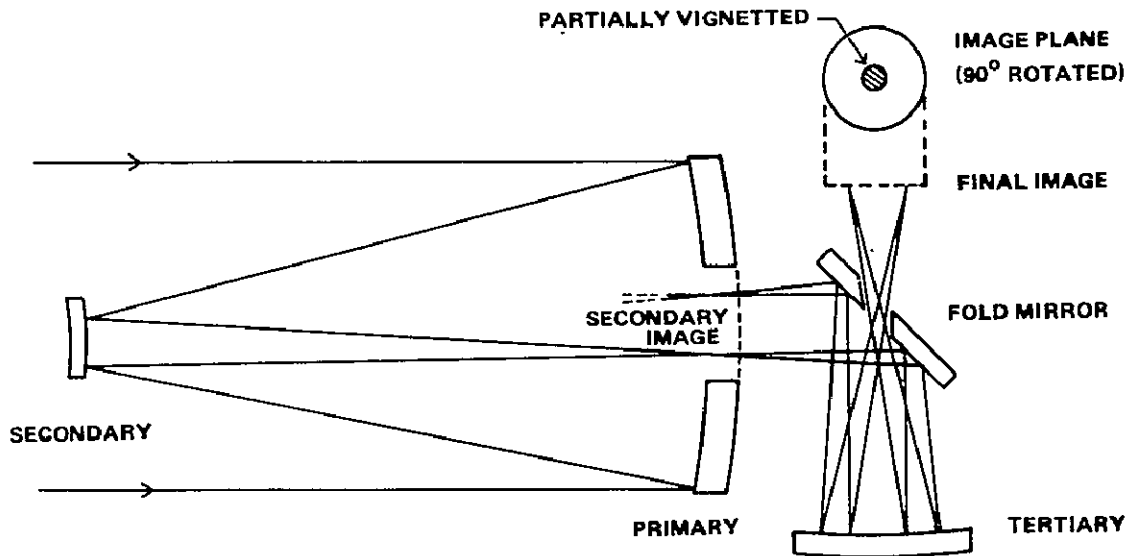


Figure 5. The Korsch three-mirror telescope (configuration II).

The mathematical condition for correcting spherical aberration, coma, and astigmatism simultaneously can be written according to References 9 and 10:

$$\begin{aligned}
 b_1\delta_1 + b_2\delta_2 + b_3\delta_3 &= b_0 && \text{(Vanishing spherical aberration)} \\
 g_1\delta_1 + g_2\delta_2 + g_3\delta_3 &= g_0 && \text{(Vanishing coma)} \\
 c_1\delta_1 + c_2\delta_2 + c_3\delta_3 &= c_0 && \text{(Vanishing astigmatism)}
 \end{aligned}
 \tag{1}$$



The  $\delta_i$  are the surface deformation constants, and  $b_i$ ,  $g_i$ ,  $c_i$  are functions of the individual mirror magnifications with respect to the object,  $m_i$ , and with respect to the pupil,  $p_i$ .

Since the system is free of astigmatism, the condition for a flat field is equivalent to the Petzval condition:

$$(m_1 - p_1)m_2m_3p_2p_3 + (m_2 - p_2)m_3p_3 + (m_3 - p_3) = 0 \quad (2)$$

The primary magnification of a telescope is  $m_1 = 0$  and  $p_1 = -1$  because the entrance pupil is at the primary mirror. The tertiary pupil magnification is made a dependent variable by solving equation (2) for  $p_3$ ,

$$p_3 = \frac{m_3}{[1 - m_2m_3p_2 - (m_2 - p_2)m_3]} \quad (3)$$

The flat field condition is, like all expressions for the aberrations, only accurate to the third order. To further optimize the flatness of the field, we introduce a small dimensionless quantity,  $h$ , so that

$$p_3 = \frac{m_3}{[1 + h - m_2m_3p_2 - (m_2 - p_2)m_3]} \quad (4)$$

Maximum flatness of the field was obtained by varying  $h$  while analyzing the image plane by means of a ray trace program. The quantities of the optimized system in equation (4) were determined to be  $m_2 = -5.60$ ,  $m_3 = 0.9740259$ ,  $p_2 = -0.1859604$ ,  $p_3 = 0.1832568$ , and  $h = 0.056$ . A list of the most relevant telescope parameters is given in Table 1. A similar design was introduced by Korsch in Reference 11.

## 2.3 OPTICAL ANALYSIS

The combination of the following characteristics distinguish the Korsch telescope from previous three-mirror designs:

- Very high resolution in a wide, flat field
- Convenient access to the image plane
- Moderate central obscuration
- A high and variable focal ratio, allows the telescope to be matched to the resolution of available detectors.

This telescope provides a flat image field of  $1.5^\circ$  in diameter with a geometric rms spot size not larger than 0.03 arc s anywhere in the field. Only a central portion of  $0.4^\circ$  in diameter is partially vignetted (Fig. 6).

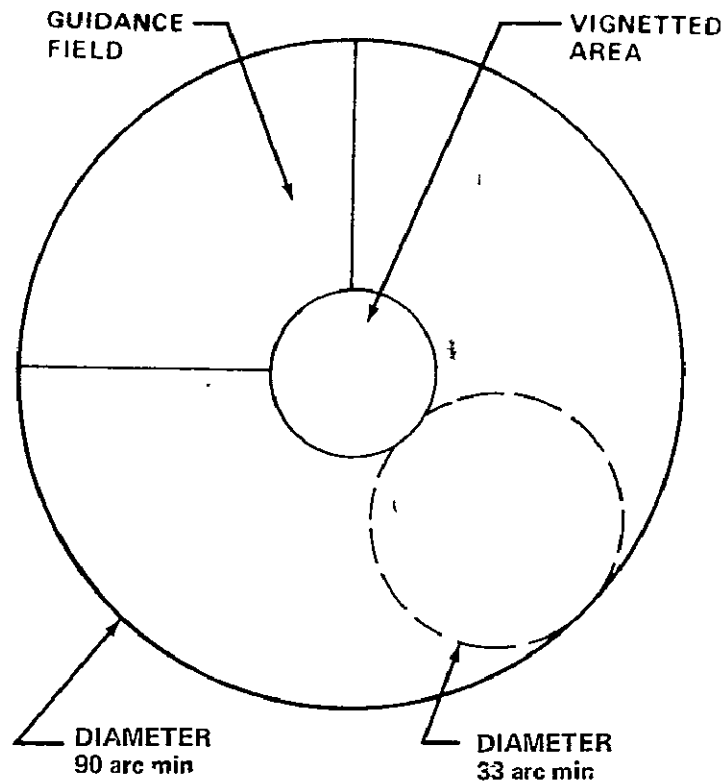


Figure 6. Field distribution.

The performance of the three-mirror telescope is demonstrated in Figure 7, where it is compared to the performance of a Ritchey-Chretien telescope and a Ritchey-Chretien plus Gascoigne corrector [12]. The geometric spot size, i.e. the diameter of the smallest circle surrounding all rays traced through the system, is plotted as a function of the field angle. The superior performance of the three-mirror telescope is not only reflected in the significantly smaller spot size but also in the fact that it is independent of the wavelength (disregarding diffraction effects), while a refractive corrector is only useful over a relatively narrow spectral range.

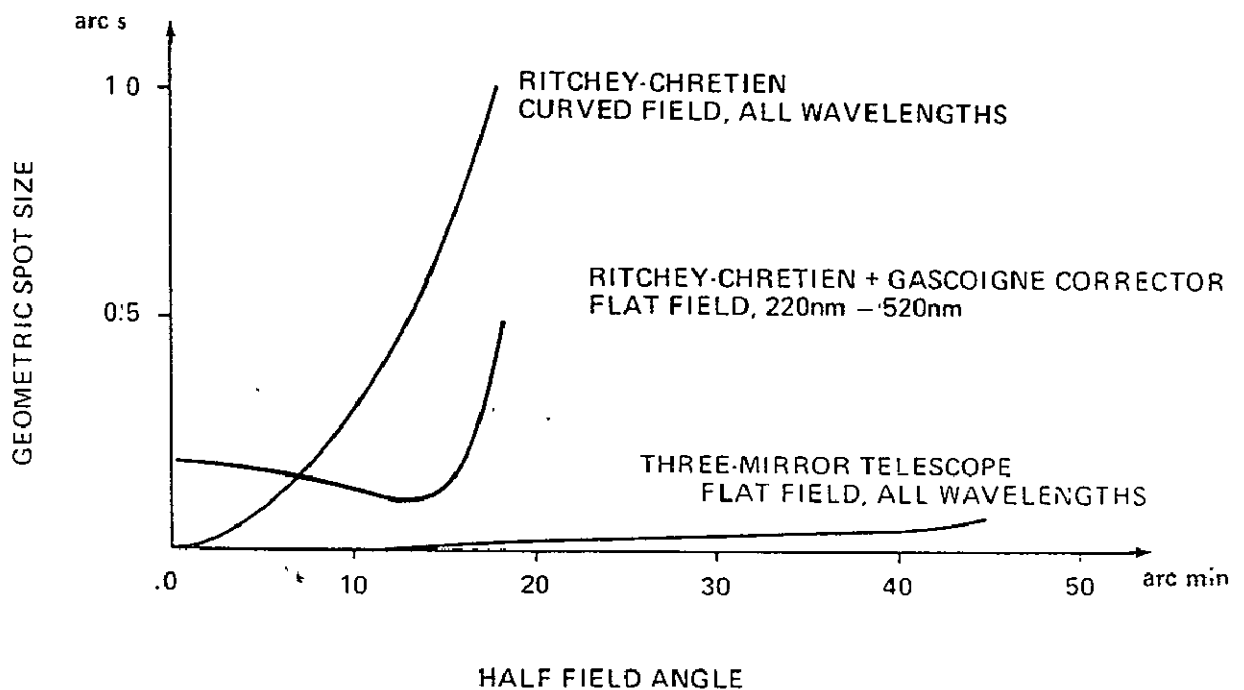


Figure 7. Performance comparison.

The analysis of the misalignment sensitivities dispels any apprehension concerning the possibility of a drastic increase in complexity due to the addition of the third mirror. Table 2 gives the effects of secondary and tertiary misalignments on the performance in terms of rms wave front errors (optical path difference) and in terms of induced aberrations (increase of spot size). It shows that the tertiary is 15 to 200 times less sensitive than the secondary.

TABLE 2. MISALIGNMENT SENSITIVITIES

	INCREASE OF RMS-OPD PER UNIT MISALIGNMENT ( $\lambda = 632.8 \text{ nm}$ )	INCREASE OF GEOMETRIC SPOT DIAMETER PER UNIT MISALIGNMENT
<u>SECONDARY</u>		
DESPACE	0.025 $\lambda/\mu\text{m}$	0.032 $\mu\text{rad}/\mu\text{m}$
DECENTER	0.0013 $\lambda/\mu\text{m}$	0.0036 $\mu\text{rad}/\mu\text{m}$
TILT	0.0008 $\lambda/\mu\text{rad}$	0.0023 $\mu\text{rad}/\mu\text{rad}$
<u>TERTIARY</u>		
DESPACE	0.0016 $\lambda/\mu\text{m}$	0.0021 $\mu\text{rad}/\mu\text{m}$
DECENTER	0.016 $\lambda/\text{mm}$	0.048 $\mu\text{rad}/\text{mm}$
TILT	0.004 $\lambda/\text{mrad}$	0.014 $\mu\text{rad}/\text{mrad}$

#### 2.4 BAFFLING

To protect the secondary image in a Cassegrain telescope effectively from stray light requires a very complex and elaborate baffling system. One major advantage of the three-mirror telescope is the natural baffling property of this configuration. The final image plane is already well protected from stray light without adding an extra baffling system. Main reasons for this effect are the folded out image plane and the exit pupil behind the tertiary forming a bottleneck in the optical train. In configuration I, Figure 8, the only stray light that can reach the final image is that scattered off the structure holding the small fold mirror. The structure, however, is so far within the system that it will not be illuminated by the Moon, Earth, or Sun. An even more efficient baffling effect is achieved with configuration II shown in Figure 9. No stray light can reach the image after only a single scattering process. Even the light that is scattered off the edges around the perforation of the fold mirror and then reflected by the tertiary through the exit pupil will be intercepted by the central vignetted portion rather than by the useful field. A further advantage is the accessibility of the secondary spider image formed by the tertiary. It is located immediately behind the exit pupil and can, at least in configuration II, easily be masked off.

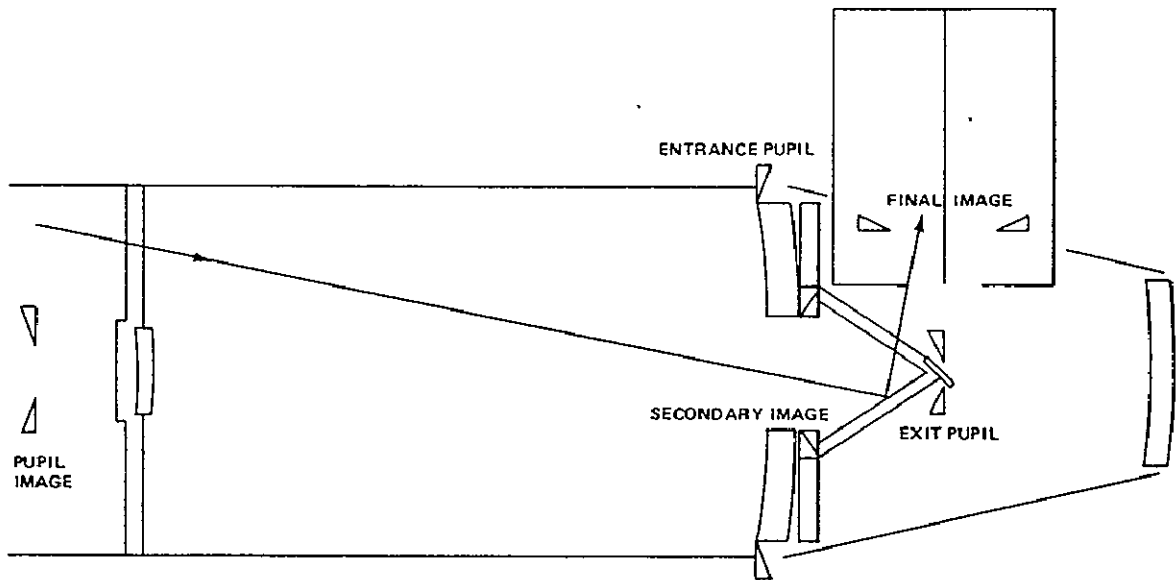


Figure 8. Stray light path in configuration I.

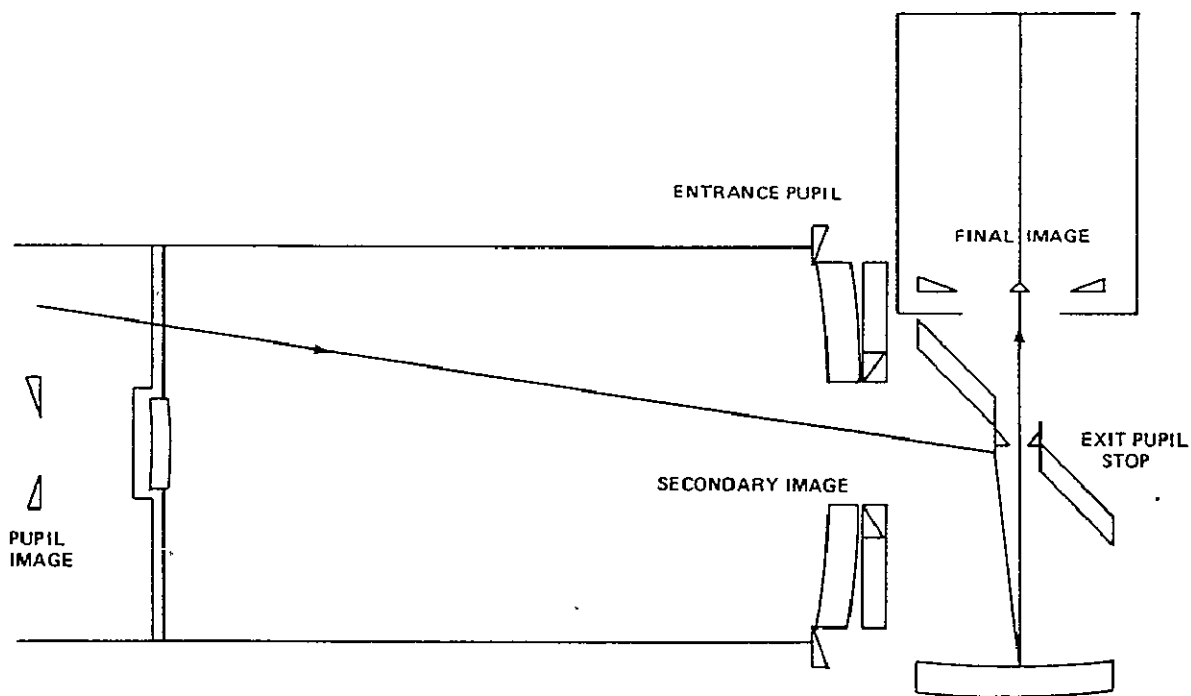


Figure 9. Stray light path in configuration II.

## 2.5 FOCAL PLANE ACCESS

The unvignetted image field is an annulus with an outside diameter of 47.1 cm and inside diameter of 12.6 cm focused at a location which provides easy access and adequate space for instruments and the fine guidance sensor (Fig. 10).

The field shape is particularly advantageous to accommodate a set of different instruments. Approximately one-quarter of the field will be assigned to the fine guidance system. The remaining field is sufficiently large for several scientific instruments (Fig. 6).

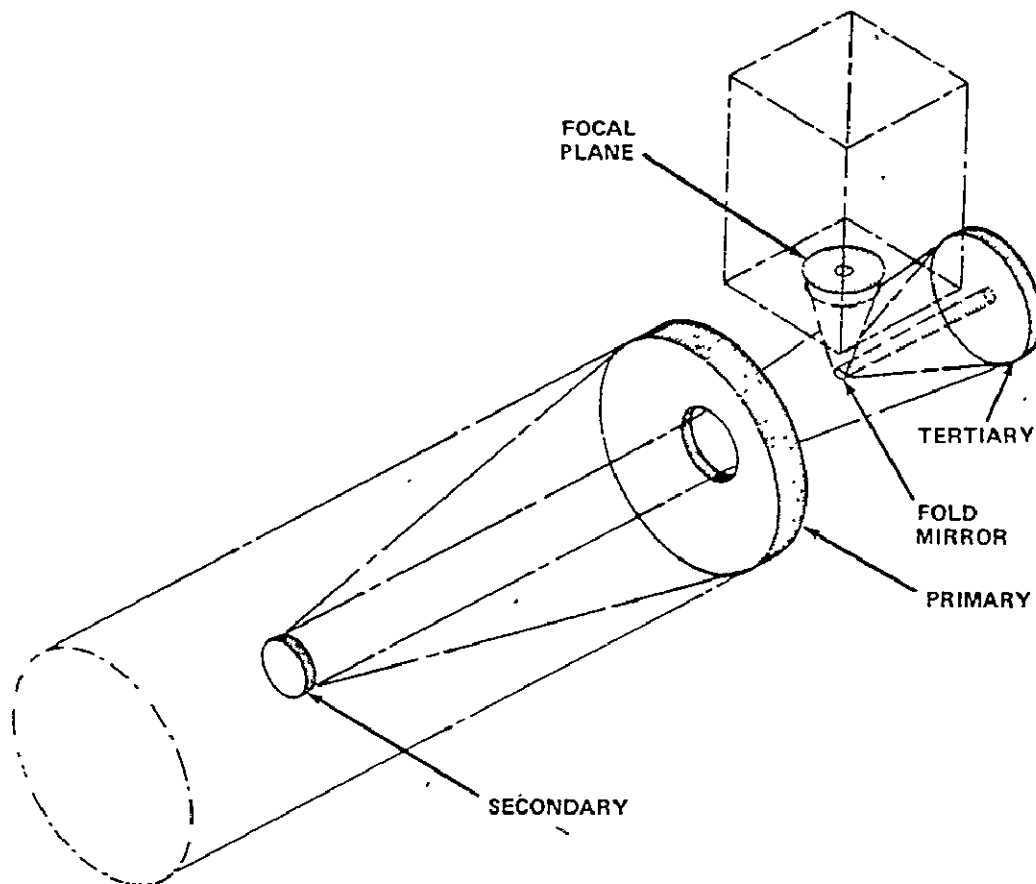


Figure 10. Telescope with instrument module.

## 2.6 INSTRUMENT INTEGRATION CONCEPT

It is desirable to have more than one instrument sharing the focal plane for the following reasons:

- To increase the versatility of the facility
- To have a backup in case one instrument fails
- To maximize the scientific gain per mission.

The last point is particularly important. However, the gain cannot be increased by merely increasing the number of instruments unless those instruments are able to operate simultaneously. A field camera is one type of instrument that can meaningfully operate simultaneously with practically any other instrument. A field camera can either be directed at a specific target or work in a serendipitous fashion, thereby leaving the freedom to point the telescope at a source of interest to a spectrograph, photometer, or any other instrument. An especially efficient mode of operation can be achieved by using three field cameras simultaneously. Each camera is centered in a quadrant of the focal plane, covers approximately  $0.5^\circ$ , and works over a different spectral band (Fig. 11). Four  $90^\circ$  rotations of the telescope about the optical axis then provides 12 pictures of 4 fields in 3 different bands. To package three relatively large cameras without mechanical and magnetic interference could conceivably be realized by using three independent electrographic cameras working within a common magnetic field. In case there is no fine guidance system available that would operate satisfactorily within the camera field, the guidance field would have to be relayed outside the coil. This is not expected to cause any significant problem.

## 2.7 ROWLAND SPECTROGRAPH CONFIGURATION

A third configuration (Fig. 12) was studied to illustrate how this three-mirror telescope design can be modified to operate as a Cassegrain configuration with only two mirror surfaces. This configuration is necessary to minimize the reflections when performing spectroscopy in the extreme ultraviolet. This requires elimination of the tertiary and fold mirrors for the instrument. A Rowland spectrograph was selected as the instrument to be accommodated. Although the primary/secondary mirror system is corrected for

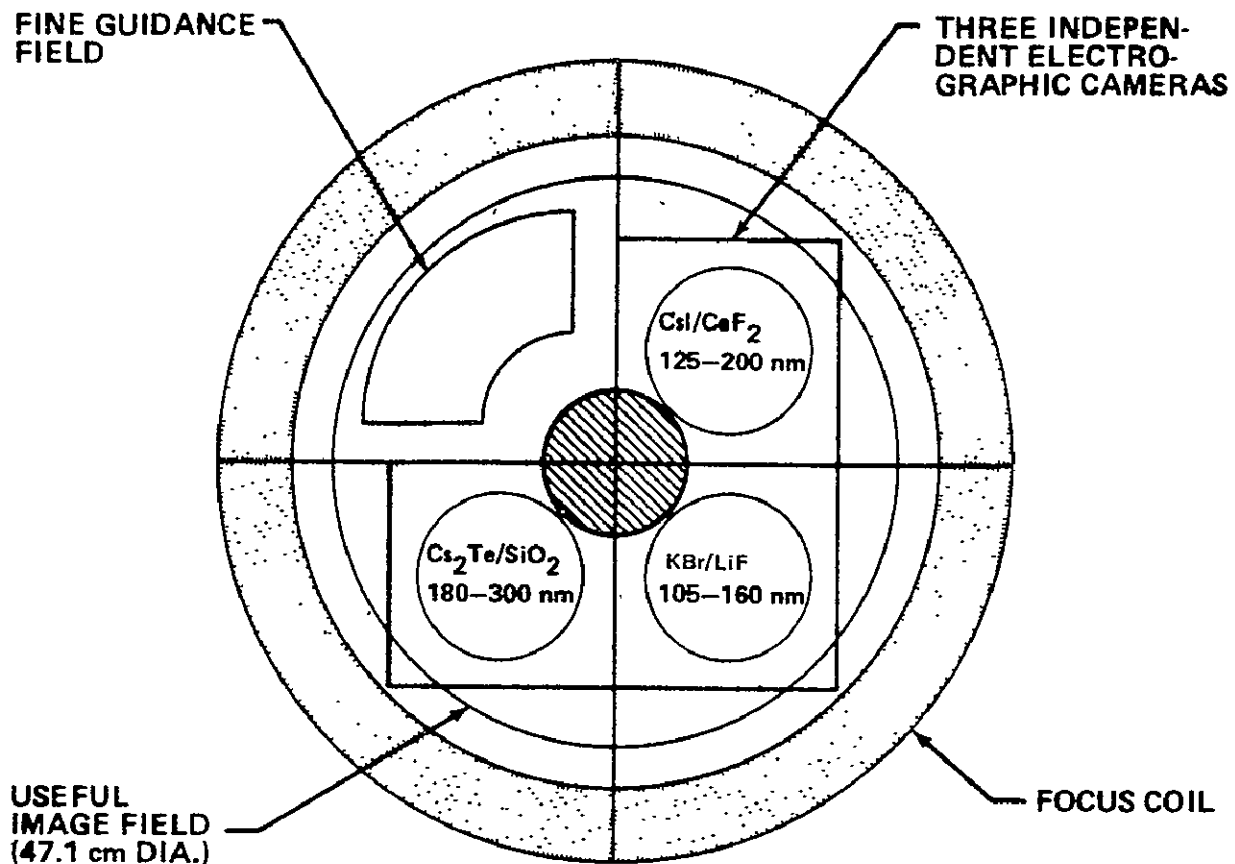


Figure 11. Three field cameras sharing focal plane.

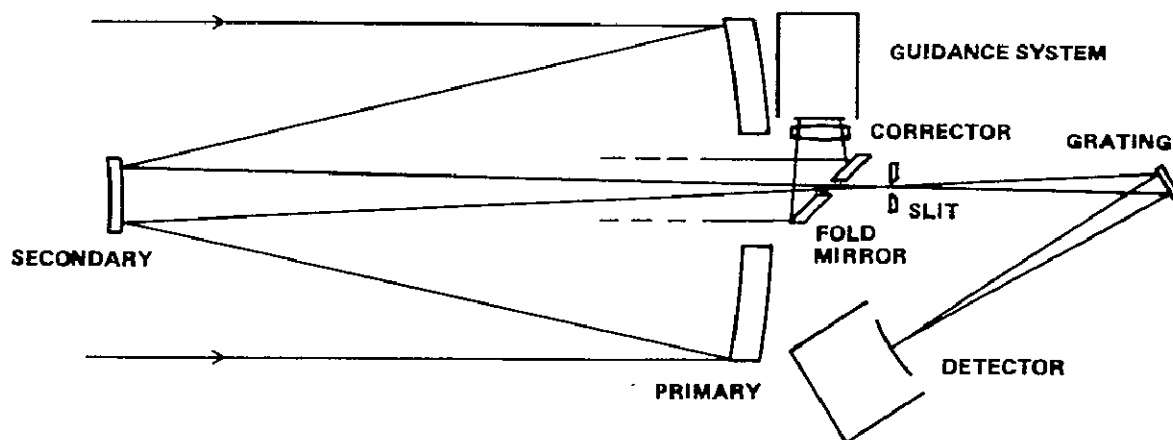


Figure 12. Korsch telescope modified as a two-mirror system with Rowland spectrograph.



spherical aberration and would provide adequate image quality for a Rowland spectrograph, a different secondary mirror is recommended that forms an image further behind the primary to ease accessibility and to improve the baffling. This secondary mirror could already have a lithium fluoride coating so that for this special mission only the primary need be recoated. Because of the limited field of view of this two-mirror system, correcting optics for the guidance system will have to be provided.

### 3. STRUCTURAL DESIGN AND MECHANICS

#### 3.1 TELESCOPE DESCRIPTION

##### 3.1.1 The Three-Mirror Telescope Configuration

The telescope facility consists of the following subsystems: optics, structures, thermal control, fine guidance, data management, and electrical power.

Preliminary analyses of these areas were performed and are presented in this report. Design aspects which have been analyzed in detail during other programs such as Space Telescope, Medium Aperture Optical Telescope (MAOT), and HEAO were used where applicable. Specifically, the detail analyses of the metering structures and the fine guidance system benefitted from past experience.

The Korsch three-mirror telescope system consists of four major modules (Fig. 13):

- a. The primary module containing the bulkhead, primary mirror, metering shell, and lightshield.
- b. The secondary module containing the secondary mirror, its support structure, and alignment actuators.
- c. The tertiary module with the tertiary mirror, fold mirror, support structure, and the aft bulkhead and tertiary metering structure.
- d. The instrument module to accommodate the scientific instruments and the telescope fine guidance system.

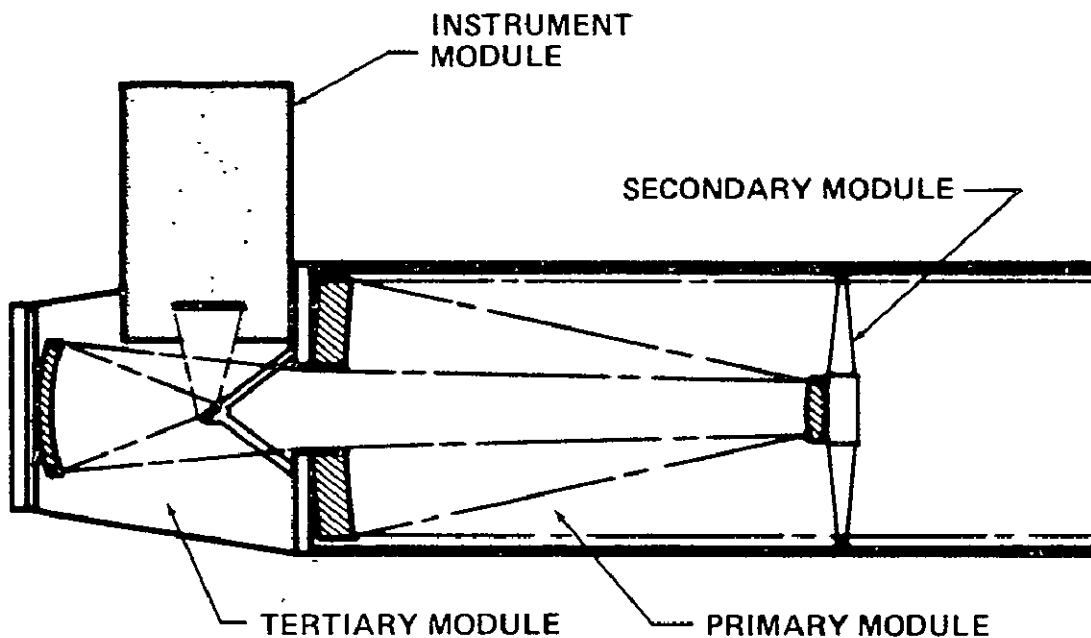


Figure 13. The four modules of the three-mirror telescope.

The central part or main structural reference within the telescope is the bulkhead of the primary module. All flight loads are directed into this bulkhead, which is the mounting base for the forward and aft metering structures and the instrument module.

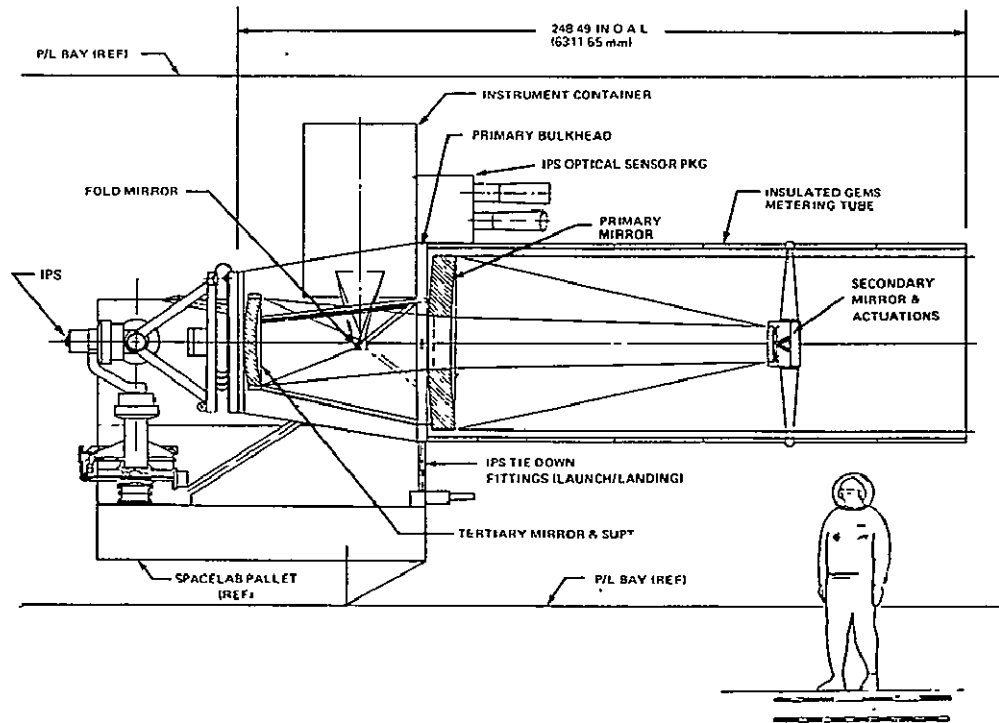
The two configurations of the three-mirror telescope under consideration are shown in (Fig 14).

The main characteristics of the four modules, including the differences between the two configurations, are summarized in Table 3.

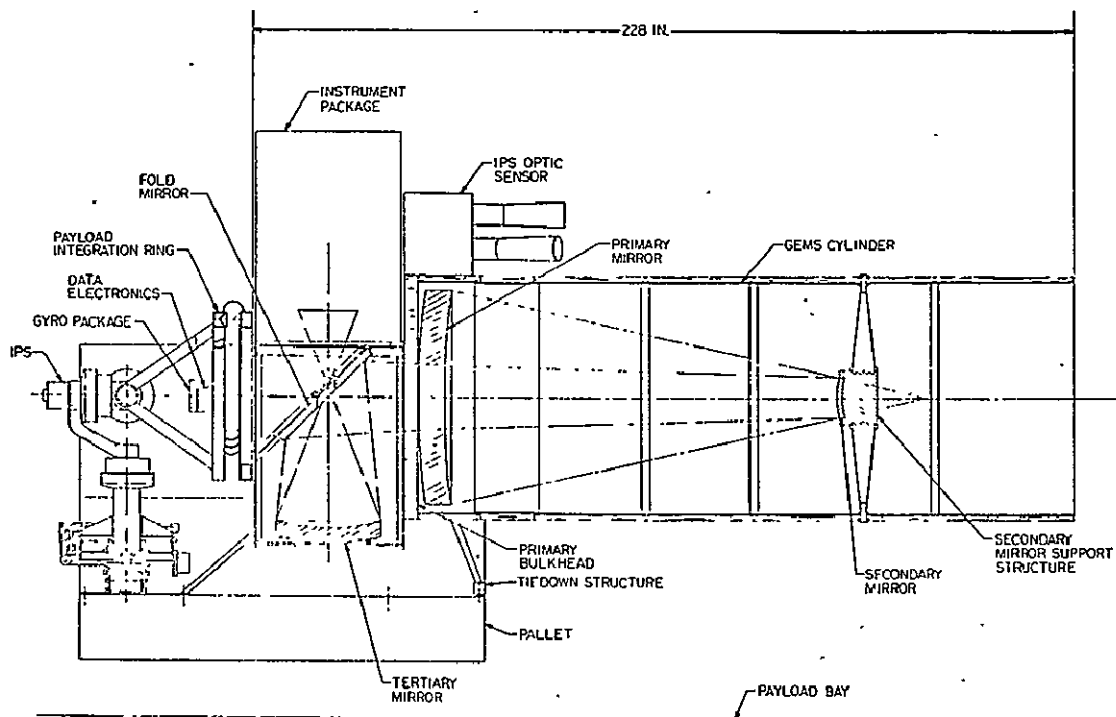
Isometric views of tertiary and instrument modules of both configurations are shown in Figure 15.

### 3.1.2 The Modified Version for a Rowland Spectrograph

The conversion of the three-mirror telescope to a two-mirror system to accommodate an ultraviolet spectrograph is easily accomplished through exchange of the tertiary module with a Rowland spectrograph module. An isometric view of the Rowland spectrograph module and a mechanical layout of the telescope with spectrograph module are shown in Figures 16 and 17.



CONFIGURATION I



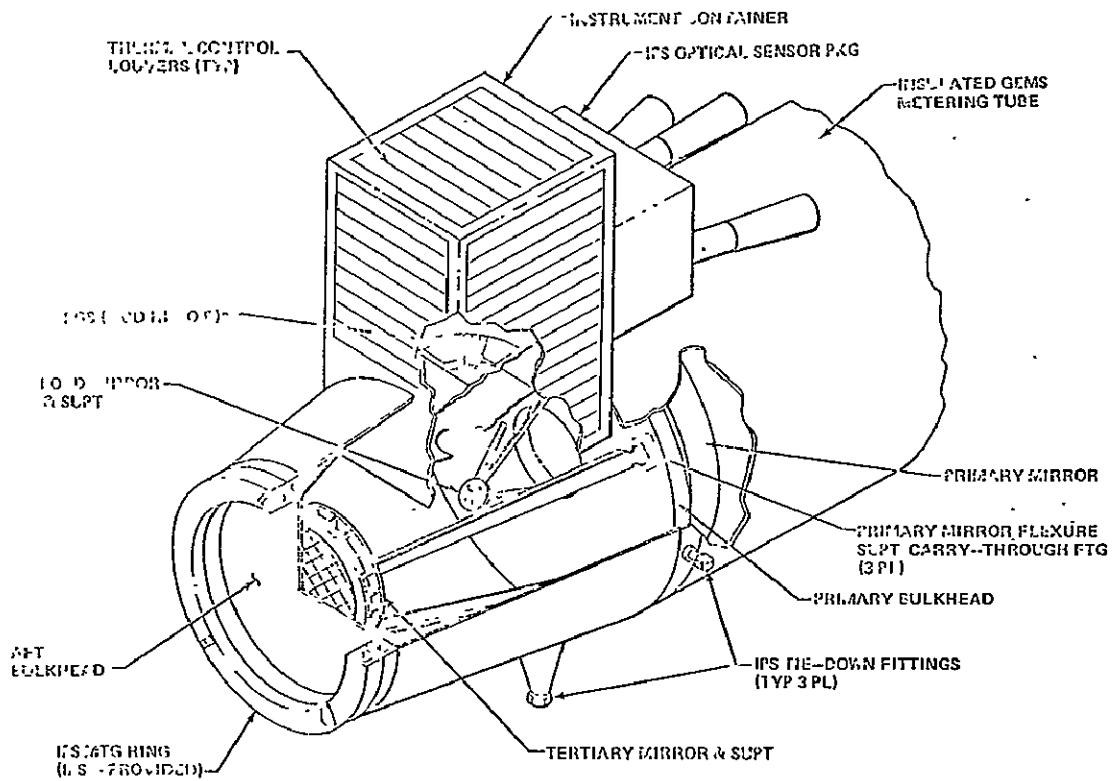
CONFIGURATION II

Figure 14. The two configurations of the three-mirror telescope.

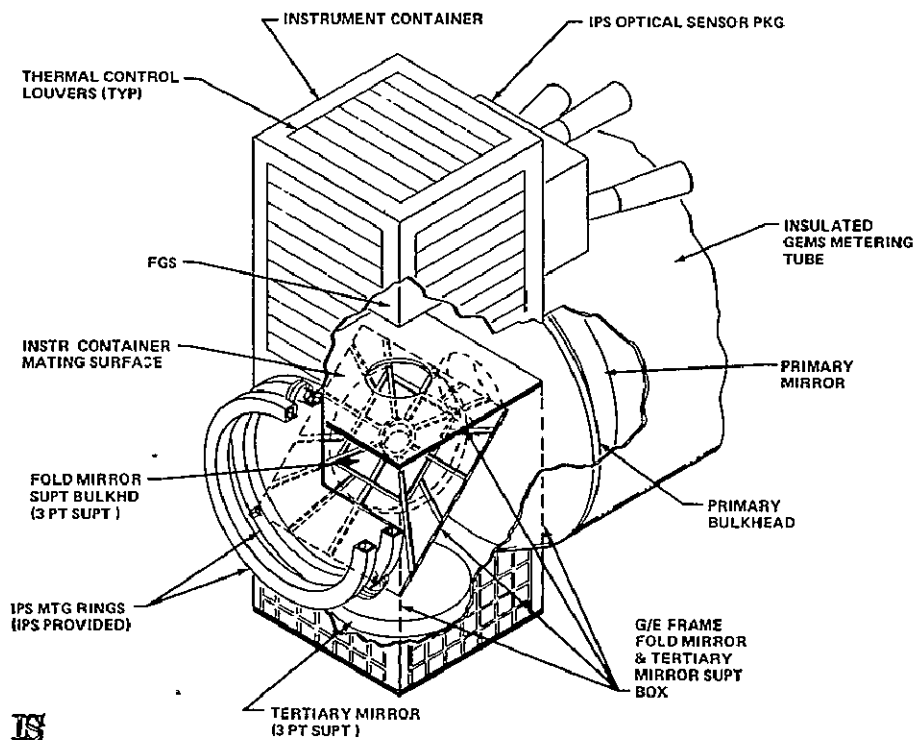
ORIGINAL PAGE IS  
OF POOR QUALITY

TABLE 3. CHARACTERISTICS OF THE FOUR MODULES

MODULE	ITEM	COMMENTS
PRIMARY MODULE	GRAPHITE-EPOXY METERING SHELL (GEMS)	ST DESIGN TEST ARTICLE -EXISTING -TESTED -NO MODIFICATION REQUIRED
	LIGHT WEIGHT ULE MIRROR	POSSIBLE USE OF EXISTING BLANK
	PRIMARY BULKHEAD AND MIRROR MOUNT FLEXURES	RESIZED ST DESIGN -HONEYCOMB CORE WITH GRAPHITE EPOXY FACING SHEETS -ALL OPTICS AND INSTRUMENTS REFERENCED TO PRIMARY BULKHEAD
SECONDARY MODULE	SECONDARY MIRROR	CONVENTIONAL MIRROR SHAPE
	GRAPHITE-EPOXY SPIDER	ST TEST ARTICLE (PROVIDED WITH GEMS)
	ALIGNMENT ACTUATORS	ST DESIGN
	ARTICULATION MECHANISM FOR IMAGE MOTION CONTROL	ST DESIGN
TERTIARY MODULE CONFIGURATION I	TERTIARY MIRROR	CONVENTIONAL MIRROR SHAPE
	FOLD MIRROR	SMALL FLAT MIRROR
	SUPPORT STRUCTURE FOR TERTIARY AND FOLD MIRROR	SUPPORTS MIRRORS OFF THE PRIMARY BULKHEAD
	AFT BULKHEAD AND ENCLOSURE	SIMPLE SYMMETRICAL STRUCTURE -MOUNTS TO PRIMARY BULKHEAD -INTERFACES WITH IPS
CONFIGURATION II	TERTIARY MIRROR	CONVENTIONAL MIRROR SHAPE
	FOLD MIRROR	LARGE PERFORATED FLAT MIRROR
	GRAPHITE-EPOXY FRAME STRUCTURE	MOUNTS TO THE PRIMARY BULKHEAD; THE TERTIARY MIRROR, FOLD MIRROR AND INSTRUMENT MODULE ARE MOUNTED TO THIS STRUCTURE -INTERFACES WITH IPS
INSTRUMENT MODULE CONFIGURATION I	INSTRUMENT MODULE	SIMPLE GRAPHITE-EPOXY AND INVAR STRUCTURE -MOUNTS TO PRIMARY BULKHEAD (FIELD SPLICE) -PROVIDES FOR RIGIDLY MOUNTING MULTIPLE INSTRUMENTS PLUS FINE GUIDANCE SENSOR
CONFIGURATION II	INSTRUMENT MODULE	SIMPLE GRAPHITE-EPOXY AND INVAR STRUCTURE -MOUNTS TO TERTIARY STRUCTURE (FIELD SPLICE) -PROVIDES FOR RIGIDLY MOUNTING MULTIPLE INSTRUMENTS PLUS FINE GUIDANCE SENSOR



CONFIGURATION I



CONFIGURATION II

ORIGINAL PAGE IS  
OF POOR QUALITY

Figure 15. Tertiary and instrument modules of configurations I and II.

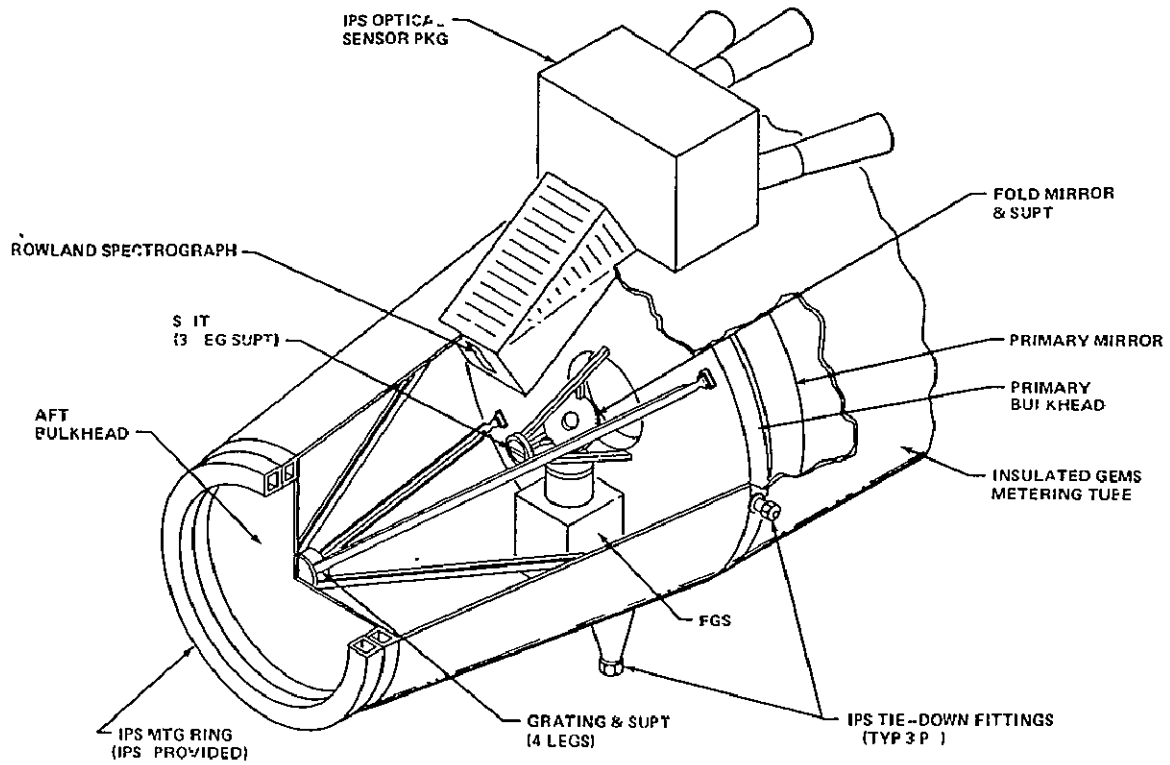


Figure 16. Rowland spectrograph module.

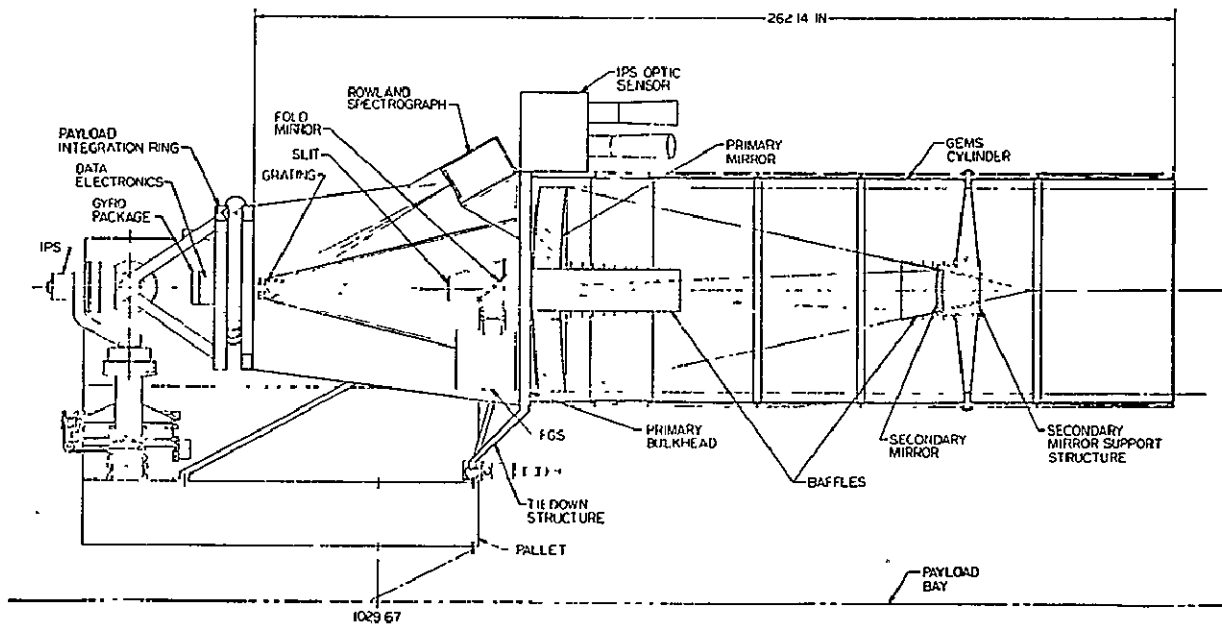


Figure 17. Rowland spectrograph configuration.

## 3.2 STRUCTURAL CONCEPT

An assessment of the requirements imposed on the telescope structure, i. e. flight loads, natural frequency to be compatible with the pointing system, and dimensional stability of the optics, was performed. Based on this assessment, it was considered necessary to evaluate only those structures providing the dimensional stability for the optics systems.

A preliminary evaluation was performed for the primary bulkhead, metering shell, primary mirror supports, secondary mirror supports, tertiary mirror supports, and the fold mirror attachment structure. Space Telescope designs were considered wherever possible and the Space Telescope graphite-epoxy metering shell (GEMS) test article (existing hardware) is proposed for the Starsat metering shell.

### 3.2.1 Requirements

The requirements for Starsat structural design are imposed by Shuttle flight loads. The critical Shuttle load is the Orbiter landing acceleration (2.8 g) in the vertical direction. The structural dimensional stability requirements for this phase of the study are as follows:

#### Primary to secondary mirror tolerances

$$\text{Despace} = \pm 2 \mu\text{m}$$

$$\text{Decenter} = \pm 50 \mu\text{m}$$

$$\text{Tilt} = \pm 50 \mu\text{rad}$$

### 3.2.2 Primary Bulkhead

The primary bulkhead consists of an aluminum honeycomb core and graphite-epoxy face sheets. An analysis of the bulkhead was not performed during this study because of the similarities to the Space Telescope design.

### 3.2.3 Metering Shell

The Starsat metering shell utilizes the existing one-half scale Space Telescope GEMS. Even though the GEMS is one-half scale, the graphite-epoxy layers are full scale. The GEMS (Fig. 18) was considered because it exists and meets the Starsat metering shell requirements.

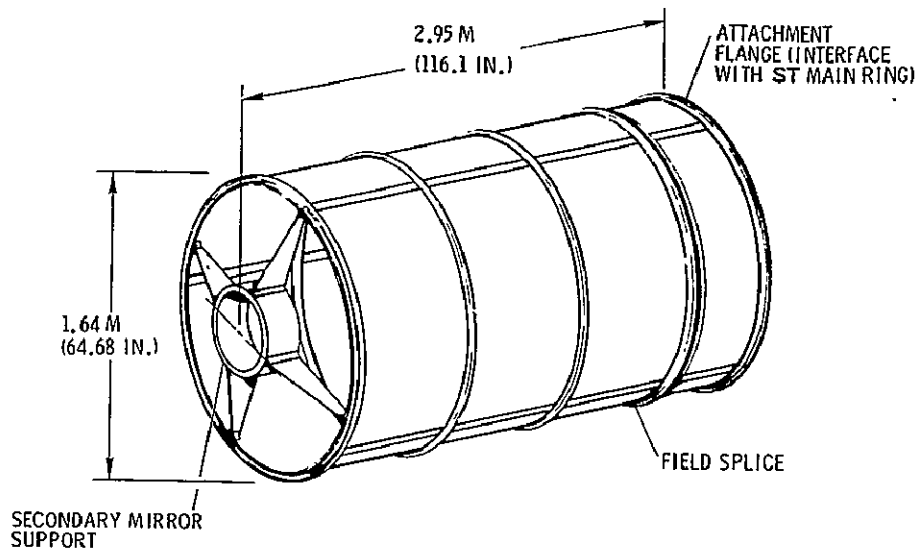


Figure 18. GEMS.

The purpose of the metering shell is to hold the alignment of the secondary mirror relative to the primary mirror. The secondary mirror is provided with an adjustment capability to correct the alignment prior to any period of observation. Following this adjustment, the metering structure must maintain the alignment within a given tolerance throughout the period of observation.

Even though the Starsat requirements are not as stringent as the GEMS, the Starsat metering shell still requires a structural material that exhibits a coefficient of thermal expansion,  $\alpha$ , close to zero. Metals were effectively ruled out in the GEMS program and should not be considered as an alternate for Starsat applications. Titanium, a low expansion metal, has an  $\alpha$  of  $7.2 \mu\text{m}/\text{m K}$ . This value would give a despace of approximately  $42 \mu\text{m}$  on the metering structure for a change of 1 K. Invar has an  $\alpha$  of  $0.54 \mu\text{m}/\text{m K}$  in the relevant temperature range, which would give a despace of approximately  $3 \mu\text{m}$  for 1 K. This is still too large for the predicted Starsat temperature range.

Static, dynamic, and thermal tests have verified that the GEMS capabilities meet or exceed Starsat requirements.



The static test performed was a 4928 N (1100 lb) side load as shown in Figure 19 which produces approximately  $6.89 \times 10^6 \text{ N/m}^2$  (1000 psi) stress levels in the structure. This is approximately the loading condition the GEMS would undergo on the Starsat. These stress levels are well below the graphite-epoxy allowable microstress level [ $6.89 \times 10^7 \text{ N/m}^2$  (10 000 psi)].

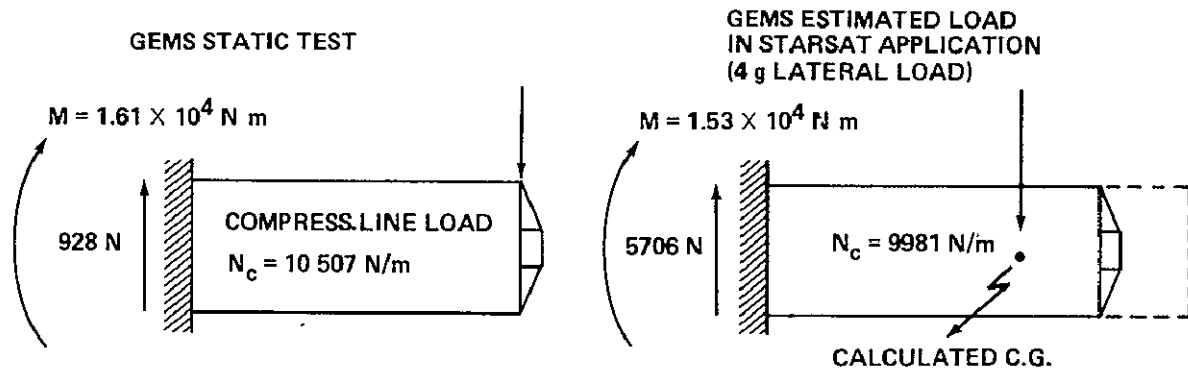


Figure 19. GEMS static test and estimated load in Starsat application.

A dynamic test was performed to determine a fixed base first mode frequency. The test showed a 38 Hz first mode natural frequency. A beam analysis of the overall Starsat configuration, using NASTRAN, shows the first mode natural frequency to be 40 Hz. The analysis and test results demonstrate that the GEMS structure is compatible with Starsat pointing requirements.

The thermal vacuum test was performed to demonstrate the dimensional stability of GEMS. The measuring was limited to despace. This is the most critical mode for Space Telescope and Starsat and is the one which can be most directly measured. The demonstrated dimensional stability of GEMS,  $1.52 \mu\text{m}$  per  $5.55^\circ\text{C}$  ( $10^\circ\text{F}$ ) approached the goal of  $1 \mu\text{m}$  per  $5.55^\circ\text{C}$  ( $10^\circ\text{F}$ ) and is lower than the  $2 \mu\text{m}$  per  $5.55^\circ\text{C}$  despace requirement for the telescope.

The GEMS structural, dynamic, and dimensional stability qualities justify its selection for use as the Starsat metering structure.

#### 3.2.4 Mirror Supports

The primary mirror supports were not considered in detail. It was assumed that, if required, the Starsat primary mirror supports would be the same or similar to the Space Telescope mirror supports. Figure 20 presents the Space Telescope support concept utilized for the Starsat.

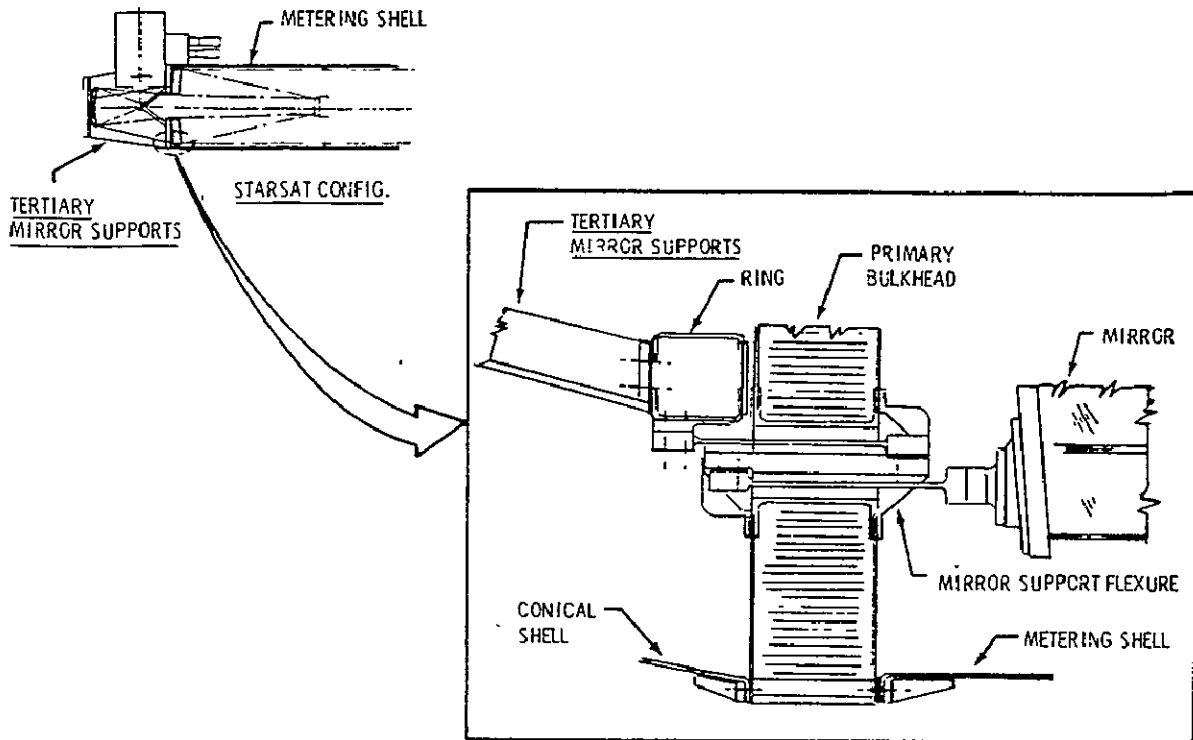


Figure 20. Primary mirror support concept.

On the Space Telescope, the flexures from the primary mirror run through the primary bulkhead and fasten on the opposite side. This allows maximum length which provides as much radial flexibility as possible.

The primary mirror mount is a dual axis Invar flexure with integral end fittings. One end fitting attaches to the primary support structure while the other fastens to an Invar pod which, in turn, is bonded to the mirror back plate through a polyurethane sheet.

Since the Starsat requirements are not as stringent as the requirements of Space Telescope, a simpler approach may be found. Further studies should address this area.

The secondary mirror is supported by four spider beams to the GEMS as shown in Figure 18. The spider beam is a one-half scale of the Space Telescope spider and, unlike the shell, the graphite-epoxy layers are half scale. The mirror is supported to the hub of the spider and has the capability to be articulated.

The test result showed that the spider withstands the static loads [806 N (180 lb) longitudinal]; however, the thermal test showed that the spider with the forward ring moves much more than predicted ( $0.24 \mu\text{m}$ ), but is well within the overall Starsat requirements.

In addition to supporting the mirror, the tertiary mirror supports must maintain the alignment of the tertiary mirror with respect to the secondary mirror. The tertiary mirror support, together with the GEMS, is considered metering structure.

The struts are attached to the mirror and the bulkhead at the same location as the primary mirror supports (Fig. 20). Graphite-epoxy was selected as the material for these supports. There are other materials that could possibly be utilized but do not have the strength and advantages offered by the low  $\alpha$  graphite-epoxy. These struts require a cross sectional area of approximately  $13 \text{ cm}^2$  and weigh 18 kg (40 lb).

The fold mirror attachments are four graphite-epoxy members attaching the fold mirror to the primary bulkhead. Graphite-epoxy was the material assumed for the fold mirror supports. These members have not been sized; however, there appears to be no structural problem with the mirror support.

#### 4. POINTING AND STABILIZATION

To achieve the desired pointing accuracy and stability, two control systems are used. Coarse control of the line of sight (LOS) is performed by the instrument pointing system (IPS) as supplied for the Spacelab program by the European Space Agency (ESA). This system also provides the only control about the telescope roll axis. Fine control of the LOS employs image motion compensation (IMC) with an articulation mechanism on the secondary mirror. This mechanism receives signals derived from the fine guidance sensor (FGS).

##### 4.1 COARSE POINTING

Coarse pointing of the Starsat system is performed by the IPS. The requirements and goals of the IPS are shown in Figure 21 and Table 4. Figure 21 defines the terminology used for the errors. Bias is the offset error from the target while stability is the movement about the offset point. The best case of  $1.6 \mu\text{rad}$  (0.33 arc s), 1 sigma, as a goal for quiescent stability error provided by the IPS is still inadequate for the fine pointing required; therefore, IMC is needed.

$$\text{POINTING ACCURACY} = \text{BIAS} + \text{STABILITY ERROR}$$

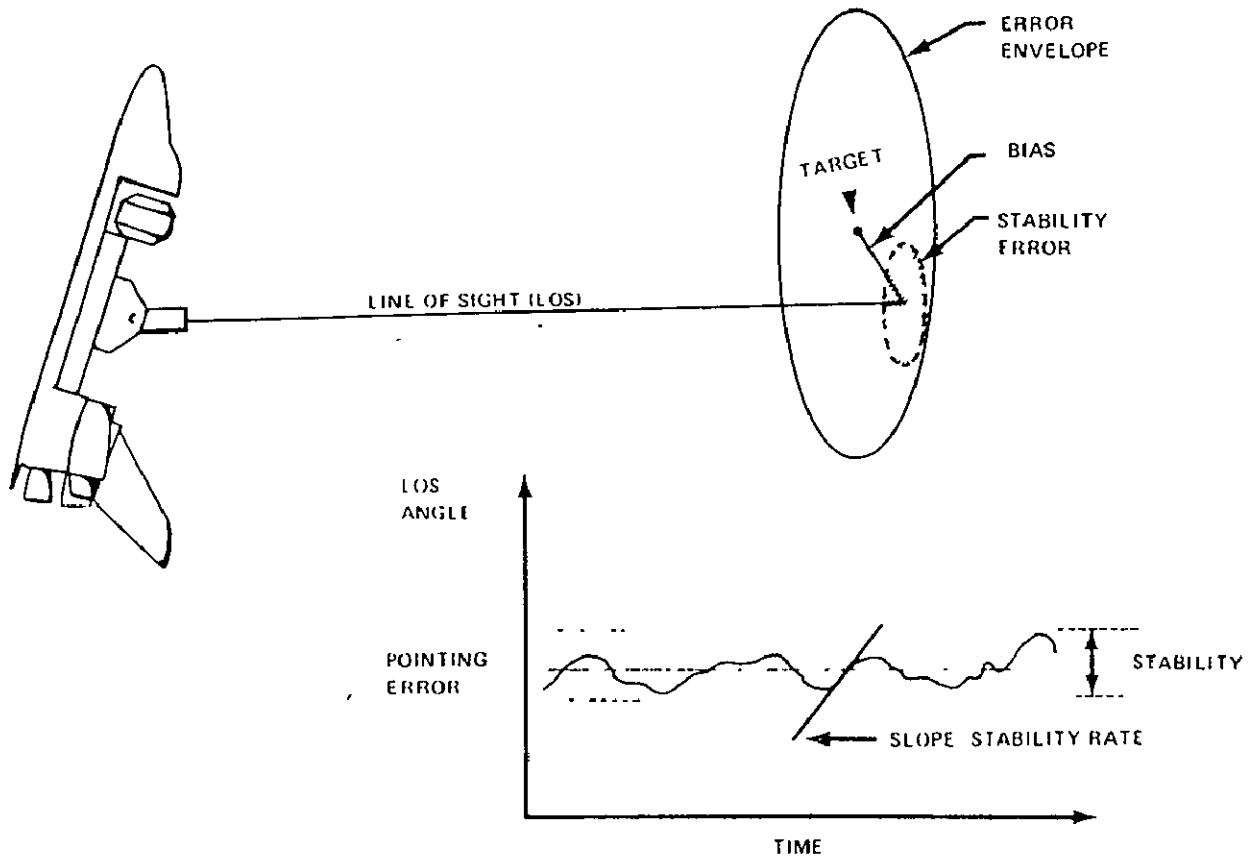


Figure 21. Error definitions.

Roll bias and stability errors contribute to image bias and stability errors in the focal plane. Assuming a  $0.013 \text{ rad}$  ( $45 \text{ arc min}$ ) maximum radius at the focal plane image and the errors given in Table 4, a bias error in LOS of  $1.0 \mu\text{rad}$  ( $0.2 \text{ arc s}$ ) is obtained if the goal of  $73 \mu\text{rad}$  ( $15 \text{ arc s}$ ) is achieved in the roll axis. Using the roll quiescent stability error of  $7.8 \mu\text{rad}$  ( $1.6 \text{ arc s}$ ) produces a stability error at the edge of the field of  $1.0 \mu\text{rad}$  ( $0.021 \text{ arc s}$ ). This type of error will be present in any telescope system using such a wide field for imaging. The magnitudes may be minimized by causing the roll of the IPS to occur about the center of one of the scientific instrument imaging fields; thereby, the stability contribution from roll is reduced to  $34 \text{ nrad}$  ( $0.007 \text{ arc s}$ ) in a particular field of  $0.5^\circ$  diameter if the IPS goal of  $7.8 \mu\text{rad}$  ( $1.6 \text{ arc s}$ ) is achieved.

TABLE 4. SPACELAB INSTRUMENT POINTING SYSTEM

PERFORMANCE REQUIREMENTS & GOALS	REQUIREMENTS	GOALS
<b><u>BIAS ERROR.</u></b>		
LOS	2 arc s	0.75 arc s 1 $\sigma$
ROLL	40 arc s	15 arc s 1 $\sigma$
<b><u>QUIESCENT STAB ERROR</u></b>		
LOS	1 arc s	0.33 arc s 1 $\sigma$
ROLL	3 arc s	1.6 arc s 1 $\sigma$
<b><u>MAN MOTION DIST. ERROR</u></b>		
LOS	3 arc s	1 arc s PEAK
ROLL	10 arc s	4 arc s PEAK
<b><u>STABILITY RATE</u></b>		
	2 arc min/s	
<b><u>POINTING RANGE</u></b>		
LOS	$\pi$ ster	
ROLL	$\pi$ rad	
<b><u>MAX. SLEWING RATE</u></b>		
	2.5 deg/s	
IPS REQUIREMENTS	DESIGN CASE	RANGE
DIAMETER	2 m	UP TO 3 m
LENGTH	4 m	ORBITER OR PALLET LIMITED
MASS	2000 kg	3000 kg (IPS) 5000 kg (PALLET)

4.2 FINE POINTING

Improvements to LOS pointing and stability may be made by controlled deflection of the optical path. An articulation mechanism at the secondary mirror provides the deflection of the light path to achieve the required stability at the focal plane. An FGS, located in the f/12 focal plane, provides

the signals for the secondary mirror. The experiment computer is used in the control loop to provide coordinate transformations, mode control, commands, and other interface functions. A block diagram of the pointing control is shown in Figure 22. Spacelab equipment (shown by dashed lines of Figure 22) will be used in coarse and fine control loops. The secondary mirror IMC and FGS together with the remote acquisition unit (RAU) and the computer constitute the fine pointing loop. The coarse loop is the IPS system.

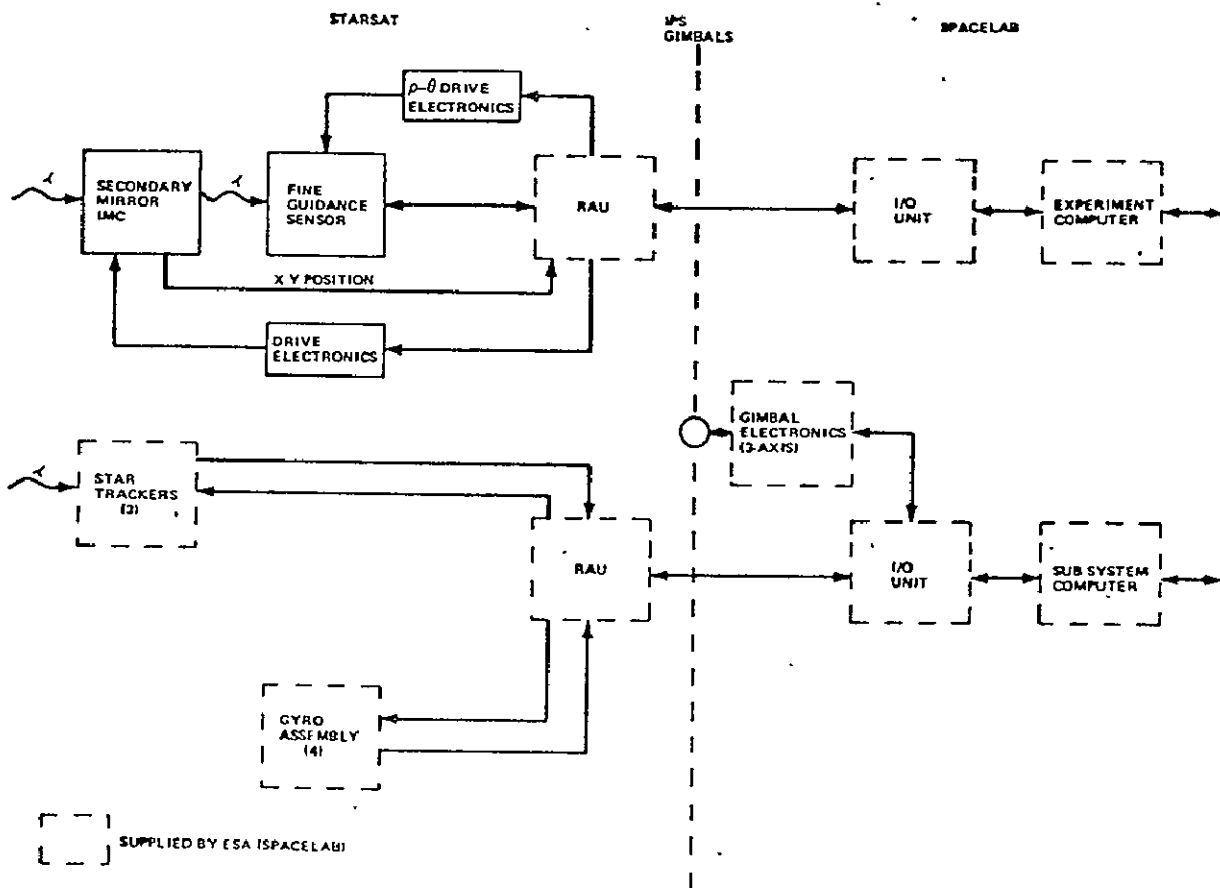
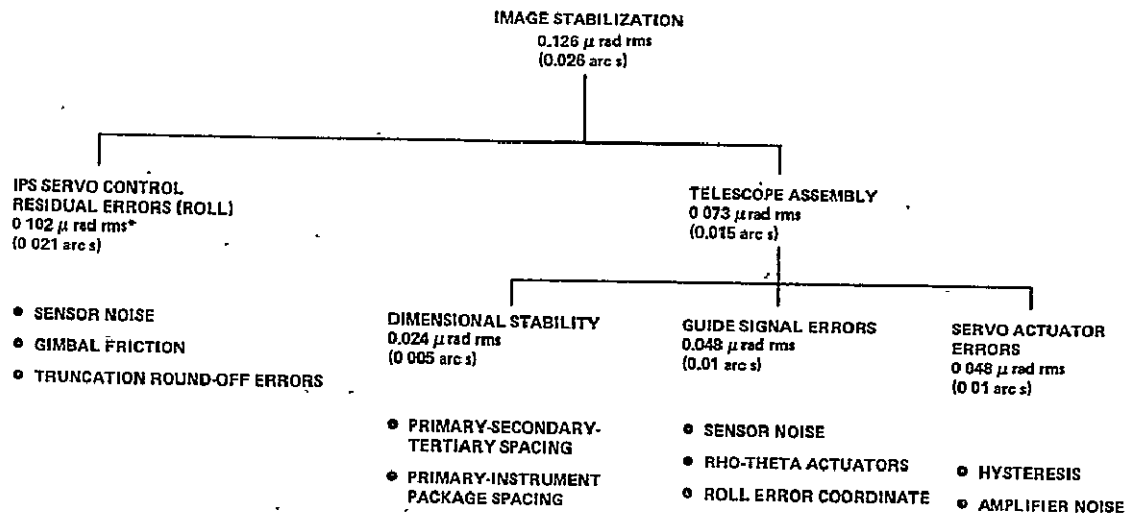


Figure 22. Pointing control block diagram.

A breakdown of the error sources for image stabilization is shown in Figure 23. The major source appears to be in the roll control of the IPS system. This is for the worst case, i.e., when the target is located 45 arc min off axis. In most applications this will not occur, but even so a stability of  $0.126 \mu\text{rad}$  (0.026 arc s) is within the desired constraints.



\*BASED ON ESA IPS ROLL STABILITY GOAL WITH TARGET 45 arc min OFF-AXIS.

Figure 23. Image stabilization.

A typical sequence for use of the Starsat is shown in Figure 24. The crew must activate the system and may follow through the entire operation manually or, if so desired, may allow the computer to control the sequence. Operation of the IPS will be determined by ESA and NASA working groups.

#### 4.3 FINE GUIDANCE SENSOR

Various means of determining guide star positions were investigated. To achieve the desired pointing accuracy and stability in the most economical way, existing sensors or sensors already under development were considered. Following are the potential candidates selected:

- HEAO-B star tracker mounted on a transport mechanism
- Charge coupled device (CCD)
- Multiaperture image dissector.
- Perkin-Elmer Space Telescope FGS.

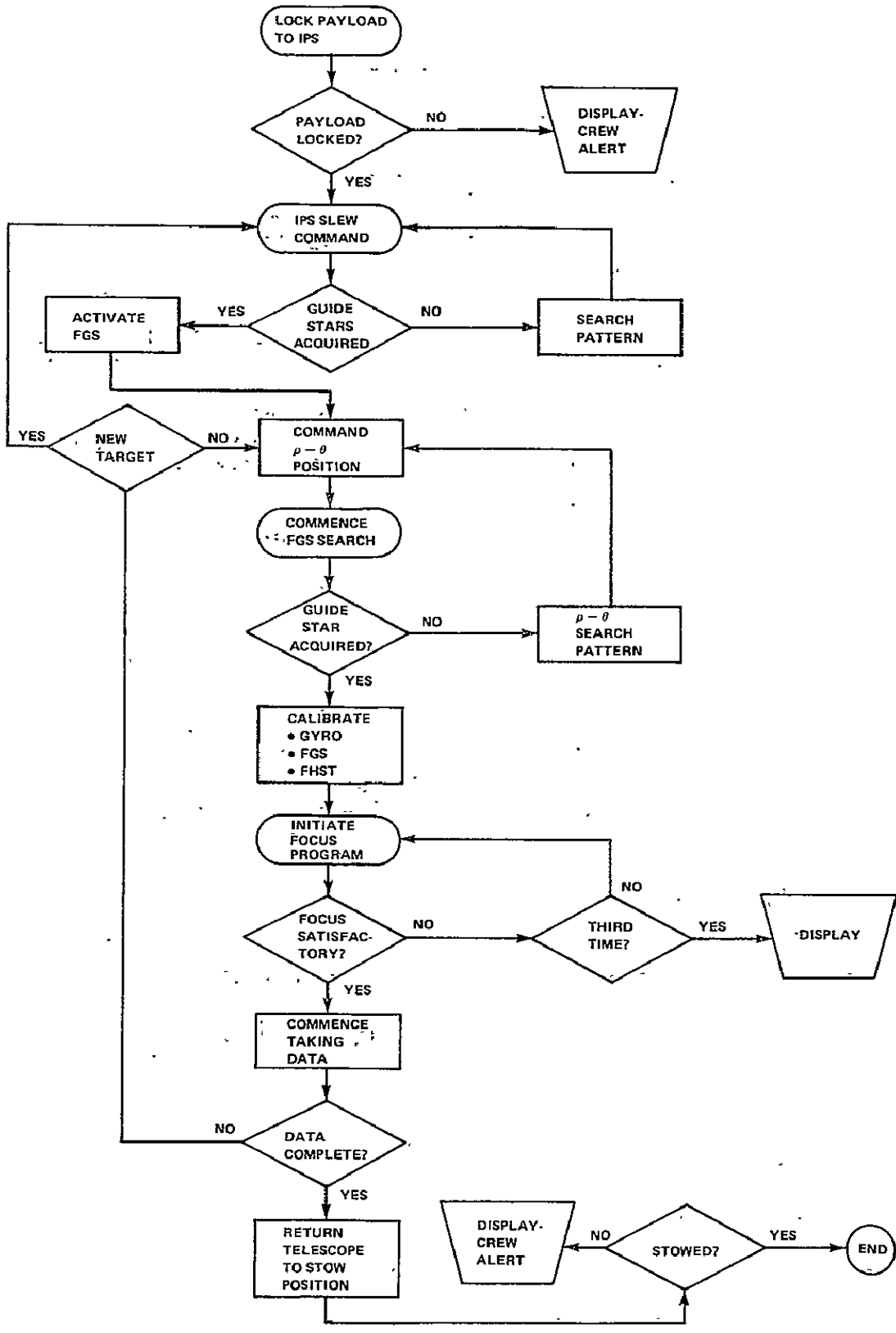


Figure 24. Starsat -- sequence flow diagram.



These systems are discussed in detail in the following sections. A system developed by Itek for Space Telescope is incompatible with the anastigmatic focal plane of Starsat and was therefore eliminated as a candidate. The moving mechanism, however, developed for this system can be used in combination with the HEAO-B star tracker.

#### 4.3.1 HEAO-B Star Tracker System

This system was selected as the baseline system. A transport mechanism mated to the HEAO-B star tracker (without optics) produces a simple, efficient system that will meet all the design goals of the guidance sensor. Two systems were considered for the transport mechanism. One system was designed by Itek to move the image dissector tube in their FGS (Fig. 25). Another very simple system was proposed by Martin-Marietta Corporation for the Space Telescope FGS as a possible cost reduction item designed to use the HEAO-B star tracker. If the design is developed for Space Telescope, it would be a simple matter to use it on Starsat (Fig. 26).

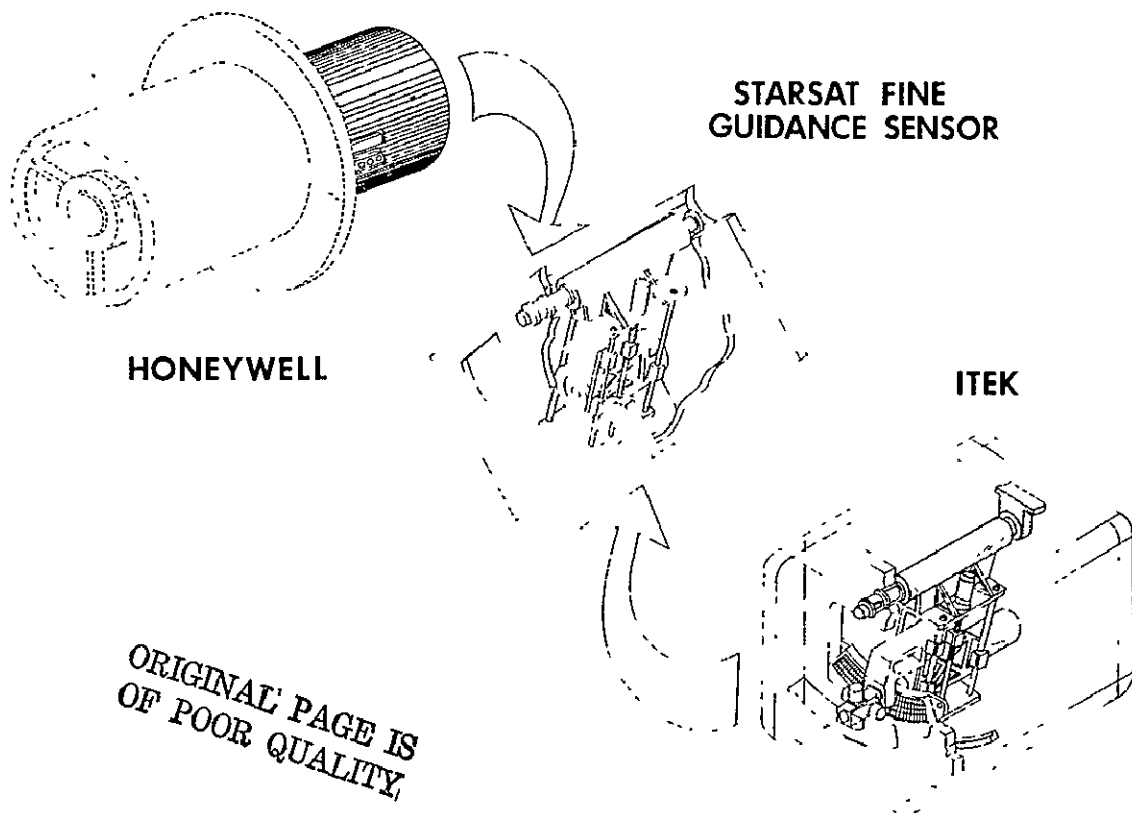


Figure 25. Starsat fine guidance sensor.

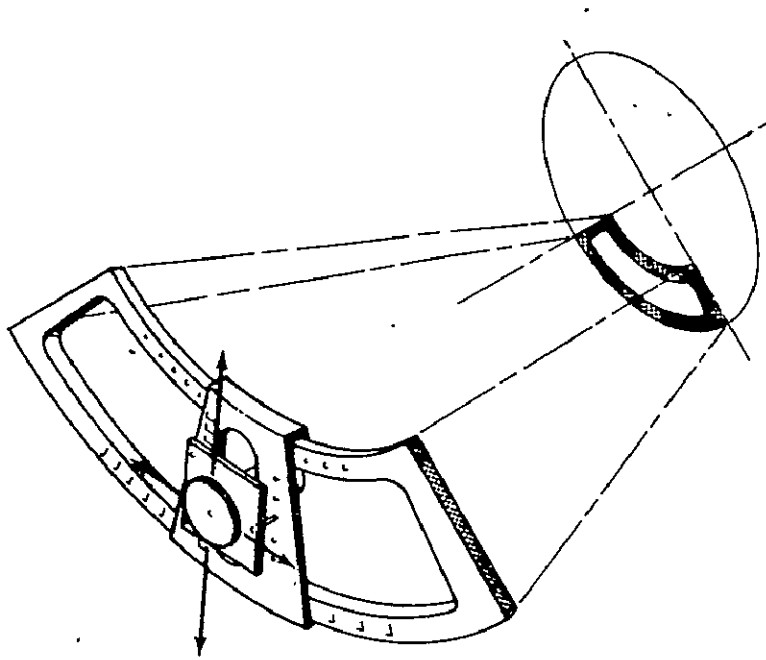


Figure 26. Martin Marietta drive mechanism.

Using only the rho-theta drive mechanism with the performance characteristics given in Reference 13, the guide field of Figure 27 is obtained. The tolerance on the repeatability of the  $\theta$  axis ( $60^\circ$  maximum in Figure 27) is  $\pm 194 \mu\text{rad}$  (40 arc s) which is equivalent to  $\pm 2.3 \mu\text{rad}$  (0.47 arc s) bias error at the edge of the focal plane. A lateral tolerance of  $\pm 0.05 \text{ mm}$  produces a  $\pm 2.8 \mu\text{rad}$  (0.57 arc s) error in the focal plane. An overall RSS value of  $\pm 3.6 \mu\text{rad}$  (0.74 arc s) is obtained for the bias error.

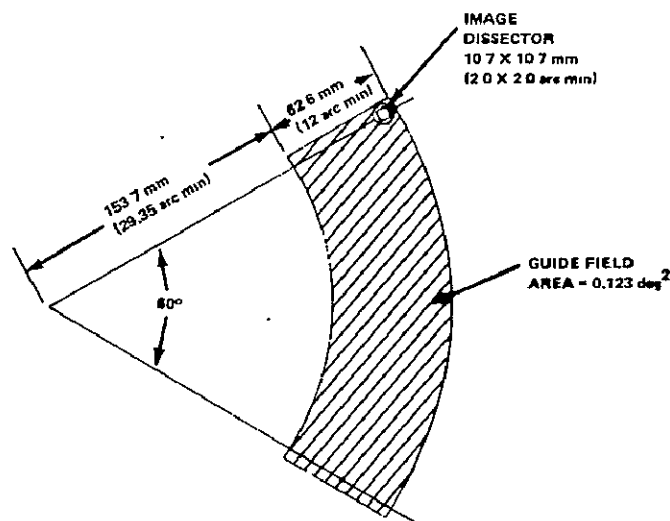


Figure 27. Guide sensor field.

The tilt tolerance on the rho-theta mechanism is listed as  $73 \mu\text{rad}$  (15 arc s) by Itek. This corresponds to a defocus of  $0.46 \mu\text{m}$ , a negligible value.

The HEAO-B aspect sensor, as described in References 14 and 15, consists of an image dissector tube (ITT F4012RP) with an S-20 photocathode. This type tube has been used in a number of star tracker programs and has been proven in space applications. Some of the characteristics of this tube are high resolution, high quantum efficiency, high transient response (nonstorage), low dark current, wide dynamic range, low power requirements, rugged construction, and electron counting capability. More detailed specifications of the tube are given in Reference 16.

Table 5 presents some of the pertinent information on the HEAO-B aspect sensor. It has two modes of operation — search and track. The search mode is a raster scan with 64 dwell points on each of the 64 lines for 4096 total elements. Figure 28 shows the search pattern, and a block diagram is shown in Figure 29. For a total scan area of  $580 \times 580 \mu\text{rad}$  ( $2 \times 2$  arc min), the

TABLE 5. FINE GUIDANCE SENSOR CHARACTERISTICS  
(HEAO-B STAR TRACKER)

	<u>LINEAR</u>	<u>ANGULAR</u>
SENSOR FIELD OF VIEW (AREA)	12,125 mm <sup>2</sup>	0.123 degree <sup>2</sup>
IMAGE DISSECTOR SCAN AREA	10.7 X 10.7 mm	2.0 X 2.0 arc min
IMAGE DISSECTOR APERTURE	0.2 X 0.2 mm	2.3 X 2.3 arc s
PROBABILITY OF ACQUIRING GUIDE STAR	95%	
MINIMUM STELLAR MAGNITUDE REQUIRED	12.5	
EFFECTIVE COLLECTING AREA-TELESCOPE	15,550 cm <sup>2</sup>	
PHOTOELECTRON COUNTING RATE	15,080 Phot. Electr./s	
SEARCH MODE		
SEARCH PATTERN	64 X 64 ELEMENT RASTER SCAN	
NUMBER OF DWELLS	4096	
DWELL TIME FOR DETECTION	2.0 ms	
SEARCH TIME	8.19 s	
TRACK MODE		
SPOT SIZE	0.3 arc s	
IDT RESOLUTION	0.1 arc s	
BANDWIDTH	5 Hz	
NOISE EQUIVALENT ANGLE	0.01 arc s	

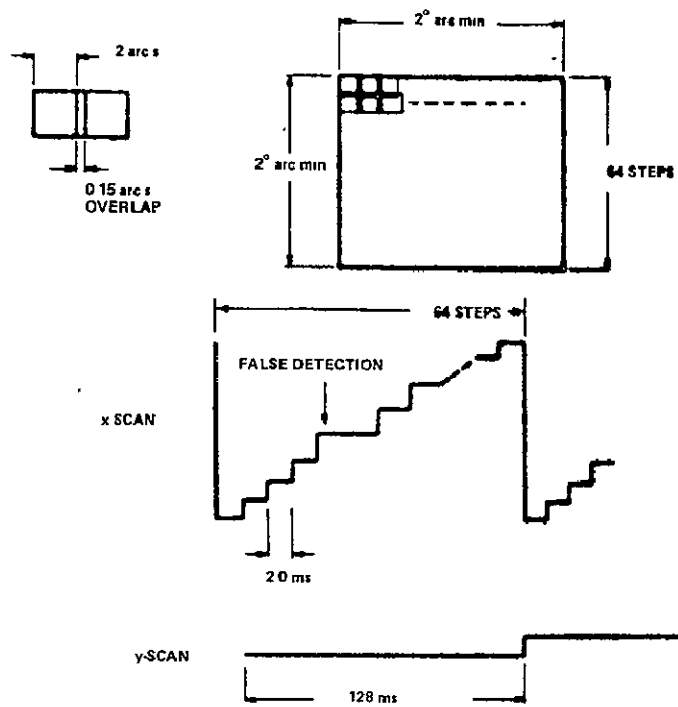


Figure 28. Search scan pattern.

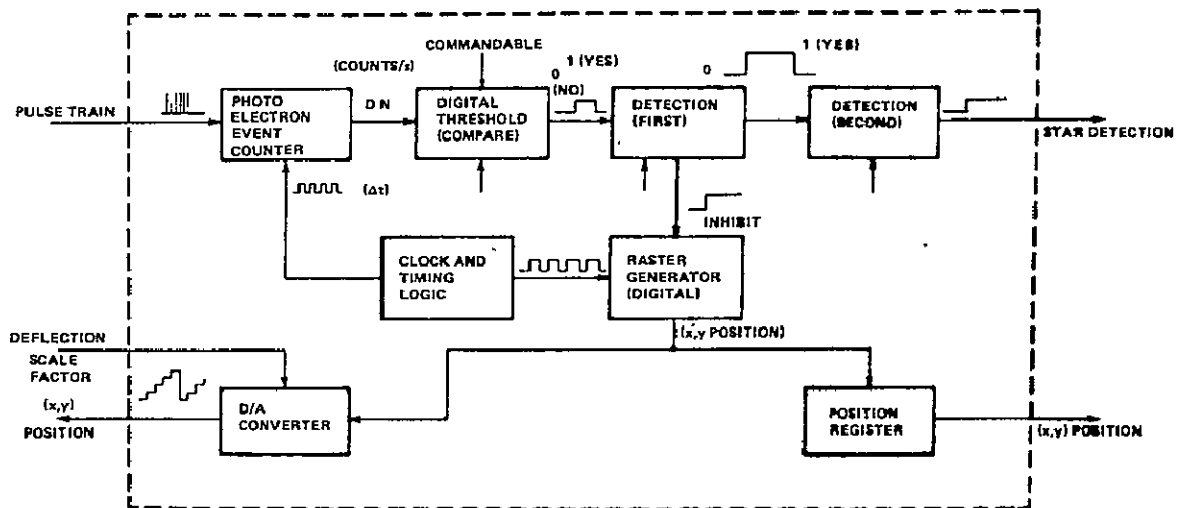


Figure 29. Acquisition mode (first guide star detection).

probability of acquiring a guide star is quite high. The IPS system is capable of pointing the telescope to within  $97 \mu\text{rad}$  (20 arc s), 1 sigma, if the pointing system requirements are used. Including some shifts in the telescope during launch, the guide star should be within the  $\pm 290 \mu\text{rad}$  (1 arc min) circle.

The probability of a star being within the total field of 0.123 square degrees is based on Poisson statistics. The probability of having  $k$  stars in the field is obtained from equation (5):

$$P_k = \left( \frac{m^k}{k!} \right) e^{-m} \quad (5)$$

where  $m = aT$  is the average number of events during the interval  $T$ . The probability of finding one or more stars in the field is  $P = 1 - P_0$ . For  $P = 0.95$  probability of acquiring one star, one obtains  $m = 3$  or in the area of 0.123 square degrees a star density of 24.39 stars per square degree is required.

A number of sources are available to determine star distribution [17,18]. The minimum stellar magnitude for the previously mentioned conditions is given to be  $m_v = 12.5$  for Mt. Wilson [17] and  $m_v = 12.1$  for Allen [18]. Using the fainter star of 12.5 visual magnitude, 15 080 photoelectrons/s are generated at the image dissector aperture based on a G2V star and the Forbes and Mitchell data of Reference 19. Assuming 30 events for 0.96 probability of detection, the dwell time at each element of the photocathode is 2.0 ms for a total scan time of 8.19 s.

Once the photoelectron count equals or exceeds the threshold level of 19 events, the sensor will automatically switch to the track mode. Figure 30 gives the track mode modulation pattern and the drive signals required on the deflection coil to obtain that pattern.

Reference 15 provides the details of the track mode. Basically the four dwell points are scanned sequentially and the photoelectrons counted during each dwell interval. At the end of a modulation cycle when all four positions are sampled, the unbalance or error count of the cycle is computed. For the X axis the normalized error count:

$$E_j(\xi, \eta) = \frac{C_{j1}(\xi, \eta) + C_{j4}(\xi, \eta) - C_{j2}(\xi, \eta) - C_{j3}(\xi, \eta)}{\sum_{i=1}^4 C_{ji}(\xi, \eta)} \quad (6)$$

where

$\xi, \eta$  = the distance between the image centroid and the modulation centroid in X, Y axis.

$E_j(\xi, \eta)$  = the error count of the jth modulation cycle as functions of  $\xi$  and  $\eta$ .

$C_{ji}(\xi, \eta)$  = sampled counts corresponding to the four phases of the jth modulation cycle.

The error count  $E_j(\xi, \eta)$  will be used to establish the displacement error.

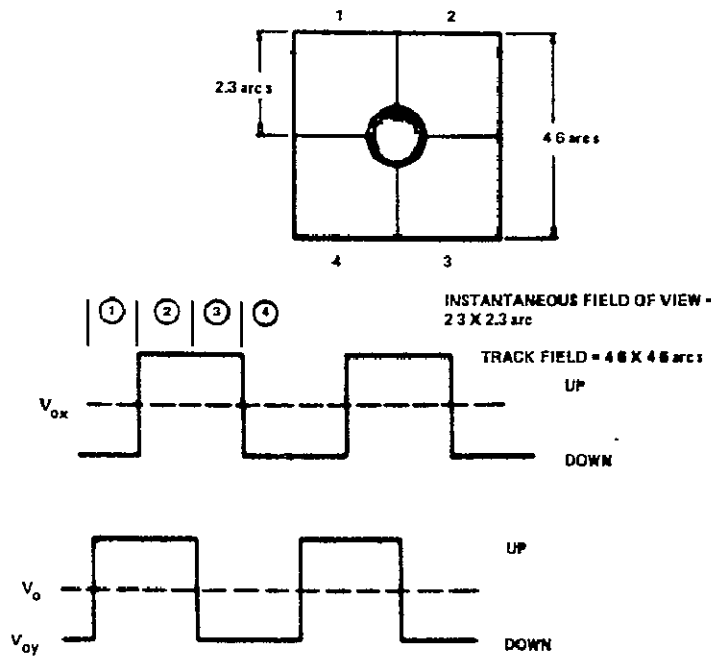


Figure 30. Modulation pattern and driving signal.

For the Starsat system the noise equivalent angle (NEA) of the FGS is the principal contributor to the instability of the image plane. At a minimum stellar magnitude of 12.5, the total photoelectron arrival rate of 15 080 photoelectrons/s is quite high for this sensor and produces a high signal-to-noise ratio. NEA may be approximated using the computations of the signal-to-noise ratio and the error angle transfer curve. A typical curve is shown in Figure 31.

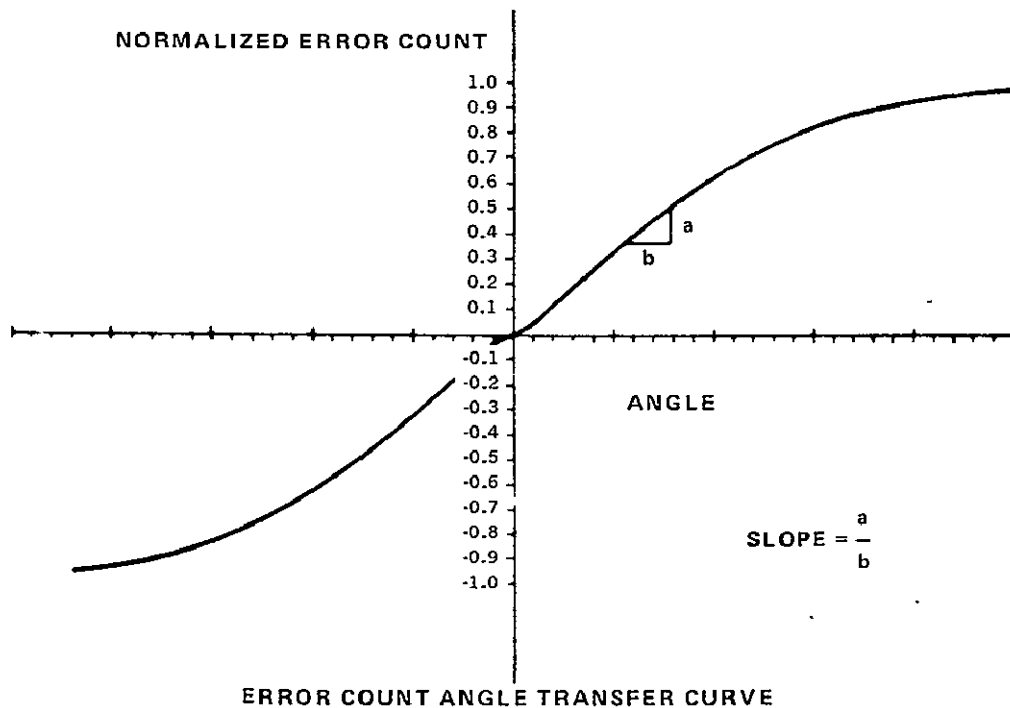


Figure 31. Error count angle transfer curve.

The modulation method shown in Figure 30 has a 25 percent duty cycle. Therefore, the signal count for each dwell is

$$S = R_s \tau \tag{7}$$

where  $R_s$  = signal emission rate and  $\tau$  = dwell time.

The noise is the statistical fluctuation of the signal, uniform background and dark emission, and is given by

$$N = \sqrt{(4R_b + 4R_d + R_s) \tau} \quad (8)$$

where  $R_b$  = background emission rate and  $R_d$  = dark emission rate. The signal-to-noise ratio is

$$\left(\frac{S}{N}\right)_{4\tau} = \frac{R_s \sqrt{\tau}}{\sqrt{4R_b + 4R_d + R_s}} \quad (9)$$

If the signal is demodulated for  $N$  cycles, the signal-to-noise ratio is

$$\left(\frac{S}{N}\right)_{T'} = \frac{R_s \sqrt{T'}}{2\sqrt{(4R_b + 4R_d + R_s) N}} \quad (10)$$

where  $T'$  = modulation cycle time and  $N = T'/4\tau$  number of cycles.

The slope of the transfer function is dependent on the image spot size and the image dissector resolution which are  $1.5 \mu\text{rad}$  ( $0.3 \text{ arc s}$ ) and  $0.48 \mu\text{rad}$  ( $0.1 \text{ arc s}$ ), respectively. For a 5 Hz bandwidth of the tracker and the previously mentioned condition, the approximation for NEA is  $48 \text{ nrad}$  ( $0.01 \text{ arc s}$ ).

This sensor may also be used as a focus sensor. A modification may be made to the square scan of the track mode which will allow for a cruciform scan as shown in Figure 32. By minimizing the time,  $t_2 - t_1$ , a best focus may be obtained. Since astigmatism and coma are not present in the Starsat design, this scheme is possible. If the spot size were not nearly circular, a best focus would be most difficult to obtain.



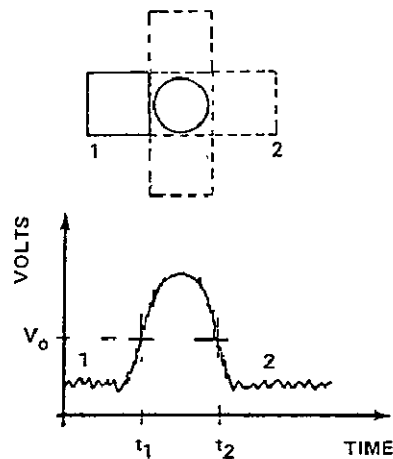


Figure 32. Focus sensor scan.

#### 4.3.2 Charge Coupled Device (CCD)

In recent years CCD's have made great progress as image sensors. The Jet Propulsion Laboratory (JPL) has done extensive work in the area of star tracking with CCD's. At the present time JPL is investigating the possibility of using multiple CCD's in the guide field of the Space Telescope to perform the fine guidance. This study is not complete at this time but does look promising. Since the pointing and stability requirements of Starsat are less stringent than Space Telescope, it seems likely that if the JPL study is favorable for Space Telescope it would also be favorable for Starsat.

The number of CCD's required in the focal plane to adequately obtain a guide star are of major concern in the CCD sensor considerations. For 95 percent probability of acquiring a star, the guide field area of the HEAO-B system would be required for 12.5 magnitude or brighter stars. JPL presently envisions six CCD chips with a field lens to effectively change the focal ratio of the system. Using the same approach for Starsat and a focal ratio of 6 for the optical system, six CCD's would produce a field of view area of 0.024 square degree — considerably smaller than the 0.123 square degree of the HEAO-B sensor.

To obtain 95 percent probability of acquisition at the galactic poles, the system would require 14.7 visual magnitude or brighter stars. Further study will be required to predict the NEA with this magnitude star. The CCD

is a storage device and does not operate on a 25 percent duty cycle as the HEAO-B sensor. Also, the spectral response of the silicon is much broader than the S-20. These advantages will probably allow the CCD to obtain the stability required of Starsat.

JPL has developed a means of interpolating the stellar coordinates within the CCD. Present technology limits the minimum size of the CCD elements to approximately 25  $\mu\text{m}$ . A spot size of 0.3 arc s at f/6 represents 13  $\mu\text{m}$ . By defocusing the spot and interpolating over four elements, JPL predicts interpolation ratios as small as 1/100th of an element width. This would make the CCD attractive for Starsat, if the cost is competitive with the other systems.

#### 4.3.3 Multiaperture Image Dissector

A study was made by ITT Gilfillan in conjunction with ITT Electro-Optical Products Division on the feasibility of using a large area precision tracking detector with diffraction-limited telescopes. This study, performed under contract NAS8-20629, was to determine the performance and configuration of such a detector. The final report of that study [20] states that such a device appears realizable within the current state-of-the-art, to the extent of work performed.

The study was made from the analytical point of view with respect to Space Telescope performance objectives. A possible application must be considered. Magnetic shielding and the ability to minimize magnetic field errors within the tube would require further investigation on Starsat.

The detector proposed by ITT is an image dissector with a 15 cm diameter photocathode. Instead of one aperture and dynode chain as in conventional image dissectors, the proposed detector has an array of apertures and dynodes — either a  $4 \times 4$  array with 16 output signals or a  $5 \times 5$  array with 25 output signals.

A 15 cm photocathode in the Starsat system represents a total field of view of 0.18 square degree if the total cathode is used. Assuming approximately 70 percent of the cathode is useful, the field of view area is equal to that of the HEAO-B system described in Section 4.3.1. If the potential magnetic shielding problem is solved, the performance should equal or exceed that of the HEAO-B tracker system as presented.

The multiaperture image dissector requires further development and for that reason appears to be too expensive for Starsat. Assuming the tube may be developed for other programs and the shielding problem is solved, this detector would be acceptable.

#### 4.3.4 Perkin-Elmer Space Telescope FGS

Perkin-Elmer has developed an FGS for the Space Telescope. This sensor is described in Reference 21. Although the Space Telescope is somewhat different, slight modifications to the sensor system make it compatible with the Starsat system.

A schematic of this sensor, shown in Figure 33, is taken from Reference 21 and shows the coarse and fine error signals available from the sensor. In the acquisition mode of operation, the acquisition mirror deflects the guide star onto a field lens which focuses the star image on an image dissector tube. The image dissector tube locks on the star and provides error signals to drive the star to the center of the acquisition mirror, where it passes through the

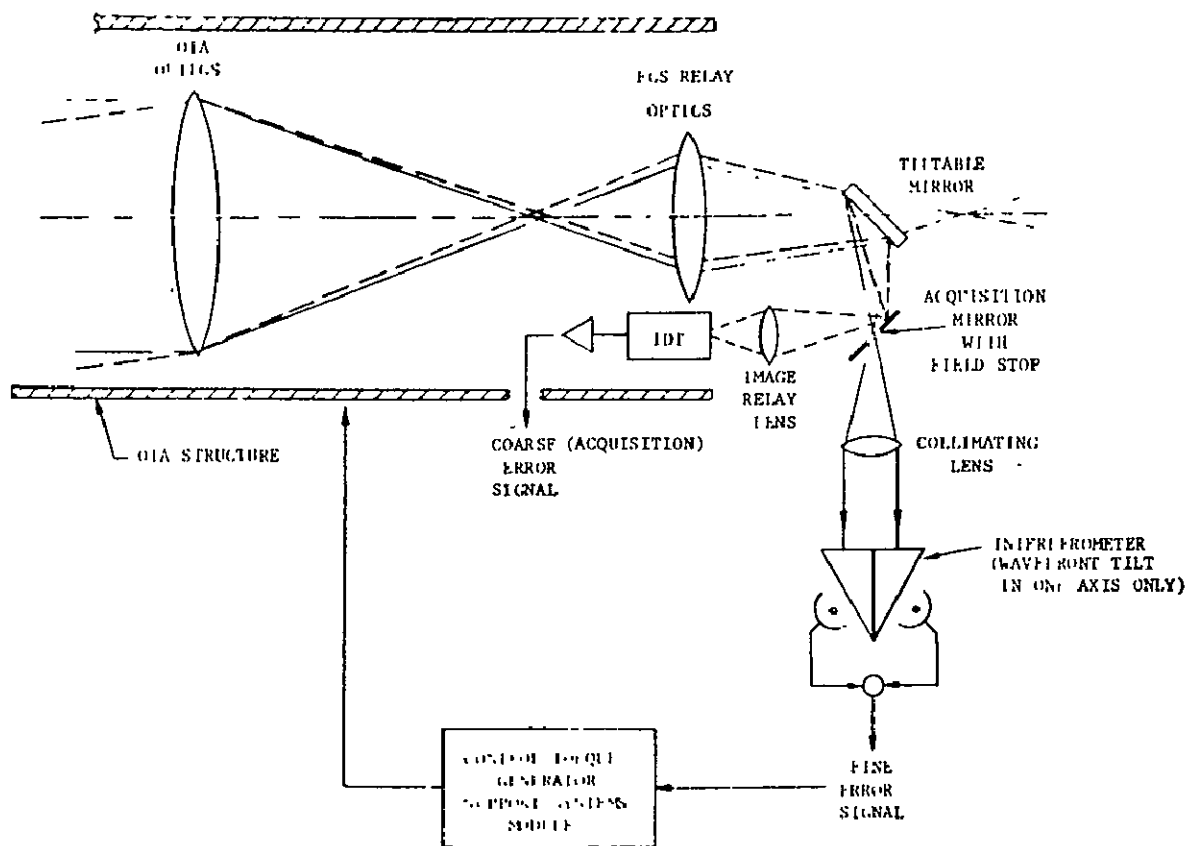


Figure 33. Perkin-Elmer Space Telescope FGS schematic.

ORIGINAL PAGE IS  
OF POOR QUALITY

hole and enters the interferometer through a collimating lens. The interferometer is a two-axis device producing an extremely accurate error output based on the interference fringe pattern. Wave front tilt is detected by four photomultiplier tubes in a photon counting mode.

To adapt this sensor to Starsat, the relay optics must be replaced with optics compatible with the f/12 Starsat system. In Space Telescope, the relay optics correct field curvature and astigmatism. Starsat with its flat focal plane will require simpler relay optics.

The Space Telescope FGS is a sophisticated system with much more stringent requirements. The cost would be quite high for the Starsat, but could provide an excellent "test-bed" for Space Telescope equipment. It appears desirable to use this sensor only in this case.

#### 4.4 SECONDARY MIRROR ALIGNMENT AND ARTICULATION MECHANISM

To remove the motion in the optical path caused by instability of the IPS, a means of deflecting the secondary mirror is required. A device to align the mirror and provide fine control is shown in Figure 34. The fine control consists of a mirror mounted on a cruciform flexure which is driven by piezo-ceramic actuators (PZT) to control the mirror tilt. Two-axis control is provided.

The cruciform flexure and ceramic actuators were designed and tested under contract for the early Space Telescope program. These actuators offer extremely fast response and high torque to the mirror. Some hysteresis exists in the actuators but should not be a problem in a closed-loop system.

In addition to the fine control, an alignment plate is attached to the baseplate by three differential beam microposition flexures equally spaced at 120° around the circumference of the baseplate. The microposition flexures provide a simple, direct means of motion reduction without introducing significant hysteresis or dead zone. This permits control of alignment plate position with resolution of several nanometers while the focus/alignment cam has sufficient displacement to minimize manufacturing problems.

The focus/alignment cams are driven by three motors. Focus motion is accomplished by driving all three motors in synchronism. Tilt alignment of

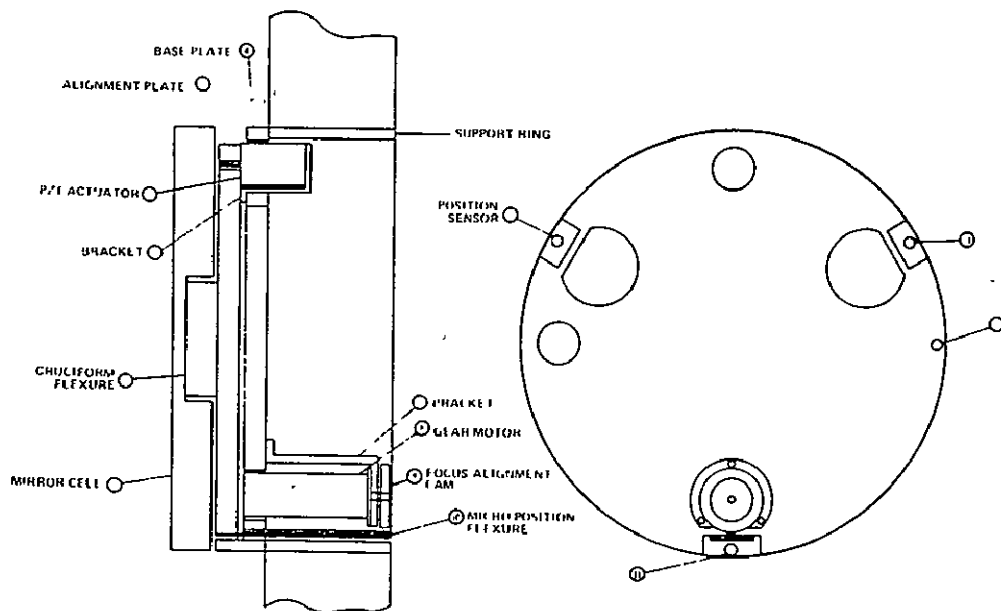


Figure 34. Mirror control system.

the mirror is accomplished by controlling each motor separately. This design is based on the assumption that tilt and focus capabilities are sufficient for on-orbit realignment.

Position sensors are provided to monitor tilt and focus motion. Position sensors are located at each of the three alignment drives. One of these sensors is opposite one of the PZT tilt actuators and also senses tilt motion. A fourth sensor is added opposite the remaining tilt actuator to avoid cross coupling problems. The sensors are eddy current loss, variable impedance transducers and have resolution to  $0.25 \mu\text{m}$ .

The system described is defined to satisfy the specified performance with high reliability and minimum cost. The key elements of the system are similar to or identical to components of systems previously developed and tested for Space Telescope.

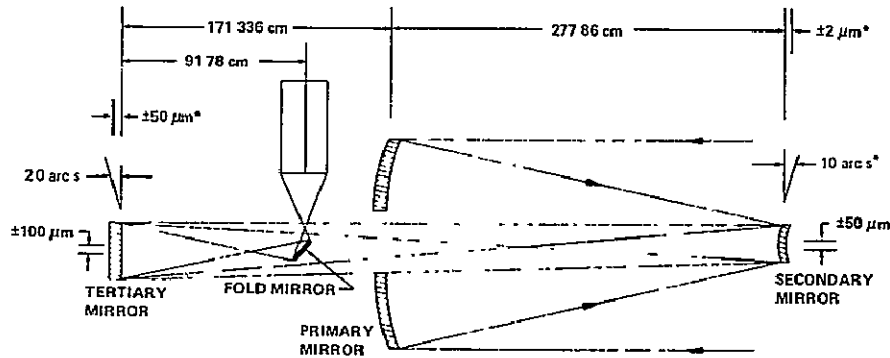
## 5. THERMAL CONTROL

The thermal design of the telescope assembly is governed by the orbital environment, error budget for optical system performance, telescope operating temperatures, materials, types of construction, operation, and

rationale adapted for maintaining reliability of the entire system. To a lesser extent, the thermal interfaces between the various units influence the thermal design. An additional implied requirement for the design is the minimization of required thermal control power.

### 5.1 REQUIREMENTS

Thermal control of the telescope metering structures is dictated by the allowable optical tolerances for despace, decenter, and tilt and the structures material selected. Based on using graphite-epoxy materials, which exhibit a coefficient of thermal expansion  $\alpha$  close to zero, and the allowable optical error tolerances defined for the telescope metering structures, thermal requirements are presented in Figure 35.



TOLERANCE	DESPLACE	DECENTER	TILT
PRIMARY TO SEC	$\pm 2 \mu\text{m}^*$	$\pm 50 \mu\text{m}$	10 arc s
THERMAL $\Delta T$	$\pm 21.6^\circ\text{C}$	$\pm 10.5^\circ\text{C}$	$13.8^\circ\text{C}$
PRIM TO TERY.	$\pm 50 \mu\text{m}^*$	$\pm 100 \mu\text{m}$	20 arc s
THERMAL $\Delta T$	$\pm 32.2^\circ\text{C}$	$\pm 16.1^\circ\text{C}$	$14.5^\circ\text{C}$
SEC. TO TERT.	$\pm 52 \mu\text{m}$	$\pm 100 \mu\text{m}$	30 arc s
THERMAL $\Delta T$	$\pm 34.7^\circ\text{C}$	$\pm 20.8^\circ\text{C}$	$15.1^\circ\text{C}$

\*COMPENSATION CAPABILITY

Figure 35. Thermal tolerances based on optical requirements.

Mirrors will be manufactured at nominal room temperature  $21 \pm 1^\circ\text{C}$  and are required to be controlled to this temperature on orbit. Control of mirror temperature is required to counter the effects of thermal expansions and contractions known to occur due to a randomly changing thermal coefficient in mirror materials.

The primary bulkhead, while not an active element, is the supporting structure and main reference for the metering structures; therefore, the requirement exists to control its temperature to  $21 \pm 1^\circ\text{C}$ . The instrument module temperature, based on predicted allowable operating ranges for instruments, is  $21 \pm 5^\circ\text{C}$ .

## 5.2 CONTROL CONCEPT

To meet all of the previously noted system requirements, a baseline concept for thermal control has been developed. This concept consists of active and passive elements described in this section. The overall thermal control system is illustrated in Figure 36.

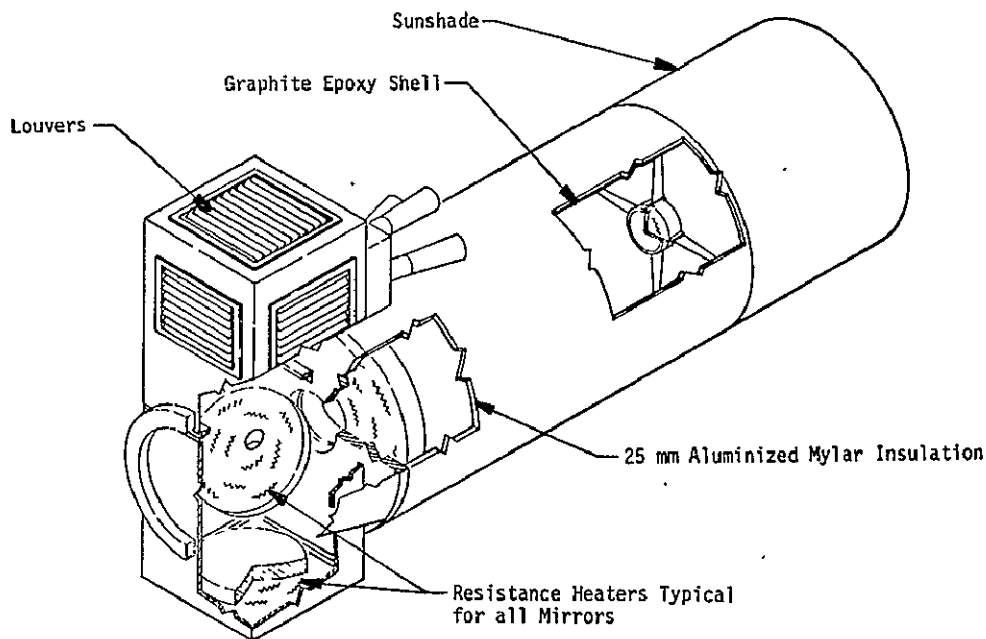


Figure 36. Thermal control concept.

Specifically, the primary, secondary, and tertiary mirrors are actively controlled at  $21 \pm 1^\circ\text{C}$  by means of multizone electrical heaters. Furthermore, these mirrors are thermally isolated from the surroundings by multilayer insulation on the back side to reduce thermal power consumption.

Passive thermal control of the metering shell between the primary and secondary mirrors is accomplished by multilayer insulation with a low  $\alpha_s/\epsilon$  exterior thermal finish. The overall telescope tube length was extended one diameter to protect the secondary mirror spider structure from large orbital temperature amplitudes.

An  $\alpha_s/\epsilon$  surface finish of 0.411 has been selected to provide for thermal control of the primary bulkhead independent of telescope orientation relative to the Sun. This value is representative of a degraded condition as it would occur after some exposure to the space environment. As the  $\alpha_s/\epsilon$  ratio increases, the primary bulkhead receives sufficient thermal loading, even with insulation, to exceed the active thermal control set point. For example with an  $\alpha_s/\epsilon$  ratio of 1, analysis indicated a maximum bulkhead temperature of 30°C (86°F).

The instrument module is designed for active-passive thermal control employing louvers, insulation, paint, and heaters. Louvers are used to minimize the heater power requirement at cold orientation.

The baseline concept is thermally compatible with all mission phases including ascent, on-orbit, reentry, and post-landing.

### 5.3 MATHEMATICAL MODEL

A thermal model consisting of 166 nodes including telescope, pallet, radiator doors, and payload bay was used to provide temperature information for comparison with the design requirements. Heater power requirements to hold the mirrors and bulkhead temperature to 21°C were also obtained from the model.

The telescope thermal model used to calculate the temperatures and power requirements is shown in Figure 37.

The graphite-epoxy shell consists of four nodal sections longitudinally, eight circumferentially, and three in cross section.

The conical shroud consists of two nodal sections longitudinally, eight circumferentially, and two in cross section. The relative alignment of the primary and tertiary mirrors is maintained by three graphite-epoxy rods.



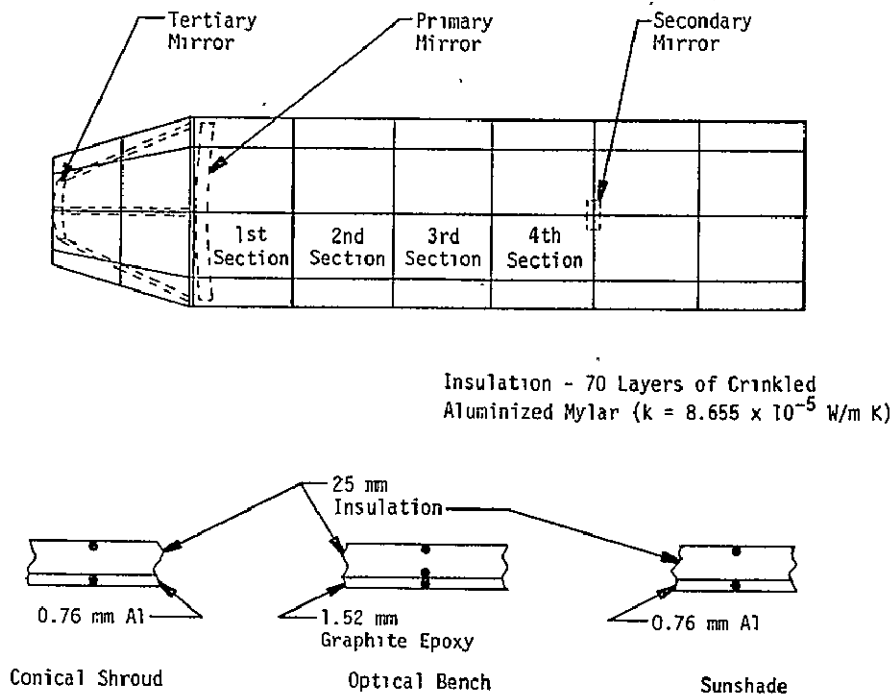


Figure 37. Thermal model.

The sunshade consists of two nodal sections longitudinally, eight circumferentially, and two in cross section. The 0.76 mm aluminum sunshade is covered with 25 mm of aluminized super insulation.

#### 5.4 ASSUMPTIONS AND INPUT PARAMETERS

The thermal analysis is based on a 250 km orbit with a  $56^\circ$  inclination for the hot case and a  $70^\circ$  inclination for the cold case to determine the incident external fluxes (solar, albedo, and Earth shine). Other orbital altitudes will affect the calculated incident fluxes; however, the overall effect of these differences is negligible on system performance.

The telescope is mounted on a pallet in the Orbiter payload bay 6 m from the aft end and pointed  $90^\circ$  to the longitudinal (X) axis (i.e. +Z axis). For the hot case, the telescope barrel is perpendicular to the Sun and, for the cold case, the barrel never sees the Sun (i.e. in the shadow of the Orbiter at all times).

The boundary conditions for the telescope are the external surface properties and the orbital heat fluxes. The external  $\alpha_s/\epsilon$  ratio used in the analysis was 0.411, where  $\alpha_s = 0.35$  represents the solar absorptivity of the telescope surface coating and  $\epsilon = 0.85$  represents the infrared emittance.

The fluxes on the configuration are a function of its position in the orbital plane and include direct solar flux, Earth, albedo, and Earth infrared emission. The direct solar, albedo, and Earth shine fluxes on the external surfaces of the Orbiter and the telescope assembly were calculated with the Lockheed Orbital Heat Rate Package (LOHARP) orbital heat flux program together with the view factor to obtain a total heat flux. The following constants were used:

Solar	1400 W/m <sup>2</sup>
Albedo	560 W/m <sup>2</sup>
Earth Infrared	296 W/m <sup>2</sup>

Table 6 presents other input data. These heat fluxes were used as inputs to a Systems Improved Numerical Differencing Analyzer (SINDA) program to determine the nodal temperature in the model.

TABLE 6. THERMAL PROPERTIES OF SURFACES AND MATERIALS

SURFACES			ABSORPTIVITY/EMISSION	
			$\alpha_s/\epsilon$	
INSIDE PAYLOAD BAY			0.2/0.5	
PALLET			0.27/0.9	
RADIATOR DOORS			0.08/0.8	
ENDS OF PAYLOAD BAYS			0.2/0.5	
EXTERIOR INSULATION OF TELESCOPE & SUNSHADE			0.36/0.85	
INSIDE TELESCOPE METERING STRUCTURE & SUNSHADE			0.91/0.86	
MIRROR			0.05/0.06	
ALL OTHER INSIDE SURFACES			0.9/0.9	
MATERIAL	THERMAL/CONDUCTANCE W/mK	DENSITY g/cm <sup>3</sup>	SPECIFIC HEAT J/grK	COEFFICIENT OF THERMAL EXPANSION cm/cmK
GRAPHITE EPOXY	12.98 (LONGITUDINALLY) 0.66 (TRANSVERSLY)	3.32	0.96	-0.066 x 10 <sup>-6</sup> -2.142 x 10 <sup>-8</sup>
ULE	1.31	2.48	0.75	
ALUMINIZED MYLAR INSULATION	8.66 x 10 <sup>-5</sup>	0.04	1.30	
ALUMINUM	156	2.72	0.92	

## 5.5 RESULTS

The effect of the two orbital orientations on the thermal model of the telescope is described in succeeding sections. An evaluation is presented to compare analytical results with previously developed thermal design criteria.

The boundary conditions described represent conservative conditions to yield maximum temperature effects for comparison with telescope requirements. For each case (hot and cold), the model was run for 30 orbital periods to give quasisteady state conditions; i. e., while there are temperature transients during an orbit, the temperature variations from orbit-to-orbit repeat quite closely. The significant temperature variations are due to vehicle orientations. Therefore, comparisons have been made with the two orientations mentioned previously (parallel and perpendicular to the Sun vector). Figures 38 and 39 show transient analysis results and give approximate equilibrium time anticipated for the telescope assembly.

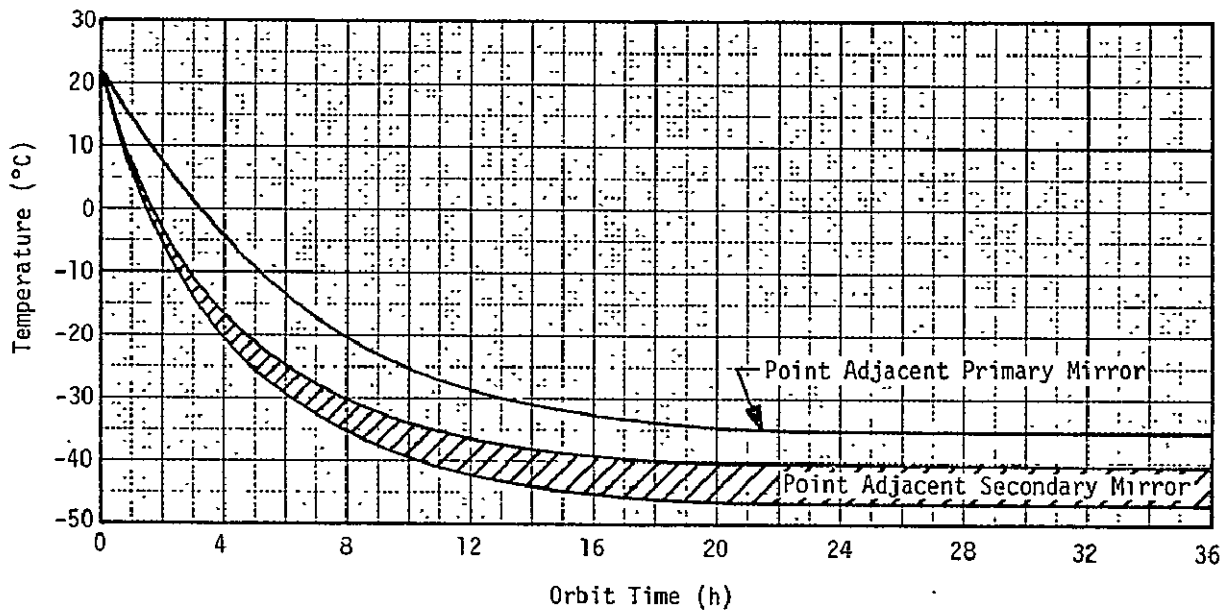


Figure 38. Temperature history of each end of the optical bench for the hot case.

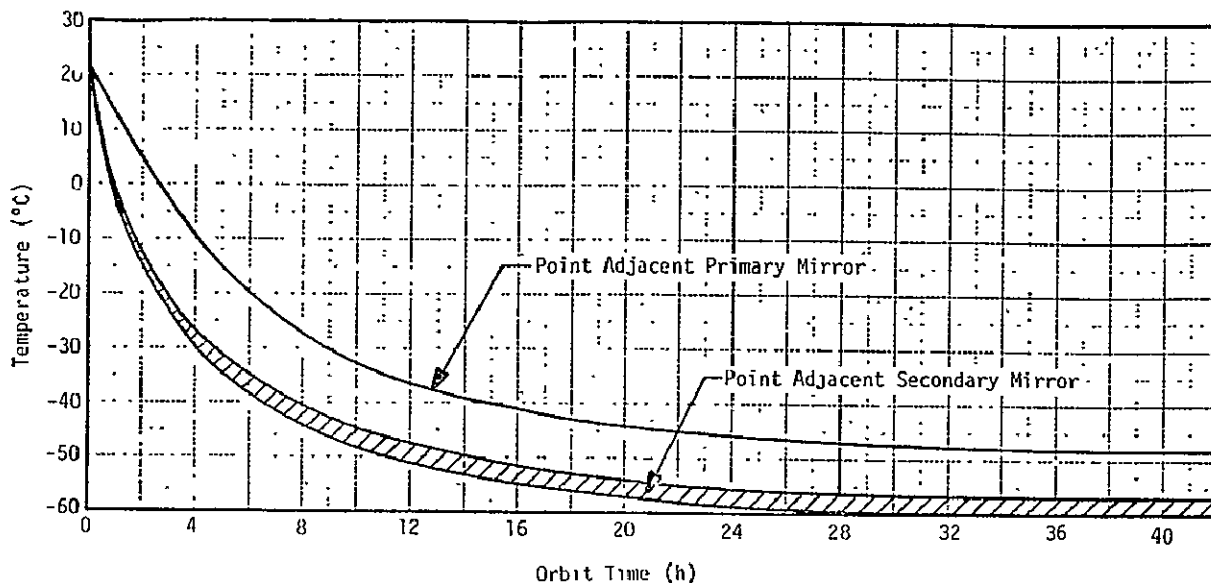


Figure 39. Temperature history of each end of the optical bench for the cold case.

Table 7 presents the computer calculated thermal control power input to the four actively controlled regions of the optics system and the louvered instrument container. Table 8 presents the equilibrium time for selected components.

TABLE 7. HEATER POWER IN WATTS TO MAINTAIN  $20 \pm 1^\circ\text{C}$

THERMAL CONTROL REGION	HOT PERPENDICULAR TO SUN	COLD PARALLEL TO SUN
PRIMARY MIRROR	26.2	29.92
SECONDARY MIRROR	3.6	5.0
TERTIARY MIRROR	0.5	0.6
PRIMARY BULKHEAD	10.0	12.0
INSTRUMENT CONTAINER		
NO LOUVER	0	804.0
WITH LOUVERS	0	120.0

TABLE 8. SYSTEM EQUILIBRIUM TIME

ITEM	APPROX. TIME (h)
PRIMARY MIRROR	22
SECONDARY MIRROR	30
TERTIARY MIRROR	7
METERING SHELL	
NEAR PRIMARY MIRROR	11
NEAR SECONDARY MIRROR	20
INSULATION SURFACE	3
*TIME FOR COMPONENT TO REACH THERMAL EQUILIBRIUM FROM 21°C (69.8°F)	

The majority of components reach thermal equilibrium approximately 20 h after launch. The times which are associated with the attainment of equilibrium temperature of the mirrors are only for the case where no heaters are used. The selected design uses heaters for active control of the mirror temperatures (21°C). (In this case the thermal analysis accounted for a constant mirror temperature.)

Before this time, the temperature gradient of the optical bench is increasing but because the entire bench temperature is decreasing, the temperature differences do not vary significantly after 7 to 10 h. The temperature change is large enough before 7 h of orbit time that adjustment is necessary every 3 h. After this time, adjustment will be necessary for a given vehicle orientation approximately once every 6 h. After 20 h, no additional adjustment will be necessary. A composite of all results is given in Table 9.

Verification of the thermal performance of the passive thermal control system is based primarily on an evaluation of the nodal response of the various cylinder members within the model. A review of the data indicates that the maximum orbital nodal temperature variation of 6.8°C occurred in the perpendicular (hot case) orientation and is located at the secondary mirror

TABLE 9. STARSAT THERMAL CONTROL RESULTS

MIRROR ALIGNMENT						
	HOT CASE*			COLD CASE**		
	PRI. MIRROR TO SEC. MIRROR	PRI. MIRROR TO TER. MIRROR	SEC. MIRROR TO TER. MIRROR	PRI. MIRROR TO SEC. MIRROR	PRI. MIRROR TO TER. MIRROR	SEC. MIRROR TO TER. MIRROR
DECENTER (TOLERANCE)	±10.5 °C	±16.1 °C	±20.8 °C	±10.5 °C	±16.1 °C	±20.8 °C
DECENTER (RESULTS)	0.907 °C	0.002 °C	6.31 °C	1.6 °C	0.002 °C	3.08 °C
DESPACE (TOLERANCE)	±21.6 °C	±322 °C	±347 °C	±21.6 °C	±322 °C	±347 °C
DESPACE (RESULTS)	2.87 °C	0.001 °C	2.871 °C	1.41 °C	0.001 °C	1.42 °C
TILT (TOLERANCE)	13.8 °C	14.5 °C	15.1 °C	13.8 °C	14.5 °C	15.1 °C
TILT (RESULTS)	6.68 °C	0.002 °C	6.682 °C	1.99 °C	0.002 °C	1.992 °C
MAX. AVERAGE TEMP CHANGE WITHIN AN ORBIT						
<u>HOT CASE</u>			<u>COLD CASE</u>			
1ST SECTION (ADJ. PRI. MIRROR)			0.84 °C	1ST SECTION (ADJ. PRI. MIRROR)		0.57 °C
2ND SECTION			1.36 °C	2ND SECTION		0.62 °C
3RD SECTION			2.99 °C	3RD SECTION		1.38 °C
4TH SECTION (ADJ. SEC. MIRROR)			6.31 °C	4TH SECTION (ADJ. SEC. MIRROR)		3.08 °C
<u>MIRROR HEATER POWER REQUIREMENTS</u>						
HOT CASE (TOTAL FOR 3 MIRRORS)				32 WATTS		
COLD CASE (TOTAL FOR 3 MIRRORS)				37 WATTS		

\* HOT CASE—ORBIT BETA ANGLE=56°, TELESCOPE POINTING PERPENDICULAR TO SUN LINE.  
 \*\* COLD CASE—ORBIT BETA ANGLE=70°, TELESCOPE POINTING AWAY FROM SUN.

spiders. A similar examination of the data for the parallel (cold case) orientation results in a temperature variation of 3.08°C. Comparison with the required stability of 20.8°C reveals that this is well within the allowable value.

Figures 40 and 41 present plots of inside surface temperature — time history for the perpendicular (cold case) and parallel (hot case) orientation for the section between the primary mirror and the secondary mirror (circumferential average).

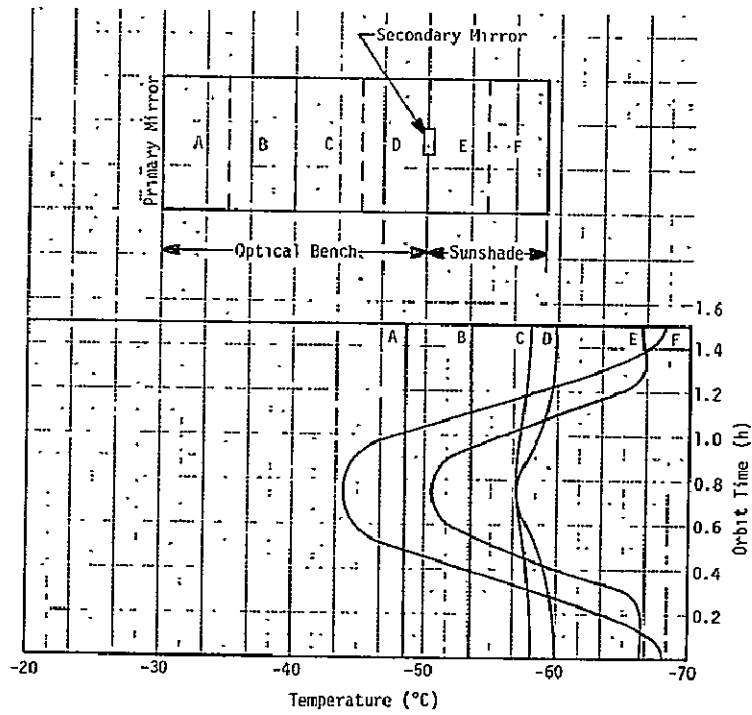


Figure 40. Average temperature variation of telescope throughout an orbit for the cold case.

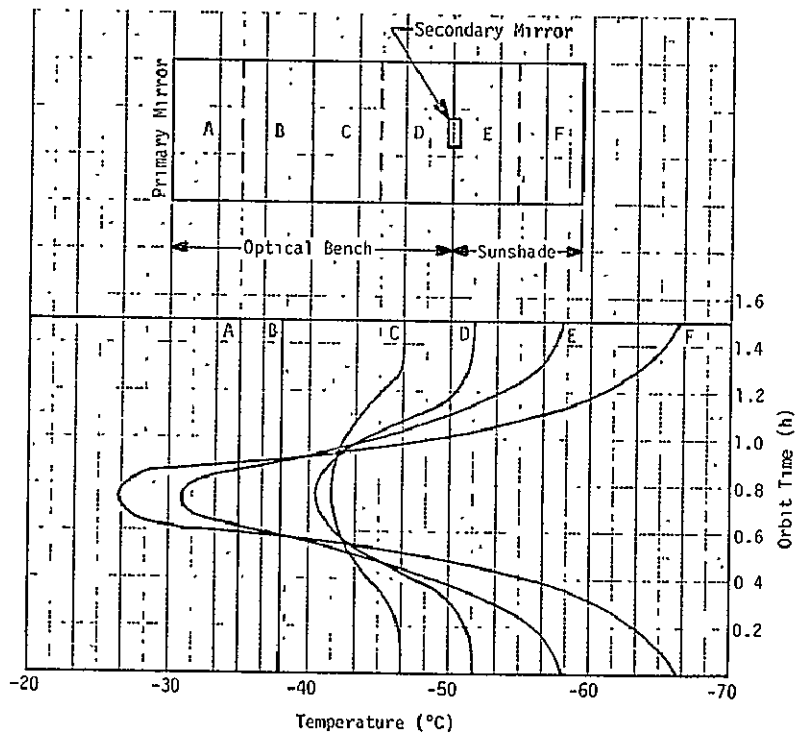


Figure 41. Average temperature variation of telescope throughout an orbit for the hot case.

The worst case temperature distributions axially down the telescope are shown in Figures 42 and 43 for the extreme hot and cold orientations. The curves of Figures 42 and 43 show the improvement obtained by the light shield. Without the light shield protecting the secondary mirror spider, the axial and lateral temperature gradients, as shown at the end of the light shield, would occur at the position of the secondary mirror causing excessive misalignment.

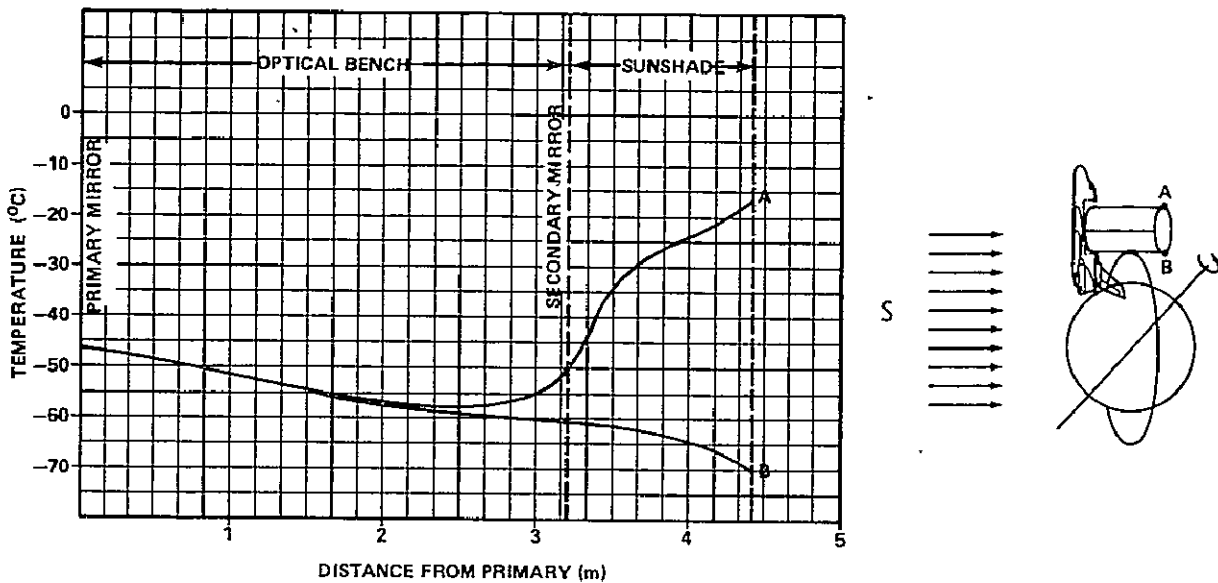


Figure 42. Temperature variation of telescope throughout an orbit for the cold case.

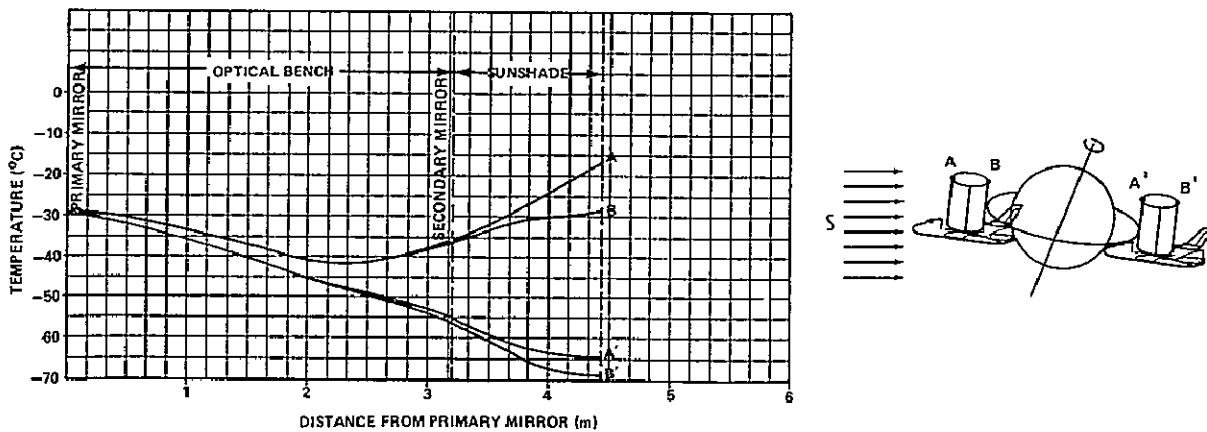


Figure 43. Temperature variation of telescope throughout an orbit for the hot case.



Figure 44 shows the attenuating effect of paint and insulation on orbital temperature amplitudes for different vehicle orientations. The result is small temperature changes on the optical bench. The impact of the changes are further reduced by the very small coefficient of thermal expansion of the graphite-epoxy.

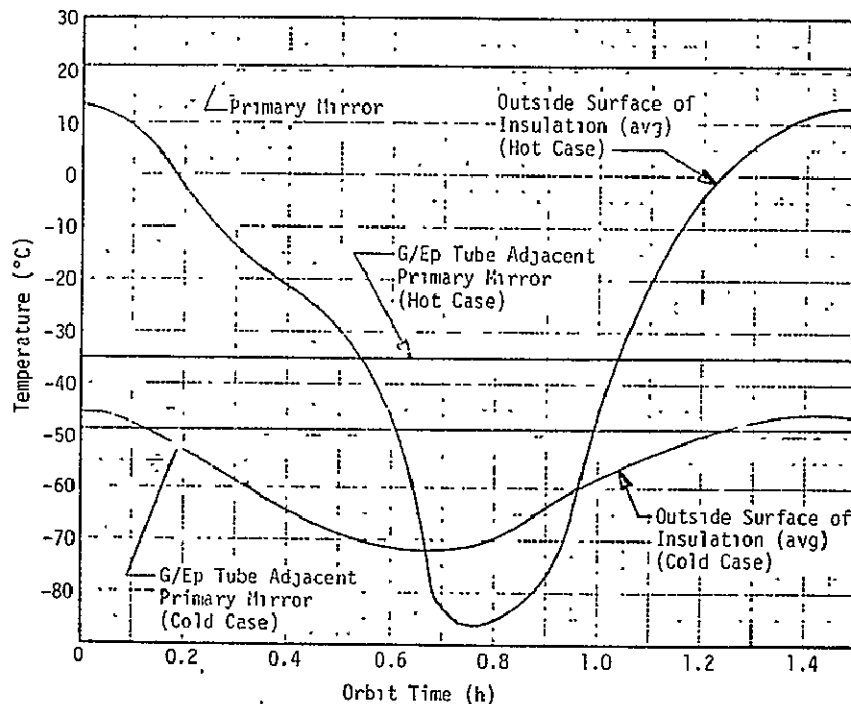


Figure 44. Temperature history of primary mirror, graphite-epoxy tube and outside surface throughout an orbit for hot and cold cases.

Figure 45 gives an indication of the payload bay orbital temperature to which the telescope is exposed. Both these temperatures are relatively low because, in all orientations studied, the payload bay is almost always in the shadow and never exposed to the direct rays of the Sun.

## 5.6 THERMAL CONTROL OF INSTRUMENT MODULE

The thermal control requirements for the instrument module are predicted on the assumptions that the operating range of the instrument is  $21 \pm 5^\circ\text{C}$  and no cryogenic sensors will be used in the near future. The maximum power used on any one camera is 170 W. When one camera is turned off, electric heaters are turned on to maintain a constant heat removal rate.

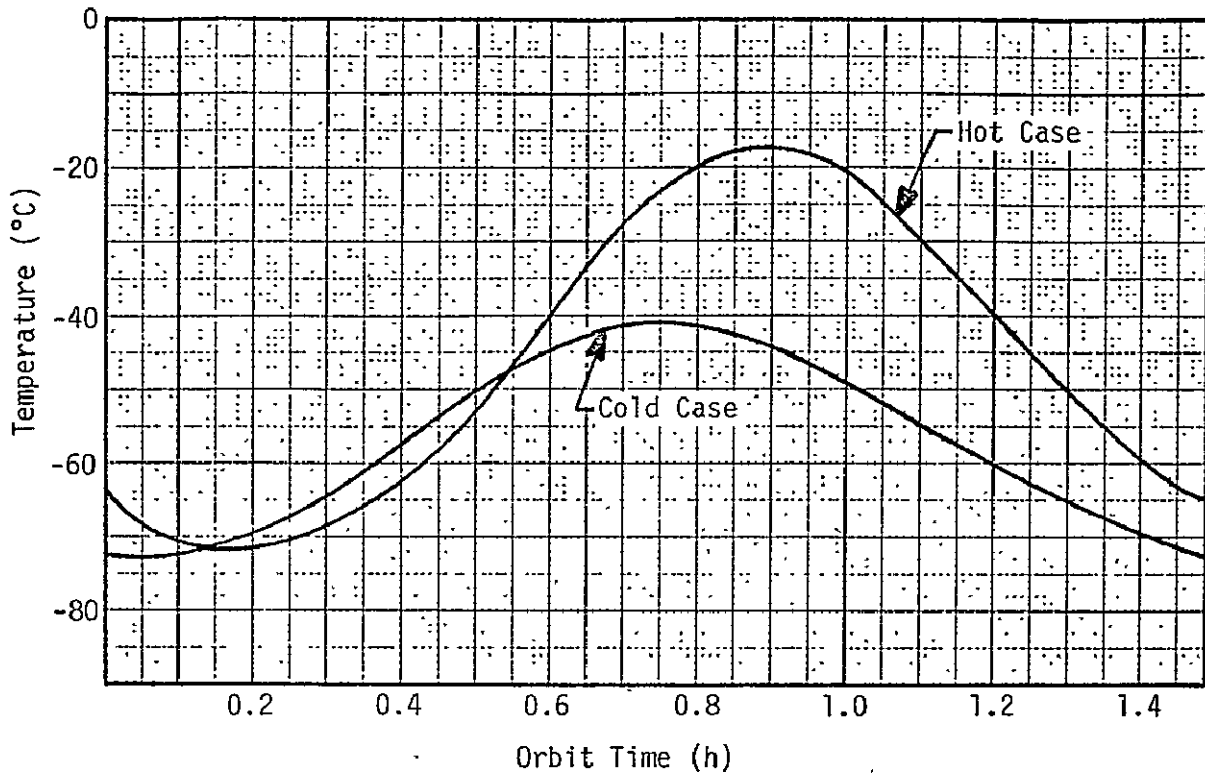


Figure 45. Average payload bay temperature throughout an orbit for hot and cold cases.

Two concepts for thermal control of the instrument module were considered: one approach is based on using a simple system of super insulation and heaters and the other concept uses a louver system with heaters sized to provide a constant temperature in the instrument compartment. The selection of the thermal control system concept must consider the maximum heater power requirements. Table 7 shows two power levels for the instrument module. The 804 W operation is based on super insulation and mosaic paint pattern in the cold orientation. Only 120 W of heater power is required with a louver control system. Because of this advantage and the proven reliability in previous space applications, a louver system is selected for the instrument modules.

## 5.7 RECOMMENDATIONS

The results of the thermal studies conducted for Starsat can be categorized for the optics and instrument module separately as follows:

1. A realistic thermal control concept has been developed that meets all current system requirements. Future work must be directed toward (a) optimizing the thermal control coating to reduce thermal power and (b) transient thermal reactions induced by telescope orientation changes must be studied in greater depth to define the limitations associated with focus and alignment maintenance after the maneuvers.

2. Two thermal control concepts for the instrument container have been assessed and both have been found to be thermally acceptable but, due to the large power savings, the louver concept is preferred. Further study is recommended with the goal to reduce the electrical heater power without impairing system performance. Variable conductance heat pipes should be evaluated as thermal control devices for the instrument module because of the flexibility which is afforded for control of variable thermal loads. These pipes were omitted in this study because of the high cost usually associated with the development of such a system.

## 6. DATA MANAGEMENT AND COMMUNICATIONS

### 6.1 DATA MANAGEMENT

The primary data management function required by Starsat is the processing of data and the generation of commands to perform pointing control. Other data management functions include focus control, telescope deployment and storage, thermal control, power distribution control, and the acquisition of engineering status data. In addition, Starsat experiments will require data management support for control and for acquisition and distribution.

Starsat will rely on the Spacelab and the Orbiter to provide data management support. The only additional telescope facility equipment required to perform a mission is command decoders and some type of buffer/formatter for telemetry. The number of command decoders and buffer/formatters required is mission dependent.

An analysis of command and telemetry requirements (Table 10) indicates that one Spacelab RAU will accommodate the telescope facility subsystem requirements with the addition of a command decoder and a buffer/formatter. A similar analysis of the command and telemetry requirements of a number of potential scientific instruments taken from Space Telescope reports indicated that one RAU would accommodate at least one or more of the instruments if a command decoder and a buffer/formatter is provided (Table 11).

TABLE 10. TELESCOPE FACILITY COMMAND  
AND TELEMETRY REQUIREMENTS

<u>COMMAND REQUIREMENTS</u>			
	<u>VARIABLE WORDS/BYTES</u>	<u>DISCRETES</u>	
- FINE GUIDANCE SENSOR	13/15	40	
- POWER DISTRIBUTION SYSTEM	0	4	
- THERMAL CONTROL SYSTEM	<u>2/2</u>	<u>3</u>	
TOTAL CHANNELS	15	47	
<u>TELEMETRY REQUIREMENTS</u>			
	<u>DISCRETES</u>	<u>SERIAL DIG. (WORDS/BYTES)</u>	<u>ANALOG 8 BITS/MEAS.</u>
- FINE GUIDANCE SENSOR	6	20/20	9
- POWER DISTRIBUTION SYSTEM	0	0	6
- THERMAL CONTROL SYSTEM	<u>41</u>	<u>0</u>	<u>41</u>
TOTAL CHANNELS	47	20	56

The Spacelab experiment computer will be used to perform all data processing and control except for control of the IPS pointing. The desired IPS pointing will be accomplished by providing secondary mirror position information to the Spacelab computer.

6.2 COMMUNICATIONS

For communications, Starsat will rely on the Orbiter communication system via its interface with Spacelab. A description of the capabilities available to Starsat is included in the section describing interfaces.

TABLE 11. COMMAND AND TELEMETRY REQUIREMENTS

<u>COMMAND REQUIREMENTS</u>			
	DISCRETE	VARIABLE WORDS/BYTES	
FIELD CAMERA			
- PERKIN ELMER	86	20/19	
- ITEK	0	19/20	
POINT & AREA PHOTOMETER (BBRC)	61	18/22	
FAINT OBJECT SPECTROGRAPH (BBRC)	18	3/2	
HIGH SPEED AREA PHOTOMETER (MMC)	21	14/18	
<u>TELEMETRY REQUIREMENTS</u>			
	DISCRETE	SERIAL DIG.	ANALOG
FIELD CAMERA			
- PERKIN ELMER	11	21	53
- ITEK	0	1/51 BYTES	
POINT & AREA PHOTOMETER (BBRC)	9	14 (10K to 160K BITS/FRAME)	44
FAINT OBJECT SPECTROGRAPH (BBRC)	2	8 PLUS (256K BITS OF SCIENCE DATA)	34
HIGH SPEED AREA PHOTOMETER (MMC)	2	2 (12X10 <sup>6</sup> BITS/SEC ICCD READOUT)	24

## 7. ELECTRICAL SYSTEM

Spacelab power is supplied from three 200 W, 28 Vdc power buses to a standard power connector on the outer gimbal of the IPS. A Starsat wiring harness interfaces with the IPS standard power connector and distributor power to the telescope facility. A detailed power analysis was performed which verified that the IPS baseline power interface is compatible with Starsat power requirements.

## 7.1 POWER REQUIREMENTS

The primary purpose of the power analysis was to determine power requirements on the outer gimbal. Although the IPS baseline was specified to be 600 W (three 200 W bases), ESA is considering increasing the capacity to 800 W. A secondary purpose for the analysis was to specify the total power interface with the Spacelab.

An assessment of power requirements on the outer gimbal was made by subdividing the mission equipment into three classifications: (1) items furnished by ESA and located on the outer gimbal, (2) instrument support equipment, and (3) scientific instruments. The approach used in determining the power level available to scientific instruments, item (3) was to subtract power required for support equipment, items (1) and (2) from the 600 W interface capacity. Support equipment requirements are tabulated in Table 12.

TABLE 12. ELECTRICAL POWER REQUIREMENTS

EQUIPMENT	AVERAGE WATTS	PEAK WATTS	REMARKS
<b>ESA PROVIDED</b>			
STAR TRACKERS (3)	20	29	PEAK DURING WARM-UP
RATE GYRO (4)	68	125	
RAU (3)	30	30	
<b>SUPPORT</b>			
DECODERS (2)	6	6	QUIESCENT PERIODS ONLY
DATA BUFFER	6	6	
OPTICS HEATERS	47	47	
INSTRUMENT HEATERS		(120)	
ALIGNMENT DRIVERS (3)	15	15	
FINE DRIVERS (2)	5	5	
FINE GUIDANCE SENSOR	9	9	
GUIDANCE SENSOR DRIVERS	15	15	
<b>TOTAL</b>	<b>221</b>	<b>287</b>	<b>EXCL. INSTR. HTRS.</b>
28V CAPACITY	600	600	
28V POWER AVAILABLE TO SCI. INSTR.	379	313*	

\*AVAILABLE TO INSTRUMENTS DURING PERIODS OF PEAK CONSUMPTION BY SUPPORT EQUIPMENT

The most significant aspect of the tabulation is the absence of baffle heaters. Baffle heaters for conventional telescope designs might be expected to require over 150 W.

It should be noted from Table 12 that the peak power total of 287 W was primarily the result of warm-up heaters for the rate gyros. Since this power would normally be available for use by scientific instruments, the average power level of 221 W was adapted as a representative power level for the analysis. It should also be noted that the power estimate of 120 W listed in the table for the instrument module was not included in the power summation because heaters would be operated only when instrument power levels fell below 120 W.

The power available for scientific instruments was thus determined to be 379 W (600 W interface minus 221 W support equipment). The power analysis was continued further to assess power required for typical instruments.

On the basis of a review of candidate instruments suitable for the Starsat, it was determined that instrument power requirements would be in a 50 to 170 W range. Examples of typical instrument requirements are as follows: (1) film and image intensifier — 70 to 150 W operating and 35 to 70 W standby, (2) high speed area photometer — 50 to 100 W operating and 25 to 50 W standby, and (3) faint object spectrometer — 100 W operating and 50 W standby.

It was the conclusion of this part of the analysis that the 379 W available to scientific instruments would be more than adequate for two instruments and would probably be ample for three instruments. The absence of baffle heaters was primarily responsible for the relatively low total power requirement. Conventional telescopes with normal baffling requirements would probably require at least an 800 W interface at the outer gimbal.

A secondary objective for the power analysis was to establish the combined IPS and Starsat interface with the Spacelab. Power requirements for the IPS were specified in the Spacelab Accommodation Handbook [22]. The level was specified as 320 W average and 1150 W peak including the star tracker and rate gyro package. The combined IPS and instrument power requirement was estimated to be 842 W average and 1576 W peak. The total electrical energy requirement for a 7 day mission was estimated to be 90 kWh for an average standby power level of 710 W. These requirements were considered to be well within Spacelab capabilities of 3000 W and 890 kWh.

## 7.2 WIRE HARNESS

Power will be routed to subassemblies located on the outer gimbal solely by a wire harness. A future trade-off study is recommended, however, to decide the need, if any, for a separate power distributor or a combined power and hardwire control distributor. The wiring harness concept is presented in Section 8.

Limited flexibility was obtained from the harness design by providing accessible connectors for the alignment drivers and fine sensors, the FGS and drivers, and the scientific instruments.

## 8. INTERFACES

Starsat is designed to interface with and be supported by Spacelab and Orbiter systems.

### 8.1 PAYLOAD BAY

The telescope facility can be mounted in the payload bay as shown in Figure 46 or can be turned around if that provides a more desirable payload layout based on c. g. constraints, field of view, or other considerations.

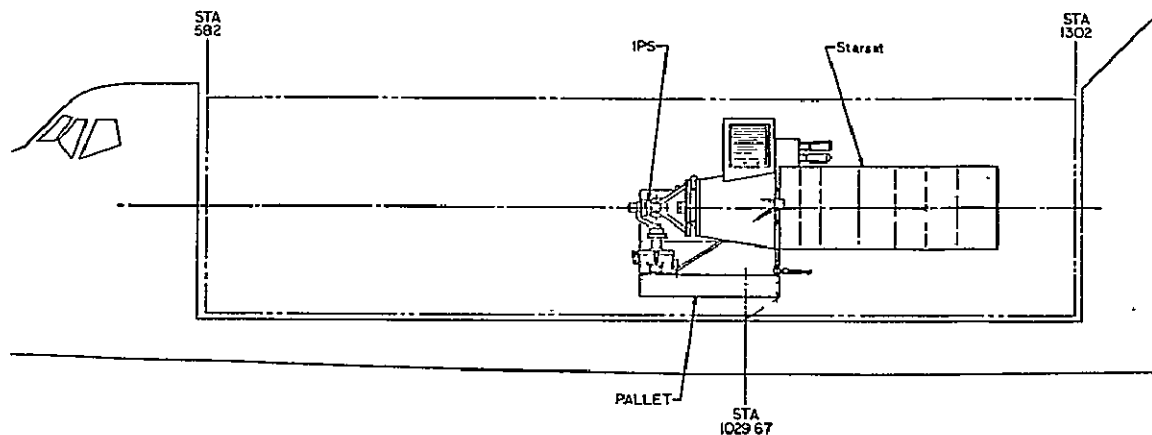


Figure 46. Starsat in Shuttle payload bay.



Figure 47 illustrates how the telescope may be articulated by the IPS. The angular telescope motion in pitch and yaw is limited by the payload bay geometry and not the IPS.

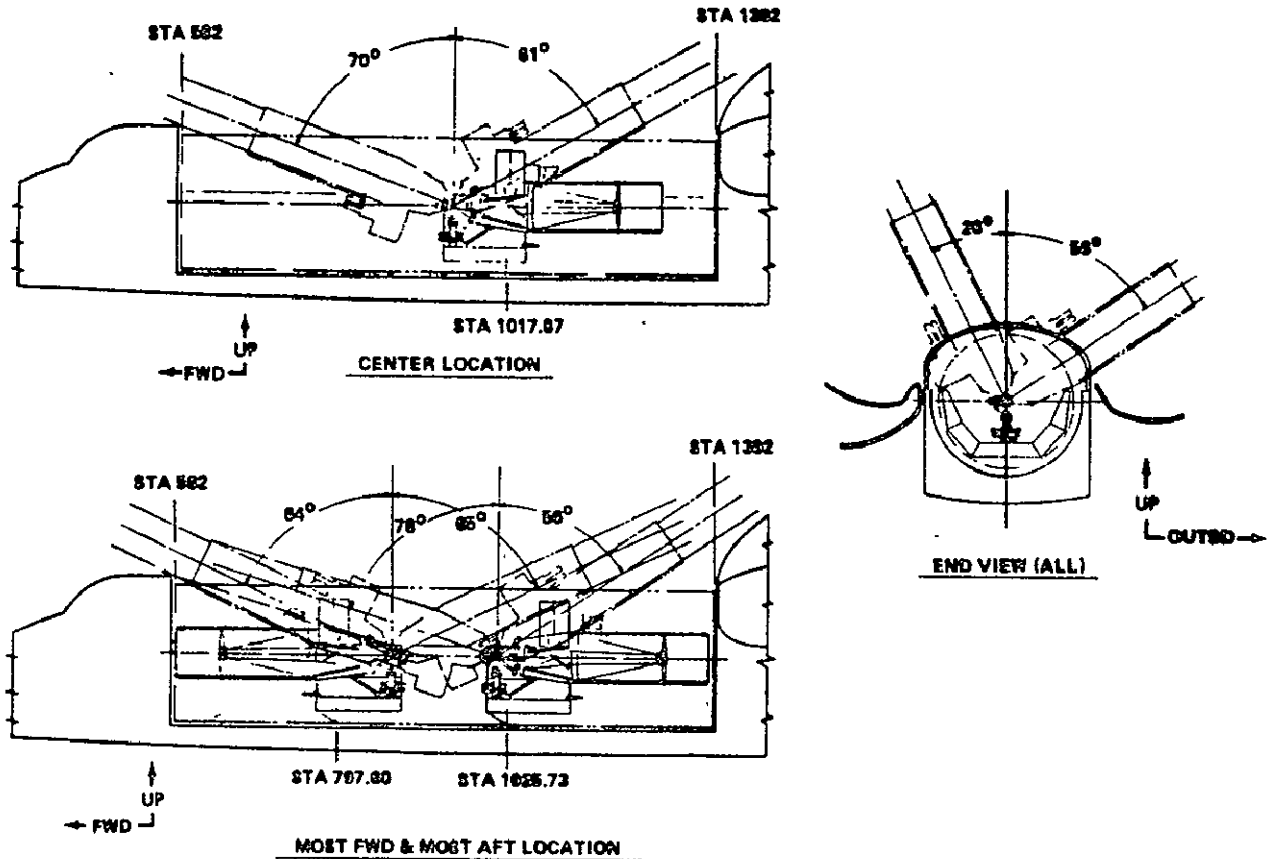


Figure 47. Allowable telescope motion in payload bay.

Figures 48 and 49 show different views of the telescope facility in the Shuttle payload bay and on the pallet.

The IPS/telescope tiedown interface works as follows (Fig. 50):

a. Launch — The telescope and IPS are separated and locked down to the pallet, connected only by the separating springs and the electrical interface.

b. On-Orbit — After the payload bay doors are open, cable-actuated locks on the telescope are unlocked by the cable actuator, the ring connector actuator pulls the IPS rings together, indexed by vee-blocks. The IPS is unlocked and the telescope rotated to the desired position with the gyro system of the IPS providing pointing and stabilization.

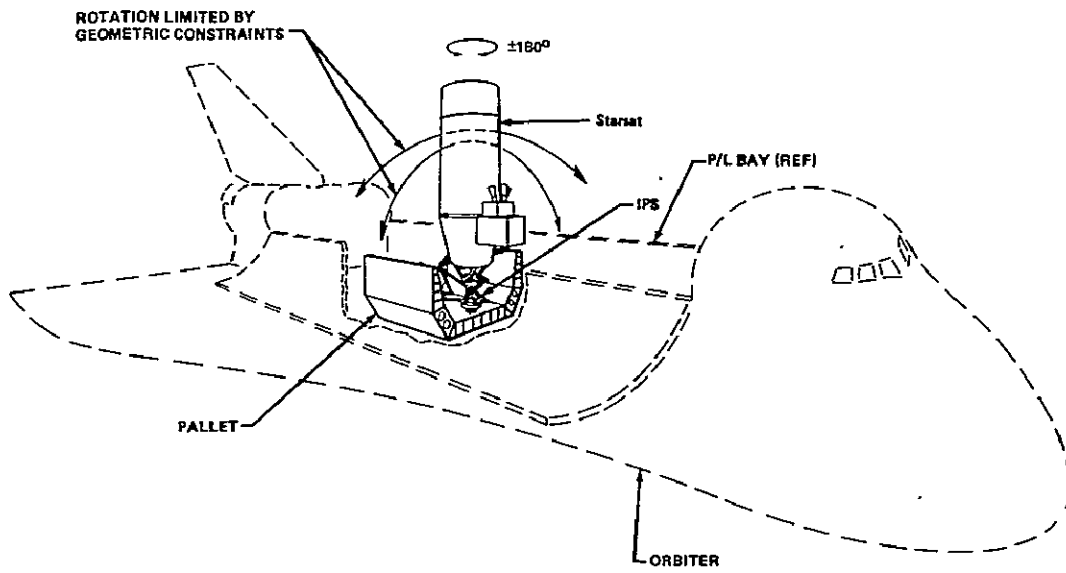


Figure 48. Telescope facility in Shuttle payload bay.

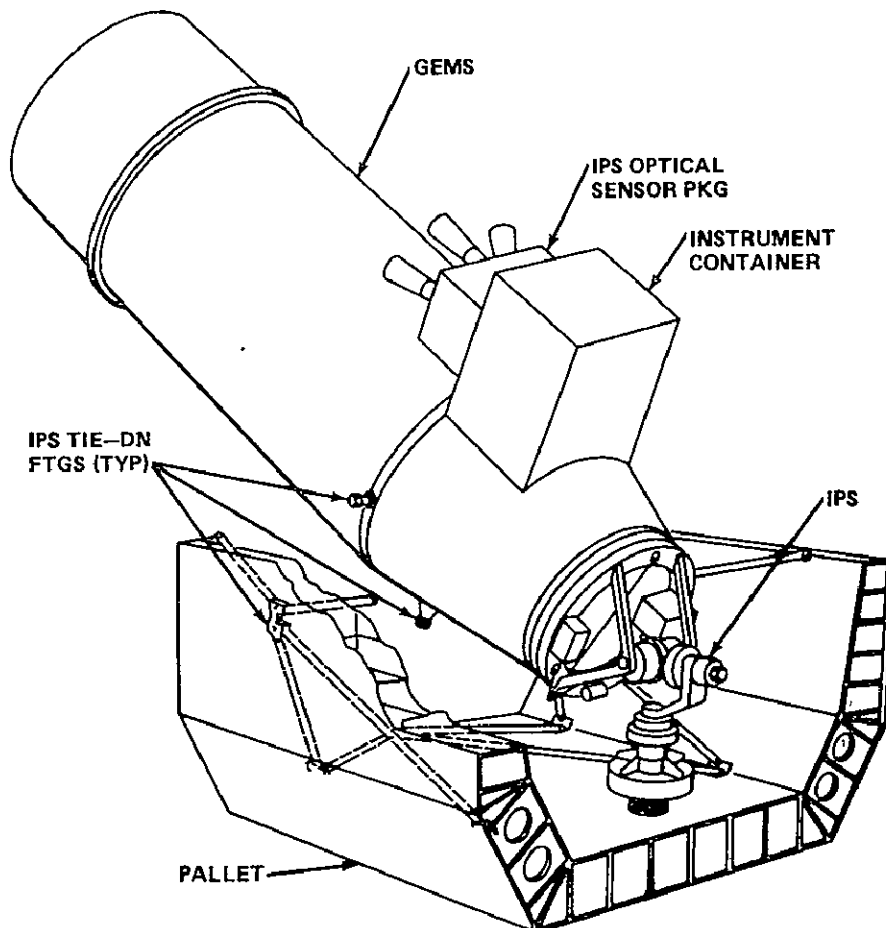


Figure 49. Telescope facility on pallet.

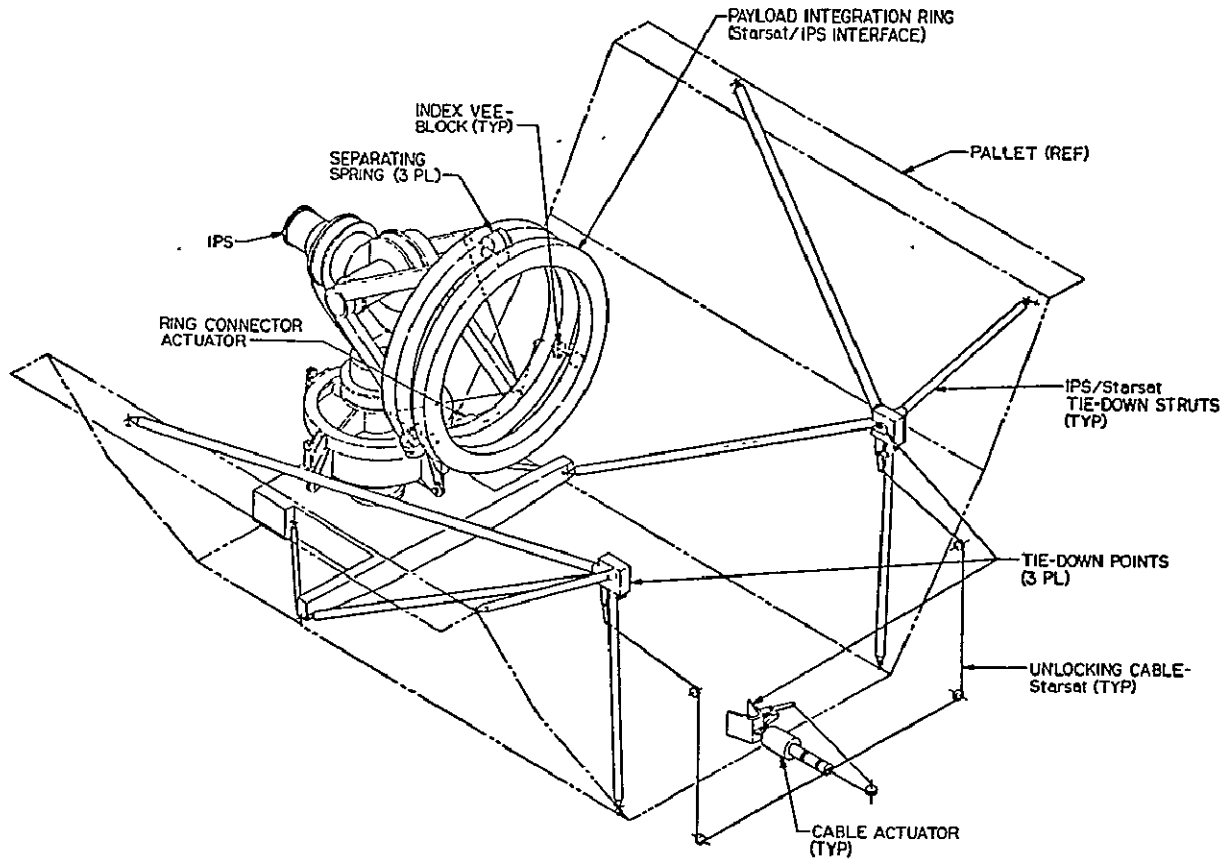


Figure 50. IPS/telescope tiedown interface.

c. Descent — The telescope is rotated back down (IPS rings separate and push the telescope into the support clamps), the pins are locked by the cable actuator to lock the telescope down, payload bay doors are closed, and reentry of the Shuttle is initiated.

## 8.2 POINTING AND STABILIZATION

Coarse control of the telescope facility LOS is performed by the IPS. This system also provides the only control about the roll axis. An IPS optical sensor package (Fig. 51) is mounted to the primary bulkhead of the telescope. This maintains the necessary alignment between the IPS optical sensor and the telescope while avoiding the requirement for the physical interface between the IPS and telescope to be accurately aligned. A detailed description of how the IPS is used to support Starsat was included in Section 4 and will not be discussed further.

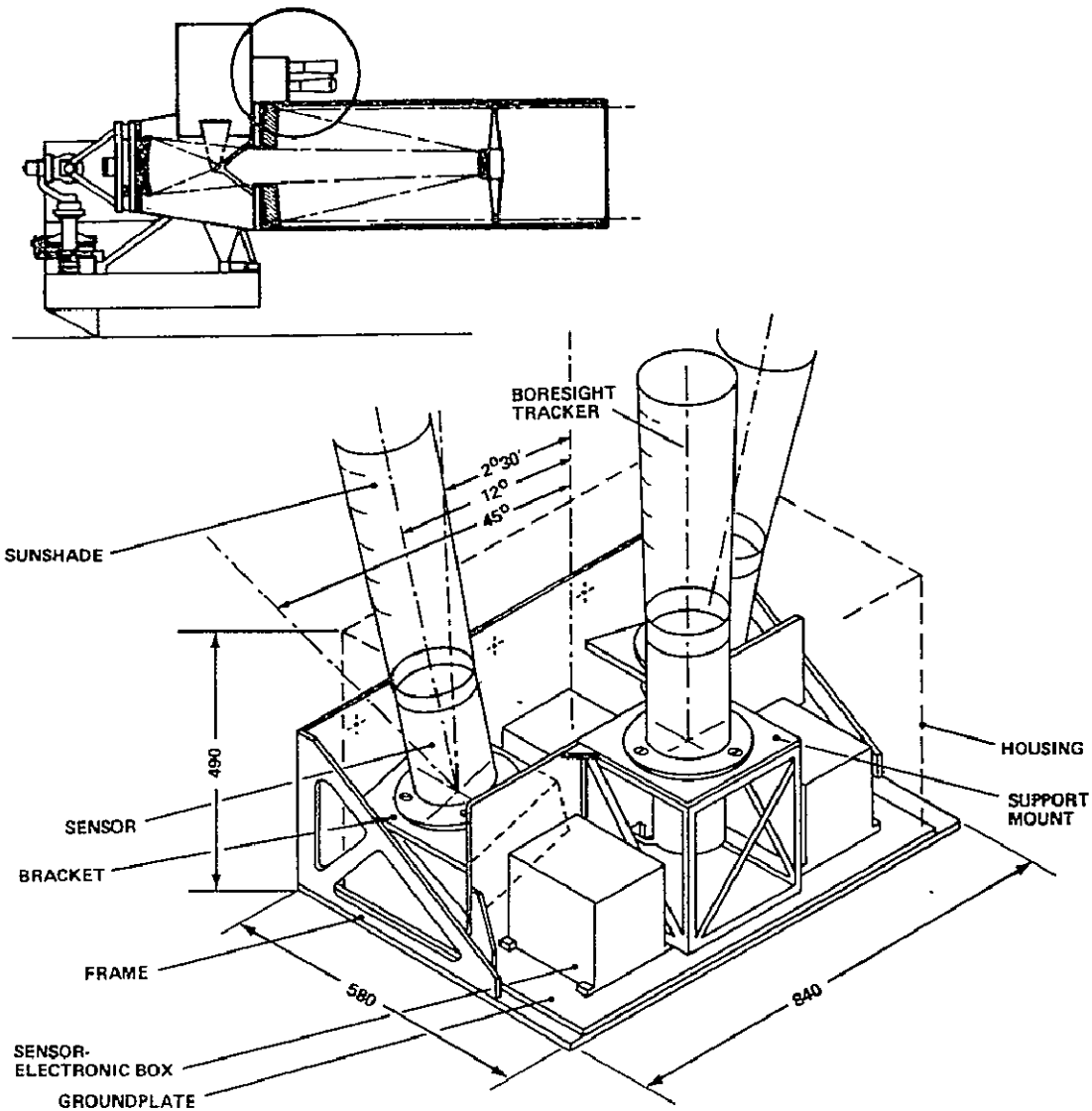


Figure 51. IPS optical sensor package.

### 8.3 DATA MANAGEMENT

Starsat will rely on Spacelab to provide data management support. A block diagram of the Spacelab CDMS and its Orbiter interface is shown in Figure 52. The Spacelab baseline presently provides for up to three RAU's and 20 coaxial cables across the IPS gimbals. Engineering and low rate science data will be acquired by the RAU's and transferred to the Spacelab experiment computer via the Spacelab experiment data bus. Any high rate digital data generated by an experiment will be transferred across the IPS gimbals via a coaxial cable. High rate digital data may be transferred to the Spacelab high rate digital multiplexer for recording and/or transmission via the Orbiter

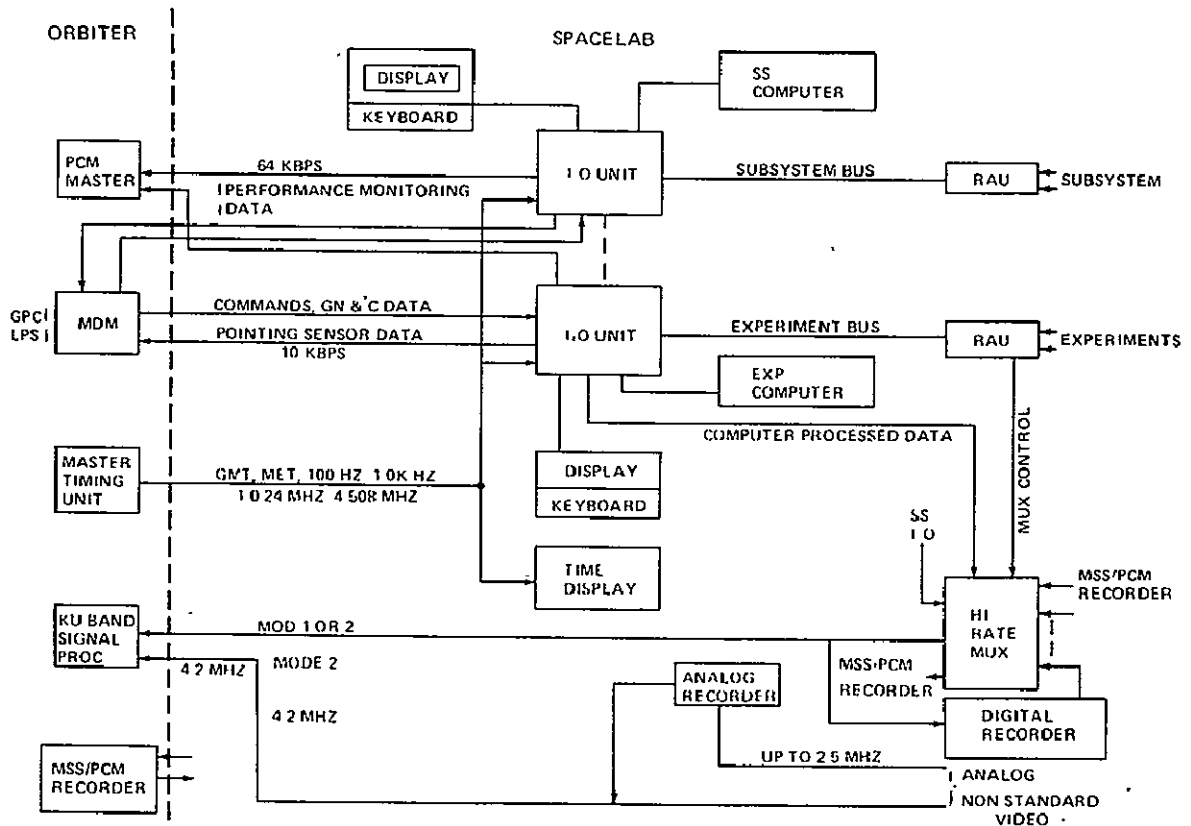


Figure 52. Spacelab CDMS and Orbiter interface.

Ku-band communications system or transferred to experiment peculiar hardware. Analog data transferred across the gimbals via a coaxial cable can be routed to the Spacelab analog recorder, to the Orbiter Ku-band communications system, or to experiment peculiar equipment. The provision of a video recorder by Spacelab is to be determined.

#### 8.4 ELECTRICAL SYSTEM

The electrical power interface with the IPS is specified at the outer gimbal. The interface is specified in the Spacelab Payload Accommodation Handbook [22] to consist of three 200 W, 28 Vdc power buses. Each bus is a two-wire interface that must not be connected to structure (Fig. 53).

ORIGINAL PAGE IS  
OF POOR QUALITY

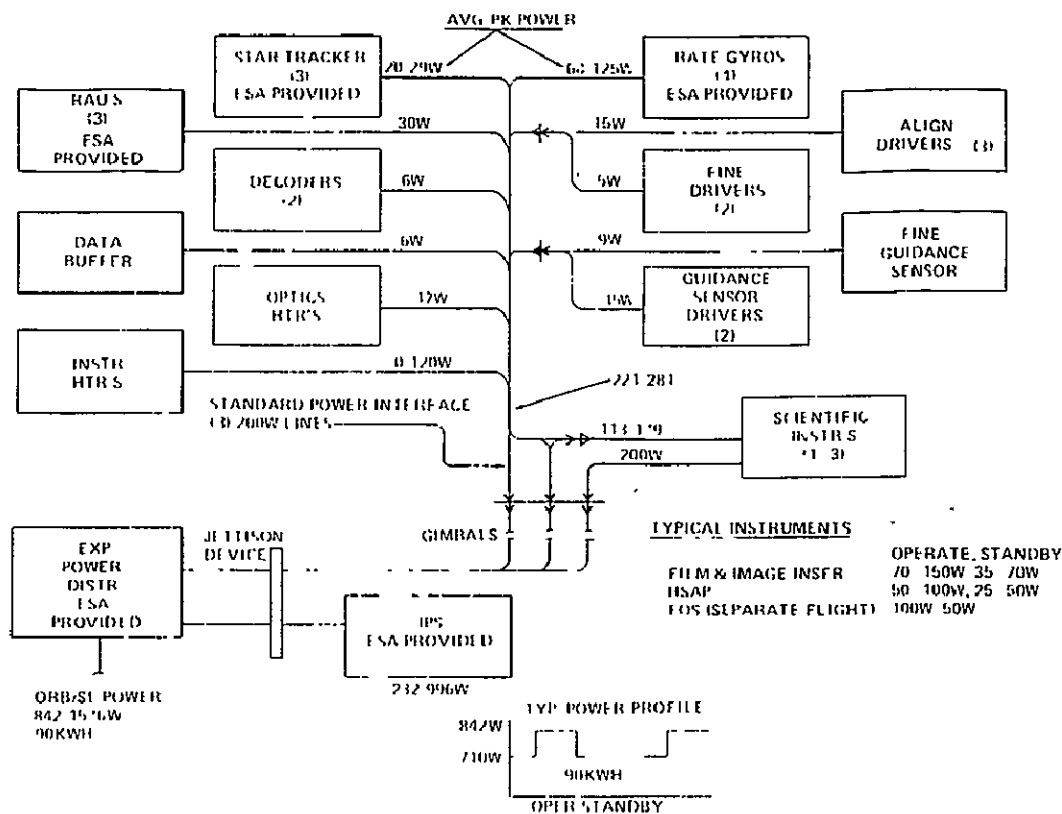


Figure 53. Electrical power distribution and interface.

## 8.5 COMMUNICATIONS

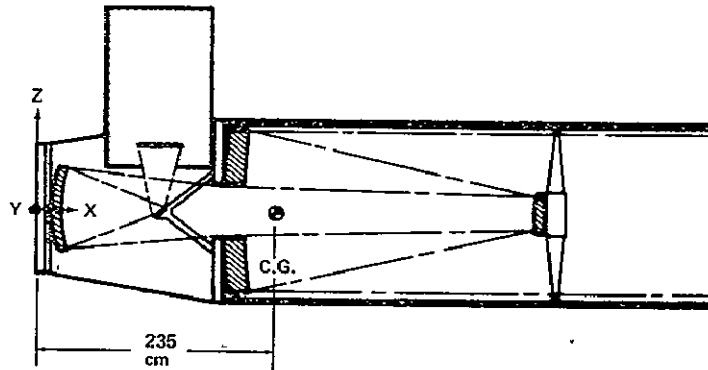
For communications, Starsat will rely on the Orbiter communication system via its interface with Spacelab. The Orbiter/Spacelab interface will permit the transmission of up to 64 kbps of engineering or housekeeping data and low rate science data to ground via the Orbiter S-band system. High rate digital data (30 Mbps or greater) and 4.2 MHz analog data can be transmitted using the interfaces between the Spacelab and the Orbiter Ku-band communications system. Although no ground commands have been identified for Starsat, the Orbiter forward link will provide 8 kbps of encoded command data with a basic command rate of 2 kbps to an attached payload. This link is time shared between the Orbiter, Spacelab subsystems, and the various Spacelab experiments.

## 9. MASS PROPERTIES

The Starsat telescope must be compatible with the Spacelab IPS weight carrying capability given in Table 4. The system and subsystem weights for Starsat are given in Table 13. The center of mass locations and moments of inertia are given in Figure 54.

TABLE 13. SYSTEM AND SUBSYSTEM WEIGHTS

	QTY	TOTAL WT. (kg)
<b>OPTICS</b>		
PRIMARY MIRROR (ULE)	1	215
SECONDARY MIRROR	1	15
TERTIARY MIRROR (ULE)	1	27
FOLD MIRROR	1	2
<b>POINTING &amp; CONTROL</b>		
FINE GUIDANCE SENSORS & ELECT	1	9
<b>STRUCTURE &amp; MECH</b>		
INSTRUMENT CONTAINER & SUPPORT STRUCTURE	1	38
METERING SHELL	1	70
LIGHT SHIELD	1	27
PRIMARY MIRROR FLEX MOUNTS	1	14
SECONDARY MIRROR SPIDER	1	18
SECONDARY MIRROR FINE GUIDANCE ACT	1	2
FINE GUIDANCE SENSOR MECHANISM	1	7
PRIMARY BULKHEAD	1	27
AFT BULKHEAD	1	27
CONICAL SHELL	1	25
SECONDARY MIRROR ALIGN. ACT	2	4
APERTURE DOOR	1	14
APERTURE DOOR MECHANISM	1	7
FOLD MIRROR SUPPORTS	1	4
TERTIARY MIRROR SUPPORTS	1	18
<b>ELECTRONICS</b>		
SECONDARY MIRROR ELECTR	-	7
HEATER ELECTR	-	4
HOUSEKEEPING DATA ELECTR	-	7
CABLES	-	9
<b>THERMAL CONTROL</b>		
INSULATION	-	9
PAINT	-	2
HEATERS	-	2
TOTAL		612
10% CONTINGENCY		61
TOTAL		673



ORIGINAL PAGE IS  
OF POOR QUALITY

C.G. LOCATIONS (cm)			MASS MOMENTS OF INERTIA (kg m <sup>2</sup> )		
$X_{cg}$	$Y_{cg}$	$Z_{cg}$	$M_x$	$M_y$	$M_z$
235	2.6	3.89	306	1411	1405

WEIGHT- 673 kg

Figure 54. Starsat center of mass and inertias.

## 10. CONCLUSIONS

Realizing that conventional telescope designs are not optimally suited for many space applications, a study was performed on a new three-mirror concept specifically designed to meet the demanding requirements of a high performance space telescope. It exhibits excellent optical performance over a wide field and broad spectral range. The accessibility of the image plane makes this design particularly attractive. This telescope is compatible with Space Shuttle and Spacelab systems and meets the performance requirements identified by the Spacelab UV-optical definition team. Some of the major subsystems for the telescope can make use of existing hardware and designs developed for other astronomy space projects. Further design and development of this telescope is recommended.



## 11. REFERENCES

1. Paul, M. : *Revue D'Optique*, 14, No. 5, 1935, p. 13.
2. Baker, J. G. : *IEEE Trans. Aer. El. Sys.*, Vol. AES-5, No. 2, 1969.
3. Lagrula, J. : *Cahiers de Phys.*, 1942, pp. 8-43.
4. Korsch, D. : *Appl. Opt.*, Vol. 11, No. 12, 1972, p. 2986.
5. Shack, R. V. and Meinel, A. B. : *J.O.S.A.*, 56, 1966, p. 545.
6. Rumsey, N. J. : *Proceedings, Opt. Instr. and Techniques 1969*, Oriel Press, p. 514.
7. Buchroeder, R. A. and Leonard, A. S. : *Appl. Opt.*, Vol. 11, No. 7, 1972, p. 1649.
8. Buchroeder, R. A. : *Technical Report No. 68*, Opt. Sc. Center, University of Arizona, 1971.
9. Korsch, D. : *J.O.S.A.*, Vol. 63, 1973 p. 667.
10. Korsch, D. : *Appl. Opt.*, Vol. 13, 1974, p. 1767.
11. Korsch, D. : *Optical Engineering*, Vol. 14, No. 6, 1975, p. 533.
12. Ball Brothers: *Telescope Opt. Des. Concepts Study in Support of the Facility Def. Team. Final Rep. July 1975, Corrected Sec. Printing, October 1975.*
13. *Space Telescope Optical Telescope Assembly/Scientific Instruments, Phase B Preliminary Design and Program Definition Study. Final Study Report, Volume IIB-Optical Telescope Assembly, Itek Corporation, Lexington, Massachusetts, March 1, 1976.*
14. HEAO-B Stellar Aspect Sensor Assembly. Vol. I Technical, a proposal to American Science and Engineering, Inc., Honeywell Radiation Center, Lexington, Massachusetts, October 11, 1974.

15. Tsao, H. H. and Wollman, H. B.: Photon Counting Technique Applied to a Modular Star Tracker Design. AIAA Paper Number 76-115, January 26-28, 1976.
16. F4012/F4012RP Technical Data Publication, Electron Tube Division ITT, Fort Wayne, Indiana, September 1970.
17. Seares, Fredrick H., Van Rhijn, P. J., Joyner, Mary C., and Richmond, Myrtle L.: Mean Distribution of Stars According to Apparent Magnitude and Galactic Latitude: Astrophysical Journal Number 62, The University of Chicago Press, Chicago, Illinois, 1925.
18. Allen, C. W.: Astrophysical Quantities. The Althone Press, University of London, 1963.
19. Forbes, F. F. and Mitchell, R. I.: Stellar Photometric Data for Six Different Photocathode Materials and the Silicon Detector. Communication Number 141 of the Lunar Planetary Laboratory, University of Arizona, December 5, 1968.
20. Preliminary Definition Study for a Large Precision Tracking Detector. Final Report, ITT Gilfillan, Van Nuys, California, January 1976.
21. Space Telescope, Phase B Definition Study. Final Report, Volume IIB, Optical Telescope Assembly, Part 4, Fine Guidance Sensor, Perkin-Elmer Corporation, March 1976.
22. Spacelab Accommodation Handbook, SLP/210a, May 1976.

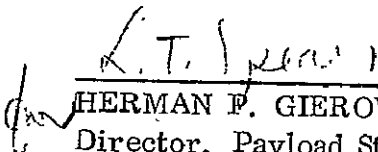
# APPROVAL

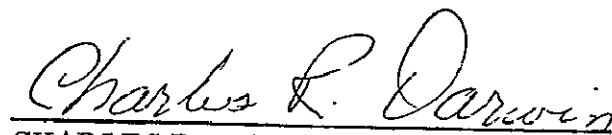
## STARSAT — A SPACE ASTRONOMY FACILITY

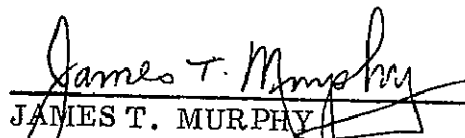
By Program Development

The information in this report has been reviewed for security classification. Review of any information concerning Department of Defense or Atomic Energy Commission programs has been made by the MSFC Security Classification Officer. This report, in its entirety, has been determined to be unclassified.

This document has also been reviewed and approved for technical accuracy.

  
HERMAN P. GIEROW  
Director, Payload Studies Office

  
CHARLES R. DARWIN  
Director, Preliminary Design Office

  
JAMES T. MURPHY  
Director, Program Development